Crosstalk Between Granulocytes, Gut Microbes, Stem Cells, And The Bone Marrow Microenvironment

by

Emily Bowers

A dissertation submitted in partial fulfillment
of the requirements for the degree of
Doctor of Philosophy
(Cell and Developmental Biology)
in the University of Michigan
2018

Doctoral Committee:

Professor Ivan Maillard, Chair
Associate Professor Maria Ken Figueroa
Assistant Professor Daniel Lucas-Alcaraz
Paul de Kruif Endowed Professor Gabriel Nuñez

Emily Bowers

bowersea@umich.edu

ORCID ID: 0000-0003-1044-6690

© Emily Bowers 2018

ACKNOWLEDGEMENTS

First, and foremost, I want to thank Daniel Lucas. You took the risk of taking me on as your first graduate student and for that, I am incredibly grateful. I have grown as a person and a scientist and owe so much of that to your guidance. You were there to push and support me every step of the way, you taught me to fight for my ideas and trust my instincts, to follow the science, and to never let anyone get in my way.

To all the members of the Lucas lab, you have been there for me every step of the way. To Ana, we saw the lab grow from the relatively empty space it was in the beginning to the lab it blossomed into by the time we left. Your encouragement and endless support – and sleepless nights – for the many experiments we did directly aided in my success in graduate school. To Margot, you were always there for me to bounce ideas off of and were always at the ready to help out with experiments. You have been an incredible support system. To Jizhou, your expertise, knowledge, and support were always available me. I am so thankful to have had the opportunity to work alongside each one of you and to have learned from each of you. I wish you all the best in your future endeavors.

To the members of my thesis committee – Ivan Maillard, Gabriel Nunez, and Maria Figueroa – your continual support and constructive feedback not only increased the

success of my projects, but helped shape me into an even better scientist. I have thoroughly enjoyed getting to work alongside and learn from each of you. I am truly grateful for you taking the time to be a part of my thesis committee and my graduate school career.

To Doug Engel, thank you for being an additional mentor. Your insight and feedback at lab meetings was always welcomed and always pushed me to think about my research in a different way.

To Jonathan Keller, I started off my time in research by joining your lab as a fresh eyed senior in high school and continued until I left for the University of Michigan. Your lab remains an incredibly special time in my life as it was these years that forever instilled in me the love and passion I have for research today.

To Kimberly Klarmann, your mentorship and friendship have been paramount to my success. You, along with Jonathan, were so imperative to helping develop my pure love for science. You taught me about myself as a scientist and as a person and were always there to guide me when needed, but were hands off when necessary. I am forever grateful for your mentorship, but more importantly, your friendship.

To all the faculty, post-doctoral fellows, and fellow graduate students who attended the Developmental Genetics meetings, thank you for all of your input and critique. Not only did it serve as a base to develop my confidence in discussing and defending my research, but you also provided incredible ideas.

To all the CDB staff, thank you for your never-ending patience and hard work. It is true that we would not be able to do any of the research if it were not for our incredible staff.

To the Michigan Research Core Facilities: the ULAM SPF mouse facilities, the Germ-Free Mouse Core, the Microscopy and Image Analysis Laboratory, the ULAM In-Vivo Animal Core, and the Flow Cytometry Core. Without the equipment, staff, and knowledge of these cores, none of my research would have been possible.

To my funding sources: The Elsa U. Pardee Foundation and Organogenesis Training Grant (T-32-HD007505) funded the research for my Nature Medicine manuscript. The Elsa U. Pardee Foundation and the Victors for Michigan program funded the gut microbiota project. Thank you for the support of my research projects.

To my friends: To Mary Lee, we may not have been in the same lab, but we might as well have been. You were always a major source of support and ideas – even if it was getting out of lab for a few minutes to grab some coffee and a snack. You were always there to

hear me vent, help me think through ideas, and throw in a joke to lighten the mood. To Jesse Sandin and Stephanie Beeman, we met outside of the research life in the craziest sport ever, but you have both been huge sources of support and laughter. You have all been so important in my development as a person over these past 5 years and each of you contributed to my success. I truly cherish your friendships.

To my mom, words cannot even begin to express the amount of gratitude and thanks that I owe you. From a young age, you instilled in me a work ethic to never take “no” for an answer and to always go after what fills me life. My successes in life are directly connected to your never ending support and the lessons you have taught me (and continue to teach me). I can easily say that I would not be at this point in my life if it were not for you.

TABLE OF CONTENTS

LIST OF FIGURES

ABSTRACT

The bone marrow (BM) is the main site of hematopoiesis in mammals and it is here that hematopoietic stem and progenitor cells proliferate and differentiate to produce all the mature cells of the blood. The BM also contains several non-hematopoietic stromal populations and these, along with hematopoietic cells and signals emanating from outside the bone marrow, communicate to regulate the production of mature cells. In this thesis I describe two novel aspects of this intricate regulation: 1) granulocytes crosstalk with BM endothelial cells to promote regeneration following bone marrow injury; and 2) neonatal gut microbes can regulate the proliferation and lineage commitment of hematopoietic stem cells (HSCs) in the BM via long distance communication.

Previous studies demonstrated that vascular regeneration was a necessary precedent for the restoration of functional hematopoiesis following BM injury. While studying the mechanisms that regulate vascular recovery, we discovered that adoptive transfer of granulocytes into recipients undergoing bone marrow transplant (BMT) led to increased recovery and function of the BM vasculature, faster recovery of hematopoietic cells in the peripheral blood, and overall increased survival of transplant recipients. A screen of BM granulocytes for angiogenic factors identified TNFα as a potential candidate for the regenerative phenotype. Genetic studies using *Tnfα*$^{-/-}$ granulocytes and TNFα receptor

null recipients validated granulocyte-derived TNFα as a newly discovered regulator of vascular regeneration.

Concurrent to this research we also discovered a new role for the gut microbiota in regulating hematopoiesis. We discovered this by initially testing whether neonatal microbes could expand granulocyte numbers in the BM; as a connection between gut microbes during neonatal development and the expansion of BM granulocytes had been previously described. Surprisingly, we did not observe any difference in granulocyte numbers when comparing germ-free and specific pathogen free (SPF) neonates. However, when analyzing the function of the HSCs in these two groups, we found reduced proliferation and increased production of myeloid and T-cells in SPF neonates when compared to their germ-free counterparts. When germ-free neonates were fostered with a SPF dam or when neonatal (but not adult) gut microbiota were adoptively transferred into adult germ-free recipients, these same HSC phenotypes were observed, suggesting that manipulation of the composition of the gut microbiota is capable of influencing hematopoiesis in the BM at all stages of development. Taking both of these projects together, these results reveal that granulocytes and gut microbes can regulate hematopoiesis during homeostasis and regeneration.

CHAPTER ONE:

INTRODUCTION

Blood cell production takes place in the bone marrow space where a complex network of hematopoietic and non-hematopoietic stromal cells interacts to form the bone marrow microenvironment. These cells form a unique three-dimensional structure to allow for the direct communication that are necessary for maintaining and regulating differentiating hematopoietic cells. In particular, this interaction of the microenvironment is essential for the proper maintenance of the hematopoietic stem cell (HSC). Years of research have allowed for the identification of several hematopoietic and stromal cells that are critical for HSC regulation and have come to be known as the HSC niche. More specifically, these HSC niche cells have been shown to produce cytokines necessary for regulating HSC numbers, as well as, trafficking to and from the bone marrow, self-renewal, differentiation, and proliferation (**1-7**).

THE HSC NICHE

Within the stromal compartment of the bone marrow, several cells have been validated as components of the HSC niche. One of the first populations identified were the endothelial cells that comprise all of the bone marrow vasculature, both sinusoidal and arteriolar blood vessels. These blood vessels are in turn almost completely ensheathed in two distinct populations of stromal perivascular cells; called the $LepR^{+}$ (also $Nestin^{dim}$ (**8-11**) or $CD45^{-}TER119^{-}CD31^{-}CD51^{+}CD140\alpha^{+}$ (**12**)) and the $Ng2^{+}$ (also called $Nestin^{bright}$ (**8**)) perivascular populations. $LepR^{+}$

cells are found in contact with all bone marrow endothelium, while $Ng2^+$ cells are much rarer and found only in contact with bone marrow arterioles. Using the LepR and Ng2 promoters for specificity, researchers have analyzed loss-of-function models to determine the involvement of these perivascular cells on HSC function. $LepR^+$- and $Ng2^+$-specific deletion of the critical HSC maintenance factors, CXCL12 and SCF, leads to severe loss of HSCs from the bone marrow and dramatically impaired hematopoiesis (**10-11, 13**). This close association to the vasculature is not unique, however. In fact, several other HSC niche components are also found in very close proximity to the blood vessels. The sympathetic nervous system innervates the bone marrow cavity and these axons follow along the vascular network. Lack of norepinephrine signaling from these bone marrow neurons leads to increased mobilization of HSCs into the peripheral blood and ultimately, loss of HSCs from the bone marrow (**14-15**).

Interestingly, mature hematopoietic cells have also been identified as HSC niche components. The Megakaryocyte is a large, multinucleated blood cell that is found in very close proximity to bone marrow sinusoids where they produce platelets. Depletion of Megakaryocytes or loss of HSC regulatory signals from these cells does not lead to immediate loss of the associated HSCs. Instead, the percent of proliferating HSCs increases and HSCs relocate farther away from the vasculature. Overtime, with continued loss of these signals, the HSC pool becomes less quiescent and eventually exhausts (**16-19**). Not all HSC niche components directly regulate the HSC pool in the bone marrow. The $CD169^+$ bone marrow macrophage has also been shown to be important for regulating expression of critical HSC regulatory cytokines, like CXCL12, on the $LepR^+$ perivascular population through clearance of aged neutrophils (**20-22**). Taken all together, this research shows the existence of a perivascular niche for HSCs and that these

multi-cellular structures work together to produce the factors necessary to promote HSC maintenance and function (**Figure 1**).

THE BONE MARROW VASCULATURE AS A KEY COMPONENT OF THE HSC NICHE

As every known HSC niche resides next to the bone marrow vasculature, this places the endothelial cells as a key constituent. The bone marrow is heavily vascularized to supply the cavity with oxygen and nutrients necessary for the constant production of blood cells. Arteries penetrate the bone marrow space where they branch off into smaller arterioles. These arterioles traverse along the endosteum – the small layer between bone marrow and bone surface – where they flow into venous sinusoids. These sinusoids make up the bulk of the complex vascular network and it is these vessels that serve as a means of egress for mature hematopoietic cells entering circulation. While initial studies using fluorescently labeled hematopoietic progenitors transplanted into irradiated recipient mice suggested that hematopoietic stem and progenitor cells (HSPCs) localize in the endosteal region of the bone marrow (**23**)**,** more recent analyses have shown that immunophenotypically-defined HSCs actually reside in very close proximity to the bone marrow vasculature (**24**). In fact, almost all HSCs in the bone marrow can be found within 5 μm of the blood vessels (**8, 10-11, 24-25**). Endothelial cells also produce a wide range of angiocrine factors, chemokines, and extracellular matrix components like CXCL12 (**10-11, 26-30**), SCF (**10-11, 31**), Pletiotrophin (**32-33**), and Notch ligands (**34-35**) and have been shown to support long-term HSC function in culture (**36-39**). While this data heavily suggested the existence of a perivascular HSC niche, the ability to validate the vasculature as a niche component has been challenging as the genetic or chemical depletion of bone marrow

endothelial cells are not compatible with life. Using vascular-specific Cre mouse lines, researchers were able to test the importance of endothelial cells as a source of HSC regulatory factors. *Scf*^{gfp} and *Cxcl12-DsRed* reporter mice revealed that endothelial cells were a major contributor of these two proteins – along with LepR^{+} perivascular cells (**10-11**). While hematopoietic cells were negative for GFP, some hematopoietic cells showed expression of the DsRed reporter. Using the hematopoietic-specific reporter *Vav1-Cre*, researchers deleted SCF (*Vav1-Cre;Scf*$^{fl/-}$ (**10**)) and CXCL12 (*Vav1-Cre;Cxcl12*$^{fl/fl}$ (**11**)) from the hematopoietic compartment and found absolutely no change to the hematopoietic system. However, when researchers used the Tie2 promoter (which targets hematopoietic and endothelial cells) to delete SCF and CXCL12, a robust phenotype was observed. Conditional deletion of SCF using the *Tie2-Cre:Scf* $^{fl/-}$ mouse model, resulted in severe depletion of HSCs in the bone marrow during steady-state and significant impairment in reconstitution of the hematopoietic system following competitive transplantation (**10**). Additionally, analysis of the *Tie2-Cre:Cxcl12*$^{fl/fl}$ mouse model also exhibited severe loss of HSCs from the bone marrow along with impaired reconstitution in a competitive transplant (**11, 29-30**).

Using the TNR.*Gfp* reporter mouse (which induces expression of Gfp upon Notch activation), researchers were able to identify endothelial cells as a source of Notch ligands, more specifically endothelial cells are a large source of Jagged 1 and Jagged 2 (**38**). Additionally, the loss of Jagged 1 (one of several Notch ligands) from endothelial cells using the *VE-Cad-Cre;Jag1*$^{fl/fl}$ mouse results in a significant decrease in the number of immunophenotypic HSCs in the bone marrow along with impaired long-term reconstitution in limited dilution assays and competitive transplants (**38**). While this data suggested a direct Notch signaling between endothelial cells

and HSCs, later studies have demonstrated that the mechanism of Notch-mediated regulation of HSCs is non-cell autonomous. Expression of the Notch inhibitor, dominant negative Mastermind-like1 (DNMAML), in the HSC pool leads to no impairment in HSC function (**40**). However, this does not discount the importance of endothelial-derived Notch ligands and their role in HSC maintenance and just further shows that the mechanism for how Notch signaling regulates the HSC pool has yet to be fully elucidated. Pleiotrophin (PTN) is another known HSC regulatory molecule and using the PTN-GFP reporter mouse, researchers were again able to restrict expression to endothelial cells and $LepR^{+}$ perivascular cells (**33**). Reciprocal transplants of wild-type BM into $PTN^{-/-}$ recipients had severely impaired donor HSC engraftment as early as four weeks post-transplant (**33**). Additionally, treatment of mice with anti-PTN (to block PTN signaling to HSC) induced HSC mobilization out of the BM (**33**).

While a lot of focus has been put on the specific signaling molecules secreted from endothelial cells that directly act on the associated HSCs, emphasis has also been placed on the intracellular signaling that influences EC function and the role of ECs as an HSC niche. Endothelial cells are continuously exposed to inflammation-inducing signals that target receptors on their surface leading to production of a range of pro-inflammatory signals like IL-1, IL-6, and TNFα. The induction of these inflammatory programs in ECs requires the master regulator, NF-kB. Researchers employed the *Tie2:IkB-SS* mouse model, which expresses a dominant negative form of IkB under the control of the Tie2 promoter which irreversibly binds NF-kB (**41**). Steady-state analysis of these mice show a significant increase in BM cellularity, an increase in the number of immunophenotypic HSCs, and a larger pool of quiescent HSCs (**41**) suggesting that loss of NF-kB signaling in ECs maintains a pro-HSC maintenance environment. While these

conditional deletion mouse models have allowed researchers to prove the importance of BMECs as a component of the HSC niche *in vivo*. However, we have only begun to scratch the surface when it comes to fully understanding the mechanisms of communication and regulation that exist between HSCs and their niche during both homeostatic and regenerative conditions.

VASCULAR REGENERATION IN THE BONE MARROW

Myeloablation is a condition where the bone marrow is severely suppressed and blood cell production dramatically drops. This is typically a side effect of the pre-conditioning regimes prior to bone marrow transplant (BMT) performed in the clinical setting. While myeloablation is necessary to deplete diseased bone marrow and provide space for donor HSCs to home and engraft, these therapies – including both the use of chemotherapy and irradiation – heavily disrupt the bone marrow microenvironment. One of the most damaged stromal populations following myeloablative therapy are the bone marrow endothelial cells, more specifically, $VEGFR2^{+}VEGFR3^{+}$ sinusoidal endothelium (**42**). In the first few days following myeloablation in mice, sinusoidal endothelial cells (SECs) begin to dilate and regress leading to a discontinuous vascular network with increased vascular permeability and impaired blood vessel integrity (**8, 42-48**), however, starting around ten days after myeloablation and BMT, vascular recovery begins with the emergence of new blood vessels and by four weeks from transplant hematopoietic output returns to normal (**42,49**).

The ability of the SECs to reform into a functional sinusoidal network is also necessary for successful engraftment and reconstitution of the hematopoietic system (**42**). More specifically, one critical pathway for vascular – and hematopoietic – regeneration is signaling through

VEGFR2. Mice undergoing BMT that receive neutralizing antibody against VEGFR2 have severe cytopenia in the bone marrow and peripheral blood leading to significantly reduced circulating white blood cells (WBCs) and platelets, have a predominance of disorganized and hemorrhagic sinusoids, and have severely impaired survival. While conditional deletion of VEGFR2 during steady-state has no impact on hematopoiesis, use of the *ROSA-Cre^{ER};Vegfr2$^{flox/-}$* mouse model during bone marrow regeneration results in life-threatening pancytopenia and severely regressed SECs for up to ten days post-transplant (**42**). Additionally, following myeloablative therapy, expression of Tie2 increases on regenerating blood vessels. Tie2 is one of two tyrosine kinase receptors expressed by blood vessels that bind the family of angiopoietin proteins. The angiopoietins are important growth factors in the formation of new blood vessels. Using the soluble decoy receptor Tie2-Fc, researchers were able to test the importance of this signaling pathway in vascular recovery. Loss of free angiopoietins after myeloablation, leads to a significant delay in sinusoidal regeneration along with dramatic reductions in circulating WBCs and platelets (**49**). Additionally, radioprotection of bone marrow SECs using the *Tie2-Cre;Bak/Bax$^{fl/fl}$* mouse model, which deletes two pro-apoptotic genes specifically from BMECs, results in increased protection of bone marrow HSCs, decreased vascular damage, and complete survival of the recipient mice post-transplant (**48**). These phenotypes were also observed in Angiopoietin 1 (*Angpt1*) global knockout models; while having no impact on the vascular network during steady-state, loss of this signaling pathway during regeneration leads to slowed vascular recovery following lethal irradiation (**46**). Conversely, loss of NF-kB signaling in BMECs during bone marrow regeneration confers a protective effect. Mice lacking NF-kB have significantly less disruption of the sinusoidal network post myeloablation compared to wild-type controls (**41**). As with SEC regeneration, loss of NF-kB in the BMECs following myeloablation

results in significantly faster recovery of mature circulating blood cells, with both red blood cells and platelets undergoing almost no change in peripheral blood concentration following irradiation and transplant compared to control mice (**41**).

These pivotal studies have since generated the current paradigm surrounding vascular and hematopoietic regeneration following severe myeloablation and bone marrow damage. We now know that vascular recovery is a necessary precedent for hematopoietic reconstitution after BMT. However, this has opened the large question of what mechanisms drive vascular regeneration and whether these pathways can be manipulated in the clinical setting to improve the efficiency of BMT. While BMT is considered a curative treatment for many hematological diseases, the procedure itself puts patients at risk for severe – and potentially life-threatening – complications; all of which predominantly stem from the impaired or delayed ability of donor HSCs to successfully engraft in the bone marrow and reconstitute the hematopoietic system. Therefore, the ability to increase the rate of hematopoietic regeneration, through manipulation of the mechanisms driving vascular recovery, post-transplant has significant clinical importance.

HEMATOPOIETIC AND STROMAL COMMUNICATION IS BI-DIRECTIONAL

The interaction between the hematopoietic system and the bone marrow stroma is not one-sided. While the importance of stromal-derived signaling for the proper function of the HSC pool is well described, studies over the past few years have implicated both mature blood cells and hematopoietic progenitors in communicating with the perivascular stromal populations in the bone marrow. More interestingly, this hematopoietic communication has been shown to

influence how the bone marrow stroma functions as niche. As mentioned above, $CD169^+$ bone marrow macrophages are involved in the circadian oscillations of CXCL12 expression on $LepR^+$ perivascular cells which directly influence the daily egress and homing of HSCs into and out of peripheral circulation (**20-21**). While the exact mechanism of communication remains elusive, chemical depletion of bone marrow macrophages using clodronate injections results in significantly decreased expression of *Cxcl12* mRNA from $LepR^+$ cells, as well as, a dramatic increase in the number of circulating HSCs (**20-21**). Additionally, genetic depletion of bone marrow macrophages using the $CD169^{DTR/+}$ mouse model, and subsequent dosing with diptheria toxin, recapitulates these results as expression of *Cxcl12* mRNA drops in the $LepR^+$ cells and the concentration of HSCs in circulation increases (**21**). Furthermore, use of macrophage-conditioned media in Dexter bone marrow cultures (**50**) leads to increased production of CXCL12 in the stromal cell line compared to the Dexter cultures grown in non-conditioned media suggesting a macrophage-derived soluble factor is involved (**21**). Additional research has linked this role of macrophage-induced regulation of the niche to clearance of aged neutrophils (**22**). Depletion of circulating neutrophils using an anti-LyG6 antibody is correlated with increases of Cxcl12 mRNA and protein levels in $LepR^+$ perivascular cells. $DsRed^+$ neutrophils injected into recipient mice also revealed that 40% of these neutrophils localize in direct contact with $CD169^+$ macrophages. Additionally, $DsRed^+$ macrophages can be found using flow cytometry, suggesting the engulfment of the aged $DsRed^+$ neutrophils. Activation of LXR (liver X receptors), important transcriptional regulators that alter gene expression in macrophages following engulfment of apoptotic cells, using the agonist GW3965 leads to increased circulation of HSCs in the peripheral blood and a significant decrease in Cxcl12 expression in the bone marrow (**22**). While the specific factors transmitted from $CD169^+$ macrophages to the $LepR^+$ cells have yet to

be identified, this research implicated the importance of mature hematopoietic cells in regulating their own production via the HSC niches. Additionally, it is well known that Megakaryocytes produce a range of pro-angiogenic cytokines including VEGF-A (**51**), FGF-2 (**52**), and MMP-2 (**53**) and the *in vitro* culturing of endothelial cells with platelets leads to increased cell proliferation and vessel tube formation (**54**). In mice lacking the protein thrombospondin 1 (TSP 1), a protein restricted to Megakaryocytes and platelets, there is an increase in density of Megakaryocytes and increase in sinusoidal vasculature (**55-56**) suggesting that Megakaryocytes have both pro- and anti-angiogenic effects during homeostasis.

The discovery that hematopoietic cells can influence the function of bone marrow stromal cells suggested that these mechanisms could have a role during regeneration. Additionally, it should be noted that following myeloablation to the bone marrow, lack of donor hematopoietic cells via a BMT not only results in lethality, but even more delayed vascular regeneration (**42**). While one explanation could be the need of BMECs for structural support provided by the presence of hematopoietic cells in the bone marrow, an alternative explanation is that hematopoietic cells communicate with the damaged BMECs to induce vascular recovery. As mentioned above, bone marrow Megakaryocytes are known to exist in a close relationship with the vasculature during homeostasis to allow for production of platelets. Under the stressed condition of hindlimb ischemia, it has also been shown that Megakaryocyte-derived cytokines found in platelets can accelerate new blood vessel formation (**55**). When researchers analyzed bone marrow regeneration following myeloablation in mice lacking the Megakaryocyte-derived anti-angiogenic factor TSP1, *TSP-DKO*, they noted faster recovery of platelets in the peripheral blood, reduced damage to the sinusoidal vasculature following 5-FU treatment, and quicker recovery of the

vascular network to normal (**56**). Platelets derived from *TSP-DKO* mice also had increased release of CXCL12 (**56**). Platelet-derived CXCL12 has been previously shown to induce recruitment of $CXCR4^{+}VEGFR1^{+}$ hematopoietic cells to the site of vascular injury to induce regeneration (**57**).

Interestingly, the ability to impact vascular regeneration does not seem restricted to mature hematopoietic cells. Expression of *Angpt1* in the bone marrow is restricted to Megakaryocytes, hematopoietic progenitors, and $LepR^{+}$ perivascular cells (**46**). Angpt1, and its receptor Tie2, are important for the development of the vascular system (**58**) and have been shown to have critical roles in vascular regeneration (**48-49**). To test the importance of $LepR^{+}$ and hematopoietic progenitor cell derived Angpt1 on vascular regeneration, researchers lethally irradiated *LepR-Cre;Angpt1*$^{GFP/fl}$ recipient mice and transplanted them with *Mx1-Cre;Angpt1*$^{GFP/fl}$ donor marrow. Mice lacking Angpt1 in both populations experienced faster recovery of hematopoietic cells in peripheral blood, increased proliferation of BMECs in the bone marrow, and a faster recovery of regressed sinusoids (**46**). It should be noted, however, that loss of Angpt1 from hematopoietic cells alone had little to no improvement on recovery suggesting that $LepR^{+}$ are the major functional source of Angpt1 in the context of vascular regeneration (**46**). Additionally, loss of Angpt1 in these transplant models did lead to higher levels of vascular permeability in the bone marrow, even 28 days post-transplant, suggesting that the vascular network in the BM is not functionally the same as before myeloablation (**46**).

In chapter one of this thesis, I will present data that bone marrow neutrophils are directly involved in the regeneration of the bone marrow SECs through production of TNFα. Infused neutrophils localize directly in contact with the regenerating vasculature. Additionally, injection of recombinant TNFα results in a milder increase in vascular regeneration, compared to the vascular recovery seen with adoptive transfer of neutrophils post-transplant. Taken together, this data suggests the potential of a regenerative neutrophil niche that is necessary for bone marrow regeneration. In chapter two of this thesis, I will present data that the composition of the gut microbiota communicates with the bone marrow to influence HSC proliferation and differentiation. Mice containing a microbiota that compositionally resembles that of a neonate contain HSCs with increased quiescence and myeloid-lineage bias in competitive transplant compared to mice harboring an adult gut microbiota. While we have yet to elucidate the mechanism driving this communication, we do know that the quiescent pool of HSCs is known to localize to the megakaryocyte (**16**) and arteriolar (**8**) niches. Therefore, this research could unveil a novel form of HSC niche modulation through signals emanating from the gut.

FIGURE

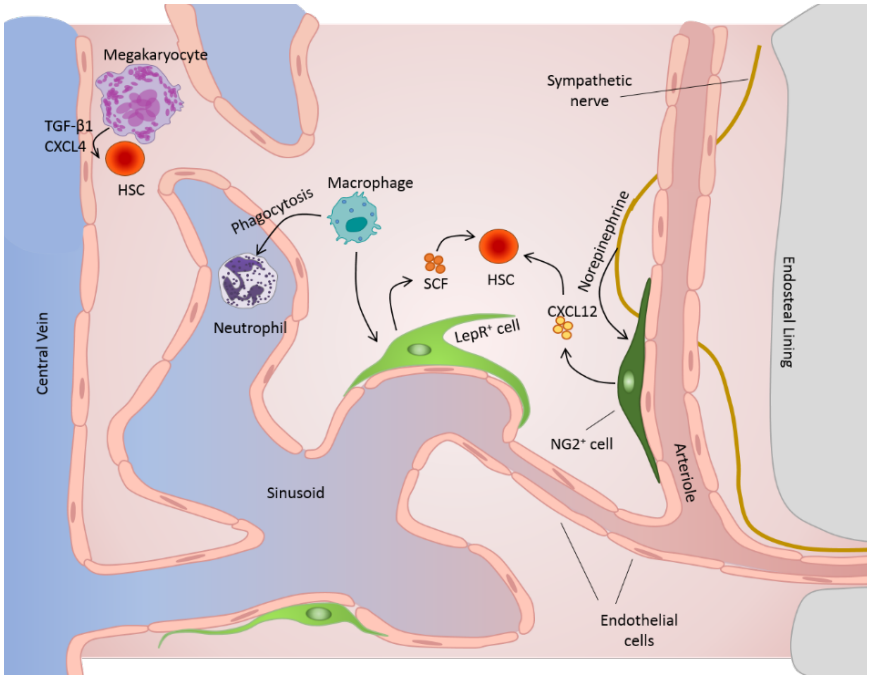

Figure 1. Schematic of the HSC niche. Hematopoietic stem cells (HSCs) reside in specific regions of the bone marrow in close association with non-hematopoietic stroma and mature hematopoietic cells. In addition, these regions are almost exclusively perivascular and can be found along both sinusoidal and arteriolar blood vessels. The endothelial network is a large component of the HSC niche and endothelial cells comprising the blood vessels secrete a variety of critical factors that maintain HSC function. $LepR^+$ perivascular cells can be found in direct contact with both sinusoidal and arteriolar vasculature and produce cytokines like CXCL12 and SCF to directly regulate the associated HSCs. $NG2^+$ perivascular cells are more restricted to the arteriolar blood vessels and are more closely associated with quiescent HSCs. Megakaryocytes are more restricted to the sinusoidal endothelium, but also regulate HSC proliferation through production of factors like CXCL4 and TGFβ. While these populations of the HSC niche directly regulate HSC function, there are several other cell populations that indirectly contribute to HSC function through interactions with the HSC niche. Sympathetic nerves follow along the arteries in the bone marrow and influence HSC mobilization and trafficking by controlling CXCL12 production of the perivascular stromal cells through secretion of norepinephrine. Additionally, bone marrow macrophages promote the retention of HSCs by also regulating the production of CXCL12 of perivascular stromal cells. While the mechanism is still unknown, this role of macrophages can be regulated by the daily clearance of aged neutrophils via phagocytosis which leads to alterations in CXCL12 production of bone marrow perivascular stromal cells. Black arrows indicate direct communication and regulation. Figure modified from one generated by Lucas lab technician, Margot May.

CHAPTER TWO:

GRANULOCYTE-DERIVED TNFα PROMOTES VASCULAR AND HEMATOPOIETIC REGENERATION IN THE BONE MARROW

SUMMARY

Endothelial cells are a critical component of the bone marrow (BM) stromal network that maintains and regulates hematopoietic cells (**10-11,34-35,42,48,59-60**). Vascular regeneration precedes, and is necessary for, successful hematopoietic stem cell (HSC) transplantation, the only cure for most hematopoietic diseases (**42,48**). Recent data suggest that mature hematopoietic cells may crosstalk with stromal cells to regulate their function (**20-22,61**). Whether a similar crosstalk regulates the vasculature is not known. Here we find that donor hematopoietic cells crosstalk with sinusoidal endothelial cells to induce host vessel and hematopoietic regeneration after transplantation. Adoptive transfer of BM, but not peripheral, granulocytes prevented death and accelerated recovery of host vessels and hematopoietic cells in mice transplanted with limited HSC numbers. Selective granulocyte ablation in vivo impaired vascular and hematopoietic regeneration after transplantation. Gene expression analyses indicated that granulocytes are the main source of the cytokine TNFα whereas its receptor, TNFR1, is selectively upregulated in regenerating vessels. In adoptive transfer experiments wild-type, but not *Tnfa*$^{-/-}$, granulocytes induced vascular recovery. After transplantation granulocytes are recruited to regenerating sinusoids suggesting that granulocytes crosstalk directly with endothelial cells. Accordingly, wild-type granulocyte

transfer did not prevent death or promote vascular regeneration in *Tnfr1*$^{-/-}$*:Tnfr2*$^{-/-}$ mice. Our results indicate that BM granulocytes generate a microenvironment that promotes vessel growth and regeneration. Manipulation of the crosstalk between endothelial cells and granulocytes may lead to new therapeutic approaches to improve vessel regeneration and increase survival and hematopoietic recovery after HSC transplantation.

INTRODUCTION

Endothelial cells are a critical component of the bone marrow (BM) stromal network that maintains and regulates the production and function of hematopoietic cells (**10-11,34-35,42,48,59-60**). During steady-state hematopoiesis, the BM vasculature produce a wide range of angiocrine factors and chemokines, like CXCL12 (**10-11**), SCF (**10-11**), Pleiotrophin (**32-33**), and Notch ligands (**34-35**), that are required for the proper proliferation, differentiation, and retention or egress of maturing hematopoietic cells. Endothelial cells also have a large role during regenerative hematopoiesis following myeloablation and transplantation by producing factors that promote hematopoietic regeneration (**33-35,48,62**). Myeloablative therapies designed to remove diseased host hematopoietic cells severely damages BM blood vessels (**8,42,48**). Regeneration of the damaged vasculature must occur before endothelial cells can support hematopoiesis (**41-42,48**). Additionally, therapies that promote vessel survival and recovery also promote hematopoietic regeneration (**41-42,48**). While the current paradigm in the BM regenerative field places vascular regeneration as a necessary precedent for hematopoietic recovery, the mechanisms that drive endothelial cell regeneration are not well investigated. After myeloablation mice that received a bone marrow transplant showed faster

vascular regeneration than the control group that received no donor bone marrow (**42**). This suggested that hematopoietic cells are needed to promote vascular recovery. This, coupled with the fact certain hematopoietic cells are capable of communicating with and influencing the function of BM stromal cells prompted us to investigate the role of hematopoietic cells in driving bone marrow vascular regeneration.

RESULTS

To test whether hematopoietic cells crosstalk with the vasculature we transplanted different amounts of $CD45.2^+$ bone marrow nucleated cells (BMNC) into lethally irradiated $CD45.1^+$ recipients. Fourteen days later the transplanted mice showed a dose-dependent increase in the numbers of hematopoietic and $CD45^-Ter119^-CD31^+CD105^+$ endothelial cells in the BM (**Fig. 2.1a,b and Supplementary Fig. 2.2a**). To analyze the vascular network of these mice we injected αCD31 and αCD144 antibodies intravenously followed by dissection and 3D whole-mount imaging of the sternal vasculature (**8**). This allowed us to distinguish between true vessels-with a perfused lumen- and vascular sheets that appear after vascular injury (**Supplementary figures 1a,b**). Mice transplanted with more BMNC showed a denser vascular network with more numerous and longer vessels when compared to mice transplanted with fewer BMNC (**Fig. 2.1c,d** and **Supplementary figures 1a,b**). In agreement with these results we found reduced vascular permeability (measured by Evans Blue extravasation, **22**) in mice transplanted with higher amounts of donor BMNC (**Fig. 2.1e**). To test whether the endothelial cells were host or donor derived we transplanted WT mice with $20x10^6$ BMNC purified from *Ubc-gfp* mice which constitutively express GFP in all cells (**63**). We found that virtually all endothelial cells were host derived (**Fig. 2.1f**). Transplant of more BMNC

led to increased endothelial cell recovery early after transplantation (**Supplementary Fig. 2.2b**) and reductions in the fraction of apoptotic and necrotic endothelial cells (**Supplementary Fig. 2.2c**) but had no effect on the cycling of endothelial cells (**Supplementary Fig. 2.2d**). These experiments demonstrate that donor hematopoietic cells promote endothelial cell survival and drive the recovery of a functional, host-derived, vascular network in the recipient mice.

The results above were surprising because hematopoietic progenitors were reported to inhibit vascular regeneration via angiopoietin-1 (**46**). We thus investigated whether the observed vascular recovery was mediated by more mature hematopoietic cells. We FACS-purified $CD45.2^+$ hematopoietic cells based on the expression of mature lineage markers. We adoptively transferred each of these populations, at the same ratios found in vivo, into γ-irradiated $CD45.2^+$ recipients together with 10^5 $CD45.1^+$ BMNC (as a source of donor HSC). Since the adoptively transferred cells are thought to have limited self-renewal capacity in vivo we adoptively transferred the same populations every 2-3 days for 2 weeks (**Fig. 2.2a**). We found that only $Gr1^+CD115^-$ granulocytes, which contain all BM neutrophils and late neutrophil progenitors (**21**), were capable of inducing rapid recovery of endothelial cells (**Fig. 2.2b**). Notably, granulocyte transfer also promoted survival (**Fig. 2.2c**) and led to faster recovery of hematopoietic cells in the periphery (**Fig. 2.2d**). In agreement with previous studies (**35,42,48**) we found a strong correlation between endothelial cell recovery and survival as moribund mice showed less vascular recovery (**Supplementary Fig. 2.3a**). Imaging of the sternal vasculature showed that granulocyte-treated mice had more blood vessels than PBS-treated controls or mice transferred with monocyte/macrophages, lymphocytes or erythroid-lineage cells (**Fig.**

2.2e,f). Granulocyte transfer also rescued vascular leakiness in irradiated mice but only when transferred at very high doses (**Fig. 2.2g**). Granulocyte-induced recovery was not mediated by induction of systemic inflammation as we did not detect significant increases in inflammatory cytokines in BM or plasma (**Supplementary Fig. 2.3b**), injury to peripheral tissues in pathology analyses (**Supplementary Fig. 2.3c**), or increased granulocyte recruitment to peripheral tissues (**Supplementary Fig. 2.3d**). We also did not find increased endothelial cell recovery in peripheral tissues in granulocyte-treated mice (**Supplementary Fig. 2.3e**). Transfer of common myeloid progenitors can protect lethally irradiated mice from death until the few host HSC that survived irradiation can restore hematopoiesis (**64**). To test if granulocytes induced survival through a similar mechanism we adoptively transferred granulocytes into lethally irradiated mice. We found that granulocytes were not capable of rescuing irradiation-induced death in the absence of donor hematopoietic stem and progenitor cells (HSPC, **Supplementary Fig. 2.3f**). We performed experiments following vascular and hematopoietic recovery up to 4 weeks after transplantation (**Fig. 2.2h** and **Supplementary Fig. 2.4a,b**). These analyses revealed that granulocyte transfer promoted endothelial cell survival early after transplantation as shown by reduced numbers of apoptotic and necrotic endothelial cells (**Fig. 2.2i**) and that was comparable to the one induced by transfer of high BMNC numbers (**Supplementary Fig. 2.2c**). In agreement, we found that granulocytes induced expression of *cFlip*, an antiapoptotic prosurvival factor (**65**), in endothelial cells (**Supplementary Fig. 2.4c**). In contrast granulocytes did not induce expression of hematopoietic supportive molecules like *Cxcl12*, *Scf*, *Notch* ligands or led to activation of *Hif1a* or its downstream targets (**Supplementary Fig. 2.4d-f**). These results indicate that granulocytes promote endothelial cell survival.

To analyze the effect of granulocytes in hematopoietic recovery we performed lineage tracing experiments (**Supplementary Fig. 2.5a**). We found that the increased peripheral blood and BM hematopoietic recovery was due to persistence of the transferred BM granulocytes (**Supplementary Fig. 2.5d,g)** and increased production of host cells in granulocyte-treated mice (**Supplementary Fig. 2.5c-h**). Importantly, adoptive transfer of peripheral blood neutrophils, which home to the bone marrow and crosstalk with CXCL12 abundant reticular stromal cells to regulate HSC trafficking (**22**), did not induce vascular or hematopoietic recovery (**Supplementary Fig. 2.5b-h).** This was probably because, in contrast to BM granulocytes, peripheral neutrophils do not persist in the recipient mice (**Supplementary Fig. 2.5d,g**). We hypothesized that increased vascular recovery might facilitate engraftment of donor-derived HSPC. To test this, we performed competitive transplants. We FACS-purified donor $CD45.1^+$ cells from the primary recipients and transplanted them together with competitor $CD45.1^+$:$CD45.2^+$ BMNC into lethally irradiated $CD45.2^+$ secondary recipients, as this strategy allowed discriminating the origin of donor, competitor and recipient cells (**Fig. 2.2a**). $CD45.1^+$ BMNC from granulocyte-treated mice displayed increased short-term T- and myeloid cell, but not long-term (16 weeks) multilineage, contribution to peripheral blood (**Fig. 2.2j**). Taken together our results demonstrate that adoptive transfer of BM granulocytes is sufficient to promote survival and drive vascular and hematopoietic cell recovery after myeloablation without exhausting the donor HSC pool.

To investigate further the function of granulocytes in regeneration we bred *Mrp8-cre-IRES-GFP* mice, in which Cre expression is largely restricted to granulocytes and a fraction of

granulocyte monocyte progenitors (GMP, **66-67**), with *iDTR* mice in which the diphtheria toxin receptor (DTR) is induced by Cre-mediated recombination (**68**). To test whether granulocytes produced by the initial BMNC graft participated in vascular regeneration we transplanted lethally irradiated recipients with $5x10^6$ BMNC purified from *iDTR* or *Mrp8-cre-IRES-GFP:iDTR* mice followed by DT treatment. This led to efficient granulocyte ablation in the mice transplanted with *Mrp8-cre-IRES-GFP:iDTR* but not control *iDTR* BMNC (**Fig. 2.3a,b**). In these mice, granulocyte ablation led to impaired vascular regeneration and increased vascular leakage (**Fig. 2.3c-e**) and impaired peripheral blood cell recovery (**Fig. 2.3f**). We also observed reductions in monocytes and macrophages in the BM of *Mrp8-cre-IRES-GFP:iDTR* mice (**Fig. 2.3g-i**). To confirm that the monocyte/macrophage loss was not responsible for the reduced blood vessels we ablated granulocytes in vivo by injection of α-Ly6G, an antibody that ablates, exclusively, granulocytes (**69**). α-Ly6G, but not isotype control, treatment depleted granulocytes (**Fig. 2.3j**) and impaired vascular regeneration (**Fig. 2.3k**). It also caused loss of BM monocytes and lymphocytes (**Supplementary Fig. 2.6a,b**). Since α-Ly6G acts exclusively in granulocytes these results indicate that loss of these populations is due to granulocyte depletion. In a complementary approach we transplanted recipient mice with a single graft of total BMNC or a graft in which the granulocytes were removed prior to transplantation via FACS. As predicted, the mice transplanted with the granulocyte-depleted graft showed reduced granulocyte numbers (**Fig. 2.3l**) and impaired endothelial and hematopoietic regeneration 6 days after transplantation (**Fig. 2.3m** and **Supplementary Fig. 2.6c,d**). These experiments demonstrate that donor-derived granulocytes are necessary for efficient vascular regeneration.

To investigate the mechanisms through which granulocytes promote vascular regeneration we profiled BM granulocytes for the expression of multiple angiogenic factors via qPCR. We detected expression of fibroblast growth factor 1 (*Fgf1*), progranulin (*Prgn*), pleiotrophin (*Ptn*), vascular endothelial growth factor a (*Vegfa*) and tumor necrosis factor alpha (*Tnfa*, **Supplementary Fig. 2.7a**). We focused on *Tnfa* because it was enriched in BM granulocytes (**Supplementary Fig. 2.7b**), its receptor *Tnfr1* was enriched specifically in endothelial cells compared to the rest of the BM stroma (**Supplementary Fig. 2.7c**), *Tnfr1* was upregulated in regenerating endothelial cells (**Supplementary Fig. 2.7c**) and TNFα induces cFLIP expression (**70**). TNFα is a powerful angiogenic factor in mice (**71-72**) and neutrophil-derived TNFα drives blood vessel formation during zebrafish development (**73**)**.** Analyses of *Tnfa*$^{-/-}$ or *Tnfr1*$^{-/-}$*:Tnfr2*$^{-/-}$ mice revealed fewer endothelial cells in the steady-state bone marrow indicating that TNFα regulates vascular homeostasis (**Supplementary Fig. 2.8**). To test whether TNFα also played a role in regeneration we myeloablated WT or *Tnfa*$^{-/-}$ mice with a single injection of 5-fluorouracil. We found that mutant mice displayed reduced endothelial cell numbers and dramatically succumbed to this treatment (**Fig. 2.4a,b**). Reduced *Tnfa*$^{-/-}$ mice survival might be due to the reduced BM endothelial cell numbers in the steady-state. Because of this we also tested whether recombinant TNFα injection could be used to improve vascular regeneration. Indeed, rTNFa injection induced faster vascular recovery in WT and *Tnfa*$^{-/-}$ mice and delayed death in *Tnfa*$^{-/-}$ mice (**Fig. 2.4a,b**). These results indicate that TNFα regulates BM endothelial cell numbers during homeostasis and regeneration and that TNFα signaling can be modulated to improve vascular regeneration. To test whether granulocytes promoted vascular regeneration specifically via TNFα we performed adoptive transfer experiments using granulocytes purified from WT or *Tnfa*$^{-/-}$ mice. To distinguish the effect in regeneration of

sinusoids and arterioles we used *Nestin-gfp* mice as in this model Nestin-GFP^{bright} cells label arterioles (**8,13**). We found that WT, but not *Tnfa*$^{-/-}$ granulocytes, induced sinusoidal vessel recovery as demonstrated by quantification of endothelial cells by FACS (**Fig. 2.4c**) and sinusoidal and arteriolar vessel numbers by 3D whole-mount immunofluorescence (**Fig 2.4d,e**). In addition WT, but not *Tnfa*$^{-/-}$ granulocytes, rescued survival and drove faster white and red blood cell recovery in the peripheral blood (**Fig. 2.4f,g**). Flow cytometry analyses showed that granulocytes express the membrane-bound form of TNFα (**Supplementary Fig. 2.9a**). Imaging analyses showed that, during regeneration, granulocytes preferentially localized to sinusoids with 76% of granulocytes found within 5μm of a sinusoid whereas a much smaller fraction (14%) localized to Nestin-GFP^{bright} arterioles (**Fig. 2.4h,i**). B lymphocytes, which do not induce regeneration (**Fig. 2.2b**), showed fewer interactions with BM vessels (**Supplementary Fig. 2.9b,c**). Granulocyte recruitment to regenerating vessels was independent of CXCR4 and CXCR2 (**Supplementary Fig. 2.9d-f**) which are the major receptors that regulate neutrophil trafficking during homeostasis (**74**) indicating that additional mechanisms regulate granulocyte recruitment to injured vessels. The results above suggested that the crosstalk between granulocytes and endothelial cells was direct. In further support for this pathway, adoptive granulocyte transfer failed to promote survival and vascular regeneration in *Tnfr1*$^{-/-}$*:Tnfr2*$^{-/-}$ mice compared to control mice after transplantation (**Fig. 2.4j,k**). To confirm that granulocyte-derived TNFα was not acting on hematopoietic cells we transplanted WT recipients with an initial graft of 10^5 WT or *Tnfr1*$^{-/-}$*:Tnfr2*$^{-/-}$ BMNC followed by adoptive transfer of WT granulocytes. During regeneration TNFα acts on HSPC to promote engraftment (**75**). In agreement, we found reduced peripheral blood and BM hematopoietic recovery in mice transplanted with *Tnfr1*$^{-/-}$*:Tnfr2*$^{-/-}$ BMNC (**Supplementary Fig. 2.10a,b**). We also found delayed

vascular regeneration (**Supplementary Fig. 2.10c**) likely due to insufficient granulocyte production (**Supplementary Fig. 2.10a**). Adoptive transfer of WT granulocytes rescued death (**Supplementary Fig. 2.10d**) and dramatically increased vascular and hematopoietic recovery in both the mice transplanted with WT BMNC mice and in the mice transplanted with *Tnfr1*$^{-/-}$ *:Tnfr2*$^{-/-}$ BMNC (**Supplementary Fig. 2.10a,b**). These experiments demonstrate that granulocytes crosstalk directly with the host BM stromal microenvironment via TNFα to drive vascular regeneration.

DISCUSSION

Myeloid cells are key players in vascular remodeling and regeneration in many tissues (**71,73,76**). Our results demonstrate that granulocytes, the most abundant cells in the BM, crosstalk with the microenvironment to drive vascular regeneration specifically via TNFα. Since both endothelial cell-derived factors (e.g. Notch ligands, EGF, Pleiotrophin (**33-35,62,77**) and vessel regeneration (**41-42,48**) are necessary for hematopoietic recovery our results suggest the existence of a bidirectional feedback loop after BM injury. In this loop endothelial cell regeneration will drive hematopoietic progenitor proliferation and generation of granulocytes which in turn support further vessel regeneration. Our results also indicate that granulocytes overcome the inhibition of vascular regeneration induced by hematopoietic progenitors (**25**). After transplantation HSC and multipotent progenitors preferentially generate myeloid cells (**40**), a preference believed to satisfy the physiological demand for peripheral neutrophils to prevent infections. Our results suggest that this myeloid bias might also contribute to recovery by forcing the differentiation of progenitors into granulocytes which in turn generate a microenvironment that promotes vessel regeneration and hematopoiesis.

The function of TNFα in regulation of HSPC is controversial. Some reports suggest that TNFα acts on HSPC to promote their maintenance in the steady state and engraftment during regeneration (**75,78-80**). Other reports suggest that TNFα acts on HSPC to inhibit their function during homeostasis and that TNFα-receptor blockade prior to transplantation promote HSPC survival (**81-82**). Our results in Supplementary Figure 9 support a pro-regenerative effect of TNFα in HSPC. Our results also suggest that, in addition to its effects on hematopoietic cells, TNFα also regulates the vasculature and that granulocytes employ TNFα to crosstalk with the microenvironment to drive regeneration. Granulocytes also produce other pro-regenerative factors like VEGF, which is necessary for BM vascular regeneration (**42**) and that can recruit angiogenic myeloid cells to the heart (**76**), and Pleiotrophin which promotes hematopoietic recovery by inducing Ras activation in HSPC (**33,62**). Future studies will determine whether these factors cooperate with TNFα in granulocyte-driven regeneration.

Our data also suggest that the composition and cellular output of the initial graft affect recovery of host vessels and hematopoietic cells. This may have implications in the context of clinical HSC transplantation; in patients especially vulnerable to myeloablation, such as those with DNA repair defects or those in which the stroma has been damaged by prior chemotherapy treatment (**83-85**), a supply of BM granulocytes can be utilized to ameliorate vascular injury and promote hematopoietic recovery.

MATERIALS AND METHODS

Mice

C57BL/6J (CD45.2^{+}) and B6.SJL-*Ptprc^{a} Pepc^{b}*/BoyJ (B6.SJL, CD45.1^{+}) were purchased from the Jackson laboratory and bred in house. C57BL/6j:B6.SJL hybrids (CD45.2^{+}:CD45.1^{+}) were generated by breeding C57BL/6J with B6.SJL mice. *Ubc-gfp* mice (**63**), *Mrp8-cre-IRES-gfp* (*Mrp8-cre,* ***66***), *iDTR* ***(68)***, *Tnfa$^{-/-}$* (**86**) mice were originally purchased from the Jackson laboratory. *Tnfr1$^{-/-}$*:*Tnfr2$^{-/-}$* (**87**) mice were also purchased from the Jackson laboratory and then backcrossed for four additional generation into C57BL/6J background and then bred in house. *Nestin-gfp* mice (**8,13**) were a gift from Paul S. Frenette. All experiments were performed in 8-14 week old male mice. All mice were housed at the SPF facility managed by the Unit for Laboratory Animal Medicine (ULAM) at the University of Michigan. Experiments were approved by the Institutional Animal Care and Use Committee at the University of Michigan.

Bone marrow isolation.

Mice were euthanized by isoflurane overdose. Bone marrow was harvested by flushing mouse long bones with 1 ml of ice-cold PEB (2mM EDTA 0.5% Bovine serum albumin in PBS). Red blood cells were lysed once by adding 1 mL of RBC Lysis Buffer (NH_4Cl 150mM, $NaCO_3$ 10mM, EDTA 0.1mM). Cells were immediately decanted by centrifugation, resuspended in ice-cold PEB and used in subsequent assays. Due to the known effect of circadian rhythm effects in granulocytes and HSC (**14,22,88-89**) we performed BM harvest at zeitgeber times 3-6 in mice under standard (12h light:12h dark) cycles.

Peripheral blood analyses.

Blood was collected from the facial vein in tubes containing EDTA. White blood cell (WBC), red blood cell (RBC) and platelet counts were obtained using an Advia Counter (Siemens) or a Hemavet 950 (Drew Scientific). Prior to flow cytometry staining and analyses, red blood cells in

peripheral blood were lysed once by adding 1 mL of RBC Lysis Buffer (NH_4Cl 150mM, $NaCO_3$ 10mM, EDTA 0.1mM). Cells were immediately decanted by centrifugation, resuspended in ice-cold PEB and used in subsequent assays.

Collagenase/Dispase digestion

To purify the stromal cell fraction of the bone marrow (including endothelial cells) we used a modified version of the serial digestion protocol developed by the Simmons laboratory (**90**). Digestion buffer was made using 2 mg/ml Collagenase Type IV (Gibco, 17104-019) and 3 mg/ml Dispase (Gibco, 17105-041) dissolved in room temperature PBS. We harvested the BM by flushing a tibia with 1 ml of digestion buffer into a 5 ml polypropylene snap-cap tube containing another 1 ml of digestion buffer. We mixed the tubes vigorously by hand and incubated at 37°C for 5-7 minutes. Following the first incubation, the tubes were mixed vigorously by hand and then placed back at 37°C for another 5-7 minutes. After this second incubation we collected the supernatant taking care of leaving any macroscopic clumps in the tube. We transferred the digested cells to a tube containing 5 ml of ice-cold PEB. Then we added one ml of digestion buffer to the snap-cap tubes and the process above repeated until all macroscopic pieces of bone marrow had been digested. The red blood cells were lysed once using RBC Lysis Buffer, filtered through a 100 µm filter (Greiner Bio-one, 542-000), and then immediately spun down in the centrifuge. The cells were resuspended in 1 ml of ice-cold PEB and used for subsequent analyses.

FACS analyses

Cells were stained for 30 minutes in PEB buffer with the indicated antibodies and analyzed in a BD LSRFortessa (BD Biosciences) or FACS-purified using a BD FACS Aria II or a Synergy SY3200 Cell sorter (Sony). Dead cells and doublets were excluded based on FSC and SSC

distribution and DAPI (Sigma) exclusion. Data was analyzed using FACS Diva software 8.0 (BDBiosciences). Antibodies used were against B220 (clone RA3-6B2, Cat No: 103224), CD3 (clone 145-2C11, Cat No:100304), CD4 (clone GK1.5, Cat No:100422), CD8 (clone 53-6.7, Cat No:100722), CD11b (clone M1/70, Cat No:101216 or 101204), CD16/32 (clone 93, Cat No:101328), CD19 (clone 6D5, Cat No: 115508), CD31 (clone A20, Cat No:110724), CD41 (clone MWReg30, Cat No:133921 or clone D7, Cat No: 108104), CD45 (clone 30-F11, Cat No:103116), CD45.1 (clone A20, Cat No:110723 or 110708), CD45.2 (clone 104, Cat No:109845, 109823 or 109814), CD105 (clone MJ7/18, Cat No:120410), CD115 (clone AFS98, Cat No:135506 or 135513), CD144 (clone BV13, Cat No: 138006), CD150 (clone TC15-12F12.2, Cat No:115904), F4/80 (clone BM8, Cat No:123122), Gr1 (clone RB6-8C5, Cat No: 108406 or 108404), Ly6-G (clone 1A8, Cat No: 127625), Sca-1 (clone D7, Cat No:108106), Secondary antibody (Goat anti-rat IgG, clone Poly4054, Cat No: 405418), and Ter119 (clone TER-119, Cat No:116220), all from Biolegend, CD117 (clone 2B8, Cat No:105828 and 105833 from Biolegend or 562417 from BD Biosciences), Ki67 (clone SolA15, Cat No:50-5698-82 from ThermoFisher Scientific), Ly6G (clone 1A8, or Cat No: BP0075-1 from Bioxcell) or isotype control (clone 2A3, Cat No: BP0089 from Bioxcell), TNFα (clone MP6-XT22. Cat No: 506303). For cell cycle analyses cells were first fixed with 4% paraformaldehyde for 20 minutes at 4°C followed by permeabilization of the plasma membrane using 0.1% Triton X-100 for 20 minutes at 4°C. The cells were then stained for 30 minutes in PEB buffer containing 0.1% Triton X-100 with Ki67 (cat No:50-5698-82). Lastly, the cells were incubated in PEB buffer containing DAPI for one hour at room temperature before being analyzed as described above. Apoptotic cells were detected using the CellEvent™ Caspase-

3/7 Green Flow Cytometry Assay Kit from Life Technologies (Cat No:C10427). Apoptotic cells were analyzed as described above.

Primary and secondary bone marrow transplantation and adoptive transfer experiments

Recipient male mice were conditioned with two doses of 600 rads, 3 hours apart, and immediately transplanted with the indicated amount of donor BMNC (retroorbital injection). For adoptive transfer experiments the indicated doses of FACS-purified hematopoietic cells were resuspended in 200µl of PBS and injected retroorbitally into the recipient mice. Due to the known effect of circadian rhythm effects in granulocytes and HSC (**14,22,88-89**) we performed adoptive transfers at zeitgeber times 10-12 in mice under standard (12h light:12h dark) cycles.

In vivo granulocyte ablation.

For diphtheria toxin-mediated granulocyte ablation we treated mice with daily intraperitoneal injections of diphtheria toxin (D0564, Sigma) (0.25µg/mouse/day) for one week starting one week after transplantation. For αLy6G-mediated depletion experiments we treated mice with 100µg (intraperitoneal) of αLy6G (clone 1A8, BP0075-1, Bioxcell) or isotype control (clone 2A3, BP0089, Bioxcell) at days 1, 3 and 5 after transplantation. Binding of αLy6G prevents staining with αGr1. This prevented us to use Gr1 to detect granulocytes in αLy6G-injected mice. Thus, in these experiments, $Ly6G^+$ granulocytes were detected by staining BM cells with isotype or αLy6G with 1µg/ml of αLy6G followed by staining with a secondary antibody (405418, Biolegend)

5-fluorouracil treatment.

For these experiments we injected mice (retroorbitally) with a single dose of 250mg of 5-fluorouracil (Sigma) per kg of body weight in PBS.

Recombinant TNFα injection.

For these we injected the mice (0.5µg/mouse, intraperitoneally) with recombinant mouse TNFα (718004, Biolegend) daily.

AMD3100 and SBD

AMD3100 (5mg/kg s.c) and SBD (0.3mg/kg, i.p. SB225002, Sigma) were injected intraperitoneally at days 1, 3, and 5 after transplantation and 1 hour before harvest.

Quantification of inflammatory cytokines in plasma and bone marrow extracellular fluid.

Inflammatory cytokines were detected by using the Legendplex Mouse inflammation panel (740446, Biolegend) and following manufacturer's instructions.

RNA isolation and qPCR analyses

RNA isolation was performed using the Dynabeads mRNA direct kit (Life Technologies) following manufacturer's instructions. cDNA synthesis was performed using the RNA to cDNA EcoDry Premix (Clontech) following manufacturer's instructions. qPCR was performed using the SYBR Green Supermix Quanta Biosciences using a ABI PRISM 7900HT Sequence Detection System (Appliedbiosystems). Results were analyzed using SDS 2.4 software (Appliedbiosystems). Oligonucleotides used for amplification are enumerated in **Supplementary Table 2.1**.

Whole-mount immunofluorescence analyses

Imaging of the mouse BM sternal vasculature has been described previously (**8**). Briefly, mice were injected (retroorbitally) with 5µg of Alexa Fluor 647 anti-mouse CD31 (110724, Biolegend) and 5µg of Alexa Fluor 647 anti-mouse CD144 (138006, Biolegend). Twenty minutes later mice were euthanized by isoflurane overdose and the sterna retrieved. For each sternum we removed muscle and connective tissue using a scalpel. The sternum was then

divided into segments and each segment cut sagitally to expose the BM cavity. Segments were fixed in 4% paraformaldehyde (Sigma) in PBS for 20 minutes at room temperature, washed thrice in PBS and imaged immediately or incubated in blocking solution (20% Goat Serum (Sigma) in PBS) for two hours prior staining with antibodies. Granulocytes or B cells were detected by staining in a solution containing 2.5µg/ml Alexa Fluor 488 anti-mouse Ly6-G (Clone 1A8, Biolegend) or Phycoerythrin conjugated anti-mouse CD19 (Clone 6F5, Biolegend), 5% Goat Serum (Sigma) in PBS for 3 days. Prior imaging each segment was glued to 35mm dishes and imaged in a Leica SP5 upright confocal microscope using a 20X, long-distance, water immersion objective, Hybrid detectors, and Leica Application Suite Advanced Fluorescence software. We acquired z-stacks (2.98µm between slices) 20-200µm depending on the position of the bone. Each slice measured 434.17 in the x axis and 434.17µm in the y axis and was 1024x1024 pixels. All images were acquired at room temperature. For Alexa Fluor 647 the wavelength of the excitation laser was 647 nm and emitted light detected between 660 to 720nm. For Alexa Fluor 488 the wavelength of the excitation laser was 488nm and emitted light detected between 500 to 540nm. For Phycoerythrin the wavelength of the excitation laser was 560nm and detection from 570 to 600nm. We used Fiji (**91**) software to generate 3D reconstructions and maximum projections from each image. Blood vessels numbers and length were counted manually in 3D reconstructions in order to be able to distinguish true vessels (with lumen) from vascular sheets (lacking lumen). Composite images of each sternum were assembled by stitching together the maximum projection images in Power Point (Microsoft).

Vascular permeability

Mice received 200 µl of 0.5% Evans Blue Dye (Sigma Aldrich, E2129) in PBS via retro-orbital injection. Thirty minutes later mice were euthanized and perfused with 5 ml of PBS to remove excess Evans Blue from the vessels. To harvest the bone marrow, one femur was flushed with 1 ml of ice-cold PEB. The cells were centrifuged and the supernatant containing the extravasated Evans Blue was removed and placed in a clean 1.5 ml tube. To analyze the amount of Evans Blue in the supernatant, samples were placed in a 96-well plate and read using a Spectramax 340PC from Molecular Devices with the absorbance measured set to 610 nm.

Pathology analyses

Mice were euthanized by isoflurane overdose. Liver, lung, and intestine were removed, processed, embedded in paraffin, sectioned, and stained with hematoxylin/eosin by a necropsy technician in the In-vivo Animal Core (IVAC). We received the sections and did imaging analysis using an Olympus BX51 with a 20X dry objective lens. Images were captured using a DP-70 digital camera and the associated software. In-depth pathological analysis was performed by the veterinary pathologist of the IVAC.

Statistics

In most graphs of data, the actual values for each mouse are plotted and the means indicated. In others the means and standard errors are plotted. Sample size was not predetermined and all mice were included in the analyses. Mice were randomly allocated to the different groups based on cage and litter size. For all experiments we aimed to have the same number of mice in the control and experimental groups. For all experiments, at the time of analyses, the investigator was blinded to the group allocation. The only exception was the blood vessel

quantification in 3D reconstructions of sternal segments. Statistical differences were calculated using two-sample T-tests (for experiments with two groups), ANOVA (3 or more groups) on log transformed data, or Log-Rank tests for survival analysis.

Data availability

The primary data that support the results described here are available upon reasonable request

References

Can be found at the end of dissertation.

Acknowledgments

We thank Margot May for excellent technical support. This work was supported by the Pardee Foundation (D.L.). E.B. was funded through a T32 training grant from the Center of Organogenesis at the University of Michigan. We thank Dr. Mark Hoenerhoff and the rest of the UM in vivo core for performing pathology analyses. We thank the mouse imaging laboratory and the flow cytometry core at the University of Michigan for their help with imaging and FACS experiments. R.K., flow cytometry and whole-mount immunofluorescence were partially supported by a core grant from the NIH to the University of Michigan Cancer Center (P30-CA46592).

Author information

Affiliations

Department of Cell and Developmental Biology. University of Michigan School. Ann Arbor. Michigan, USA.

Emily Bowers, Anastasiya Slaughter, Daniel Lucas

Center for Organogenesis, University of Michigan School of Medicine, Ann Arbor, Michigan, USA.

Emily Bowers, Daniel Lucas

Ruth L. and David S. Gottesman Institute for Stem Cell and Regenerative Medicine Research, Albert Einstein College of Medicine, Bronx, New York, USA.

Paul Frenette

Department of Cell Biology, Albert Einstein College of Medicine, Bronx, New York, USA

Paul Frenette

Department of Biostatistics, University of Michigan School of Medicine, Ann Arbor, Michigan, USA.

Rork Kuick

The John Goldman Center for Cellular Therapy, Hammersmith Hospital, Imperial College Healthcare NHS Trust, London, UK

Oscar Pello

The University of Michigan Comprehensive Cancer Center, University of Michigan, Ann Arbor, USA.

Daniel Lucas

Contributions

E.B. and D.L designed the study; E.B., A.S. and D.L. performed and analyzed experiments. O.P, suggested and designed experiments. R.K. performed statistical analyses. P.F. provided *Nestin-gfp*, *Tnfa*$^{-/-}$, *Tnfr1*$^{-/-}$ and *Tnfr2*$^{-/-}$ mice and designed experiments, E.B and D.L wrote the manuscript with help from all coauthors. D.L. supervised the manuscript.

Competing financial interests

None.

Corresponding author

Correspondence to Daniel Lucas (dlucasal@umich.edu)[Field]

Publication

This manuscript was published in Nature Medicine.

Bowers E, Slaughter A, Frenette PS, Kuick R, Pello OM, Lucas D. Granulocyte-derived TNFα promotes vascular and hematopoietic regeneration in the bone marrow. Nat Med. 24;95-102 (2017).

FIGURES

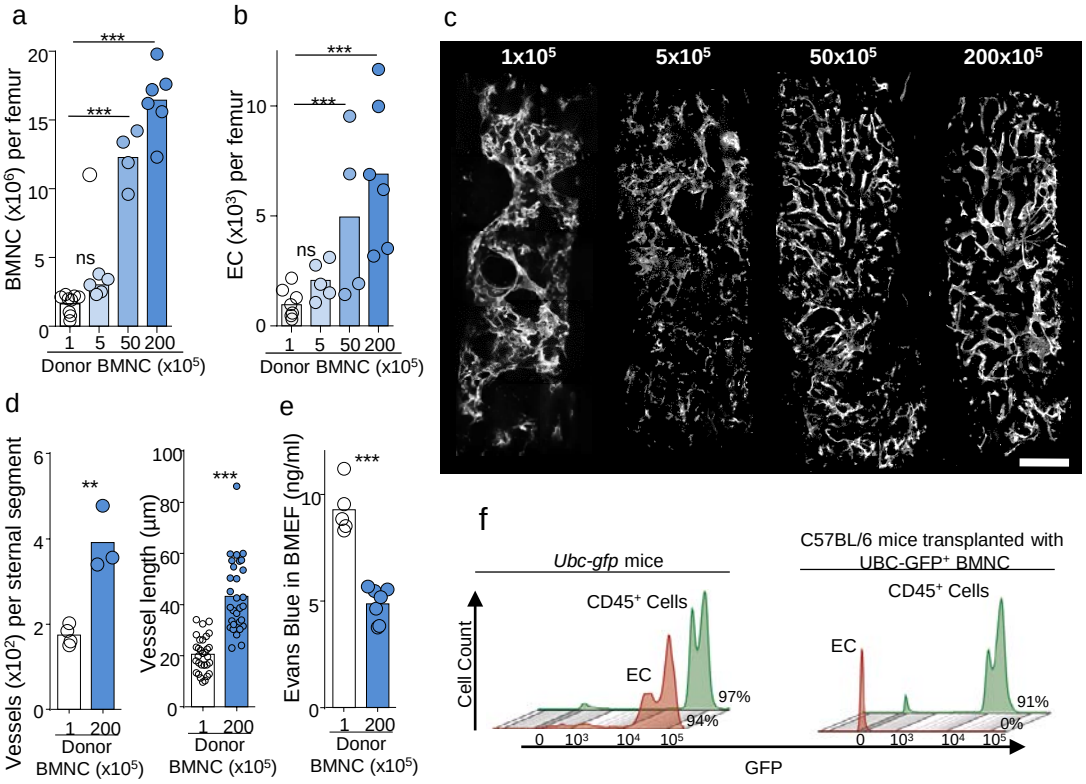

Figure 2.1. Donor hematopoietic cells drive endogenous vascular regeneration after transplantation. (**a,b**) Number of bone marrow nucleated cells (BMNC, a) and endothelial cells (EC, $CD45^-Ter119^-CD31^+CD105^+$, b) in the femur of B6-SJL mice 14 days after lethal irradiation and transplant with the indicated amount of $CD45.2^+$ BMNC. p-values were calculated using 1-way ANOVA model comparing the 3 higher doses to the lowest dose. (**c**) Representative composite image showing blood vessels (white, CD31/CD144) in the sternum of mice treated as in a. Scale bar 200mm. (**d**) Quantification of intact blood vessel segments (left, one dot=one mouse) or average vessel length (right, one dot=one vessel) in the sternum of mice treated as in a. p-values were calculated using Two-sample T-test. (**e**) Quantification of extravasation of the dye Evans Blue in the bone marrow extracellular fluid of mice treated as in a. p-values were calculated using Two-sample T-test. (**f**) Percentage of GFP^+ endothelial cells in B6-SJL $CD45.1^+$ recipients transplanted with $20x10^6$ BMNC purified from *Ubc-gfp* mice. Unless otherwise indicated each dot corresponds to one mouse. For all panels the graphs show the pooled data of at least two independent experiments.

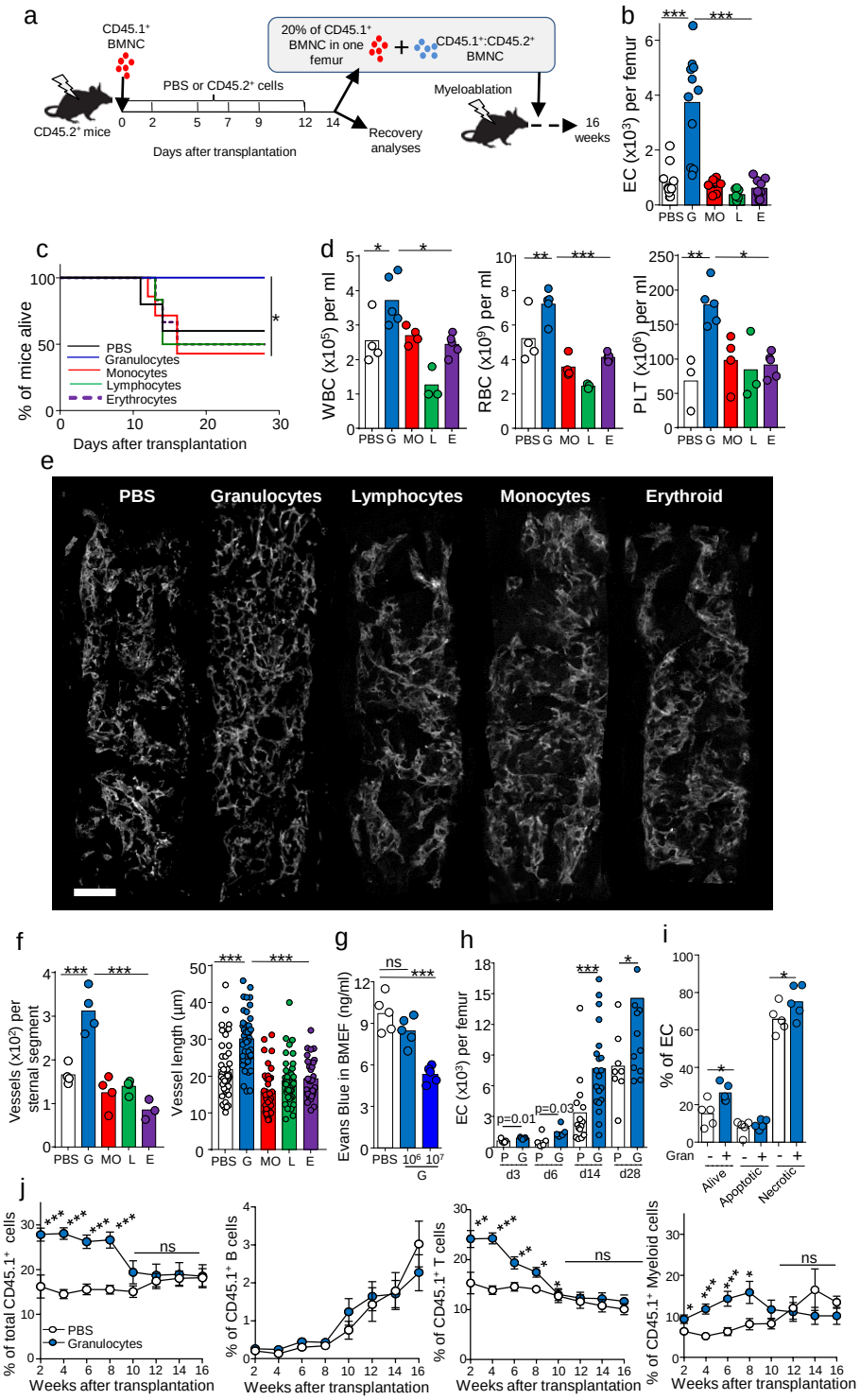
a
CD45.1+ BMNC
CD45.2+ mice
PBS or CD45.2+ cells
0 2 5 7 9 12 14
Days after transplantation
20% of CD45.1+ BMNC in one femur
CD45.1+:CD45.2+ BMNC
Recovery analyses
Myeloablation
16 weeks
b
EC (x10³) per femur
PBS G MO L E
c
% of mice alive
PBS
Granulocytes
Monocytes
Lymphocytes
Erythrocytes
Days after transplantation
d
WBC (x10⁵) per ml
RBC (x10⁹) per ml
PLT (x10⁶) per ml
e
PBS
Granulocytes
Lymphocytes
Monocytes
Erythroid
f
Vessels (x10²) per sternal segment
Vessel length (µm)
g
Evans Blue in BMEF (ng/ml)
h
EC (x10³) per femur
p=0.01
p=0.03
d3 d6 d14 d28
i
% of EC
Gran
Alive
Apoptotic
Necrotic
j
% of total CD45.1+ cells
% of CD45.1+ B cells
% of CD45.1+ T cells
% of CD45.1+ Myeloid cells
Weeks after transplantation
ns

Figure 2.2. Granulocytes promote vascular regeneration. (**a**) Experiment design, (**b**) Number of endothelial cells (EC, $CD45^-Ter119^-CD31^+CD105^+$) in the femur of C57BL/6 mice 14 days after lethal irradiation and transplant of 10^5 $CD45.1^+$ BMNC followed by adoptive transfer of all the granulocytes (G: $Gr1^+CD115^-$, $1x10^6$), monocytes and macrophages (MO: $CD115^+$ or $F4/80^+$ cells within the $Gr1^-CD4^-CD8^-B220^-$ gate, $1x10^5$), lymphocytes (L: $CD4^+$, $CD8^+$ and $B220^+$ cells, $7.5x10^5$) and erythroid (E: $Ter119^+$, $1x10^5$) cells found in $2x10^6$ $CD45.2^+$ BMNC. p-values were calculated using 1-way ANOVA model. (**c,d**) Survival curves (c, PBS n=5, G n=6, MO n=7, L n=6, and E n=6) and peripheral blood recovery for mice treated as in b; each dot represents one mouse. p-values were calculated using Log Rank analyses or one-way ANOVA. (**e**) Representative composite image showing blood vessels (white, CD31/CD144) in sternal segments purified from PBS, granulocyte, monocytes and macrophages, lymphocytes or erythroid cells-treated mice fourteen days after lethal irradiation and transplantation. Scale bar 200µm. (**f**) Quantification of intact blood vessel segments (left, one dot=one mouse) or average vessel length (right, one dot=one vessel) in the sternum of the mice shown in e. p-values were calculated using one-way ANOVA. (**g**) Quantification of extravasation of the dye Evans Blue in the bone marrow extracellular fluid of transplanted mice treated with PBS or serial adoptive transfer of 10^6 or 10^7 granulocytes fourteen days after the initial transplant. p-values were calculated using one-way ANOVA. (**h**) Kinetics of endothelial cell recovery in PBS or granulocyte (G) treated mice at the indicated time points. Each dot represents one mouse. p-values were calculated using Two-sample T-test. (**i**) Frequency of live, apoptotic or necrotic endothelial cells, determined by caspase 3 staining, in the BM of mice treated with PBS or granulocytes 6 days after transplantation. Each dot represents one mouse. p-values were calculated using Two-sample T-test. (**j**) $CD45.1^+$ cell engraftment in total, B, T or myeloid cells in secondary recipients after transplantation of $2.5x10^5$ $CD45.1^+$:$CD45.2^+$ competitor BMNC and 20% of the $CD45.1^+$ cells in one femur of granulocyte- or PBS-treated mice 14 days after initial transplant. PBS, n=18 for weeks 2-8, n=13 for weeks 10-16; Granulocytes n=17 for weeks 2-8, n=12 for weeks 10-16. p-values were calculated using Two-sample T-test. For all panels the graphs show the pooled data of at least two independent experiments.

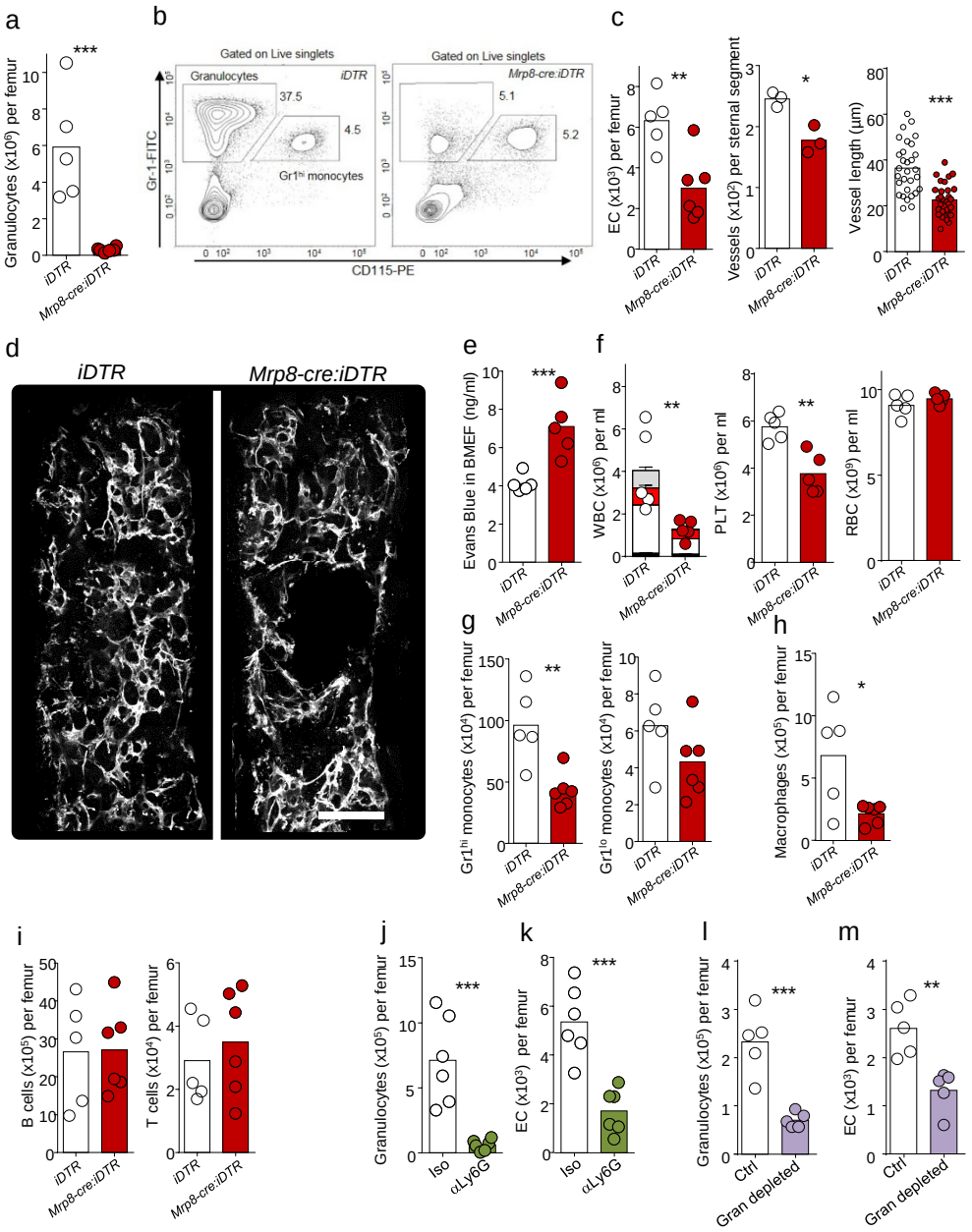
a
b
c
d
e
f
g
h
i
j
k
l
m
Granulocytes (x10⁶) per femur
iDTR
Mrp8-cre:iDTR
Gated on Live singlets
Granulocytes
37.5
4.5
Gr1ʰⁱ monocytes
5.1
5.2
Gr-1-FITC
CD115-PE
EC (x10³) per femur
Vessels (x10²) per sternal segment
Vessel length (µm)
Evans Blue in BMEF (ng/ml)
WBC (x10⁶) per ml
PLT (x10⁶) per ml
RBC (x10⁹) per ml
Gr1ʰⁱ monocytes (x10⁴) per femur
Gr1ˡᵒ monocytes (x10⁴) per femur
Macrophages (x10⁵) per femur
B cells (x10⁵) per femur
T cells (x10⁴) per femur
Granulocytes (x10⁵) per femur
Iso
αLy6G
Ctrl
Gran depleted

Figure 2.3. Granulocytes are necessary for vascular regeneration. (**a, b**) $Gr1^{+}CD115^{-}$ granulocyte quantification (a) and representative FACS plots (b) showing granulocyte depletion in lethally irradiated C57BL6/J mice fourteen days after transplant of $5x10^{6}$ *iDTR* or *Mrp8-cre:iDTR* BMNC followed by diphtheria toxin treatment. (**c**) Number of endothelial cells (EC, $CD45^{-}Ter119^{-}CD31^{+}CD105^{+}$) in the femur (left panel) and number and length of vessels in the sternum (right panel) of the mice analyzed in a. (**d**) Representative composite image showing blood vessels (white, CD31/CD144) in sternal segments of C57BL/6J mice treated as in a. Scale bar 200µm. (**e**) Evans Blue in the bone marrow extracellular fluid of the mice shown in a. (**f**) Number of white blood cells (one dot = one mouse) and frequency of T cells (black bar), B cells (white bar), monocytes (red bar) and neutrophils (grey bar), platelets and red blood cells in the peripheral blood of mice treated as in a. (**g-i**) Monocyte (g), macrophage (h), and lymphocyte (i) numbers in the bone marrow of the mice shown in a. (**j,k**) $Ly6G^{+}$ granulocytes (j) and endothelial cells (k) in the BM of lethally irradiated C57BL6/J mice 6 days after transplantation of 10^{6} BMNC and treatment with isotype control (Iso) or αLy6G antibodies. (**l,m**) Granulocytes (l) and endothelial cells (m) in the BM of lethally irradiated C57BL6/J mice 6 days after transplantation of 10^{6} BMNC (Ctrl) or a graft containing all other hematopoietic cells but in which granulocytes have been removed via FACS. For all panels p-values were calculated using Two-sample T-test and the graphs show the pooled data of at least two independent experiments.

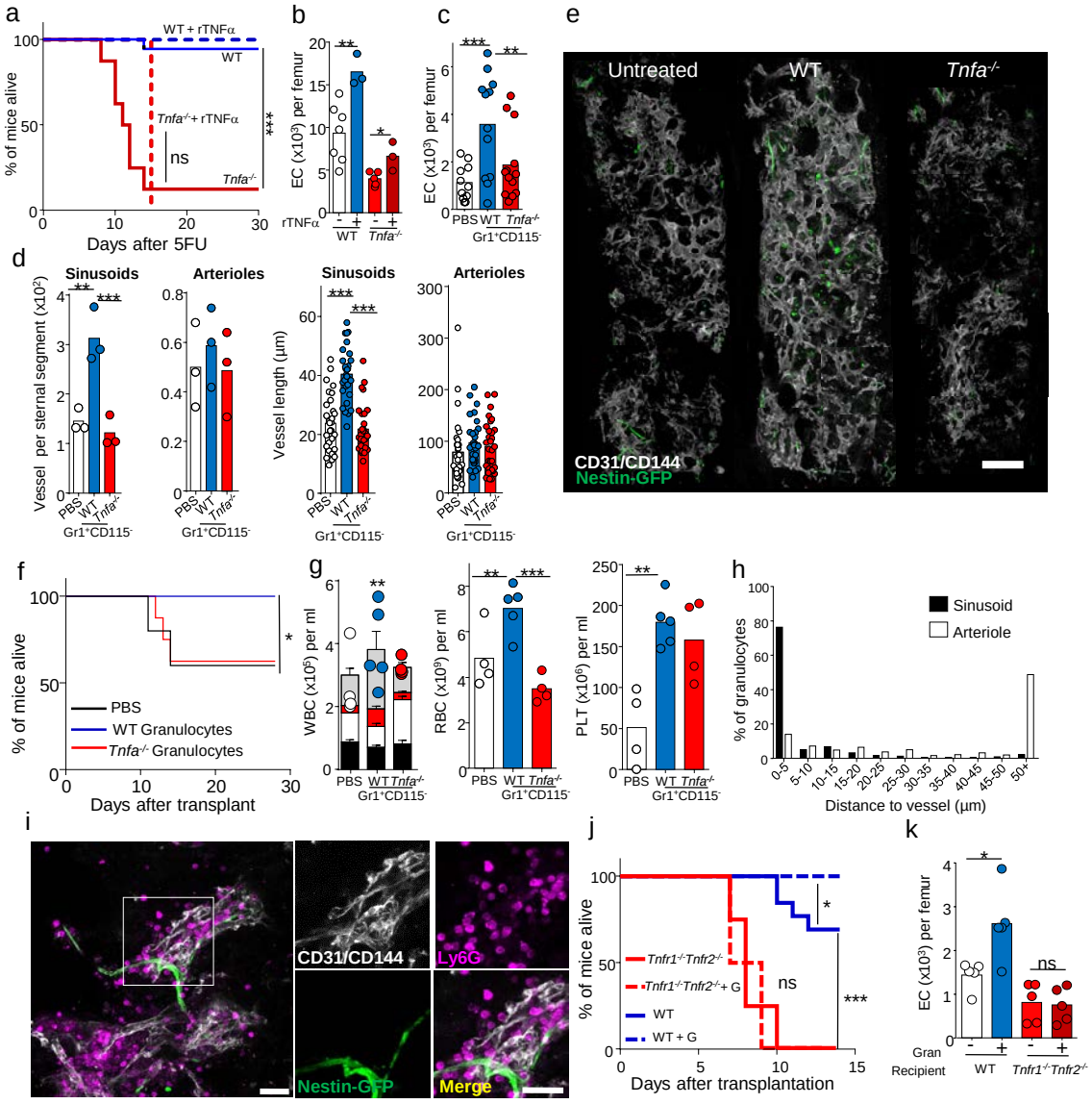
a
WT + rTNFα
WT
Tnfa-/- + rTNFα
ns
Tnfa-/-
% of mice alive
Days after 5FU
***
b
EC (x10³) per femur
rTNFα
WT
Tnfa-/-
c
EC (x10³) per femur
PBS WT Tnfa-/-
Gr1+CD115-
e
Untreated
WT
Tnfa-/-
CD31/CD144
Nestin-GFP
d
Sinusoids
Arterioles
Sinusoids
Arterioles
Vessel per sternal segment (x10²)
Vessel length (μm)
PBS WT Tnfa-/-
Gr1+CD115-
f
% of mice alive
PBS
WT Granulocytes
Tnfa-/- Granulocytes
Days after transplant
g
WBC (x10⁶) per ml
RBC (x10⁹) per ml
PLT (x10⁶) per ml
PBS WT Tnfa-/-
Gr1+CD115-
h
Sinusoid
Arteriole
% of granulocytes
Distance to vessel (μm)
0-5
5-10
10-15
15-20
20-25
25-30
30-35
35-40
40-45
45-50
50+
i
CD31/CD144
Ly6G
Nestin-GFP
Merge
j
% of mice alive
Tnfr1-/-Tnfr2-/-
Tnfr1-/-Tnfr2-/- + G
WT
WT + G
ns
Days after transplantation
k
EC (x10³) per femur
Gran
Recipient
WT
Tnfr1-/-Tnfr2-/-
ns

Figure 2.4. Granulocytes promote vascular regeneration via TNFα. (**a**) Survival curves for WT or *Tnfa*$^{-/-}$ mice after injection of 250mg/kg body weight of 5-fluorouracil (5FU) and treatment with either PBS (WT n=18, *Tnfa*$^{-/-}$ n=16) or recombinant TNFα (WT n=7, *Tnfa*$^{-/-}$ n=4). p-values were calculated using Log Rank analyses. (**b**) Number of endothelial cells in the femur of C57BL/6 mice treated as in a, 8 days after 5FU injection. p-values were calculated using Two-sample T-test. (**c**) Number of endothelial cells in the femur of C57BL/6 mice 14 days after lethal irradiation and transplant of 10^5 CD45.1$^+$ BMNC followed by treatment with PBS or adoptive transfer of WT or *Tnfa*$^{-/-}$ mice granulocytes. p-values were calculated using 1-way ANOVA model. (**d**) Quantification of the number (one dot=one mouse) and length (one dot= one vessel) of intact sinusoidal and arterial segments in the sternum of the mice shown in c. p-values were calculated using 1-way ANOVA model. (**e**) Representative composite image showing blood vessels (white, CD31/CD144) in sternal segments of mice treated with PBS, WT or *Tnfa*$^{-/-}$ granulocytes. Scale bar=200µm (**f**) Survival curves for the mice treated as in c (PBS n=5, WT n=6, *Tnfa*$^{-/-}$ n=8). (**g**) Number of white blood cells (one dot = one mouse) and frequency of T cells (black bar), B cells (white bar), monocytes (red bar) and neutrophils (grey bar), platelets and red blood cells in the peripheral blood of mice treated as in c. p-values were calculated using 1-way ANOVA model. (**h**) Percentage of granulocytes (n=305 granulocytes from two mice) found at the indicated distances from sinusoids (black) or arterioles (white) in *Nestin-gfp* mice 6 days after lethal irradiation and transplant of 10^6 BMNC. (**i**) Immunofluorescence analyses showing the association between transferred granulocytes (magenta, Ly6G) and regenerating sinusoids (white, CD31/CD144) and arterioles (white and green, CD31/CD144$^+$Nestin-GFP^{bright}) in the mice shown in h. Scale bar=25µm. (**j**) Survival curves for WT or *Tnfr1*$^{-/-}$*:Tnfr2*$^{-/-}$ mice after lethal irradiation and transplantation of 10^5 CD45.1$^+$ BMNC followed by treatment with PBS (WT n=13, *Tnfr1*$^{-/-}$*:Tnfr2*$^{-/-}$ n=4) or adoptive transfer of WT granulocytes (WT n=12, *Tnfr1*$^{-/-}$*:Tnfr2*$^{-/-}$ n=6). p-values were calculated using Log Rank analyses. (**k**) Endothelial cells per femur in mice treated as in j but 6 days after the initial transplant. p-values were calculated using 1-way ANOVA model. In panels a-k the graphs show the pooled data of at least two independent experiments.

SUPPLEMENTAL FIGURES

a

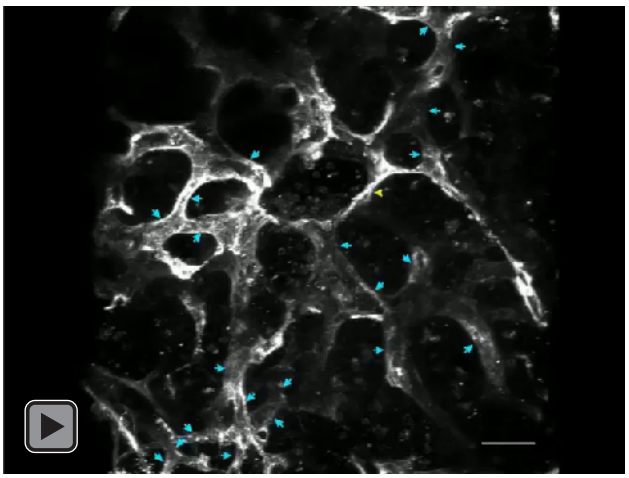

b

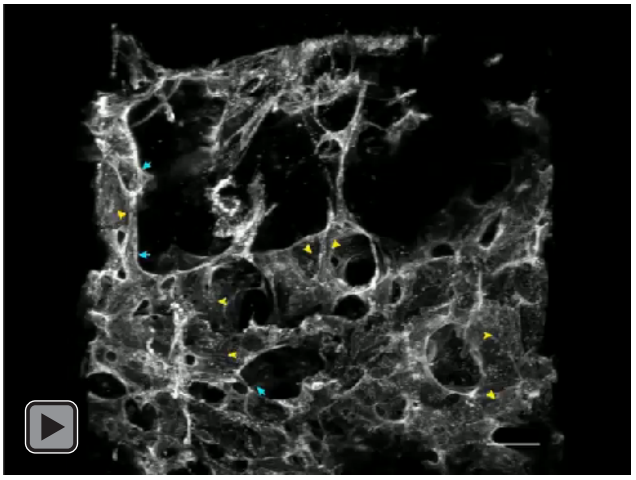

Legend for Supplementary Movies 2. (**a,b**) 3D reconstruction of endothelial cells (CD31/CD144^{+}, white) in the sternum of a lethally irradiated mouse fourteen days after transplantation of 20x10^{6} (a) or 0.1 x10^{6} BMNC (b). True vessels (with lumen) are indicated by blue arrows and can be easily distinguished from vascular sheets that appear after irradiation (yellow arrows).

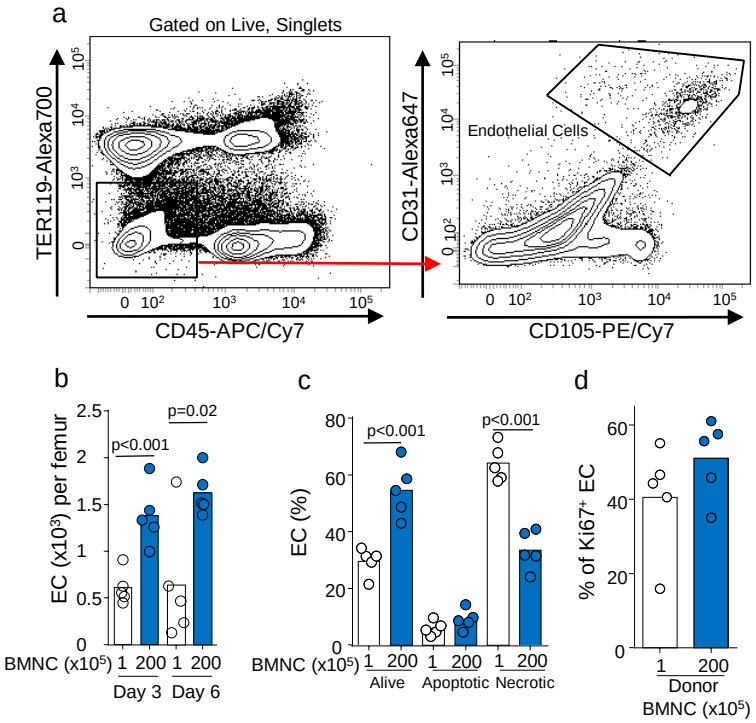

Supplementary Figure 2.2. Kinetics of endothelial cell recovery. (**a**) Gating strategy for the quantification of $CD45^{-}Ter119^{-}CD31^{+}CD105^{+}$ endothelial cells. (**b**) Number of live endothelial cells per femur in C57BL/6 mice 3 and 6 days after lethal irradiation and transplant of the indicated amounts of BMNC (1: n=5 for day 3 and day 6; 200: n=5 for day 3 and day 6). (**c**) Frequency of live, apoptotic, or necrotic endothelial cells, determined by caspase 3 staining, in the BM of mice treated as in panel b, 6 days after transplantation (1: n=5; 200 n=5). (**d**) Frequency of proliferating ($Ki67^{+}$) endothelial cells in the BM of mice analyzed in panel c, 6 days after transplantation (1: n=5, 200: n=5). p values were calculated using a two-tailed Two-sample T-Test. Each dot represents one mouse. Graphs show the pooled data of at least two independent experiments. Bar graphs represent the mean.

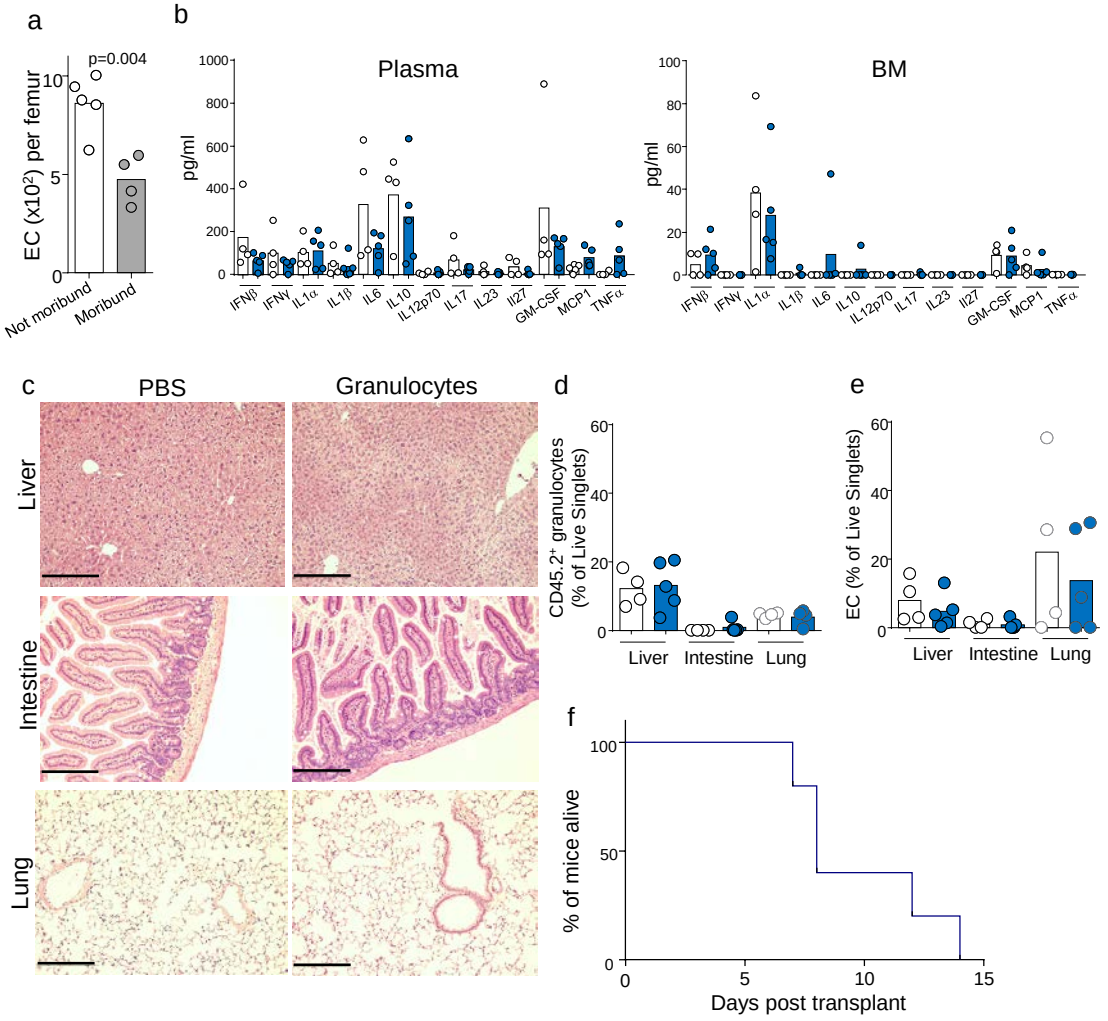

Supplementary Figure 2.3. Donor granulocytes do not induce inflammation. (**a**) Endothelial cells per femur in moribund (n=4) or non-moribund (n=5) C57BL/6 mice 14 days after lethal irradiation and transplant of 10^5 BMNC. (**b**) Levels of the indicated inflammatory cytokines in plasma or bone marrow extracellular fluid in C57BL/6 mice 14 days after lethal irradiation and transplant of 10^5 BMNC followed by treatment with PBS (white, n=4) or adoptive granulocyte transfer (blue, n=5, as in Fig. 2a). (**c**) Representative histology microphotographs of hematoxylin/eosin stained sections of the indicated organs in the mice analyzed in panel b (PBS: n=4, Granulocytes: n=5). Scale bar 200µm. (**d-e**) Percentage of granulocytes (d) or endothelial cells (e) in the indicated organs of the mice analyzed in panel b (white: n=4, blue: n=5). (**f**) Survival curves of C57BL/6 mice after lethal irradiation and treated with adoptive transfer of granulocytes. n = 5. p values were calculated using two-tailed Two-sample T-Test. Graphs show the pooled data of at least two independent experiments. Bar graphs represent the mean.

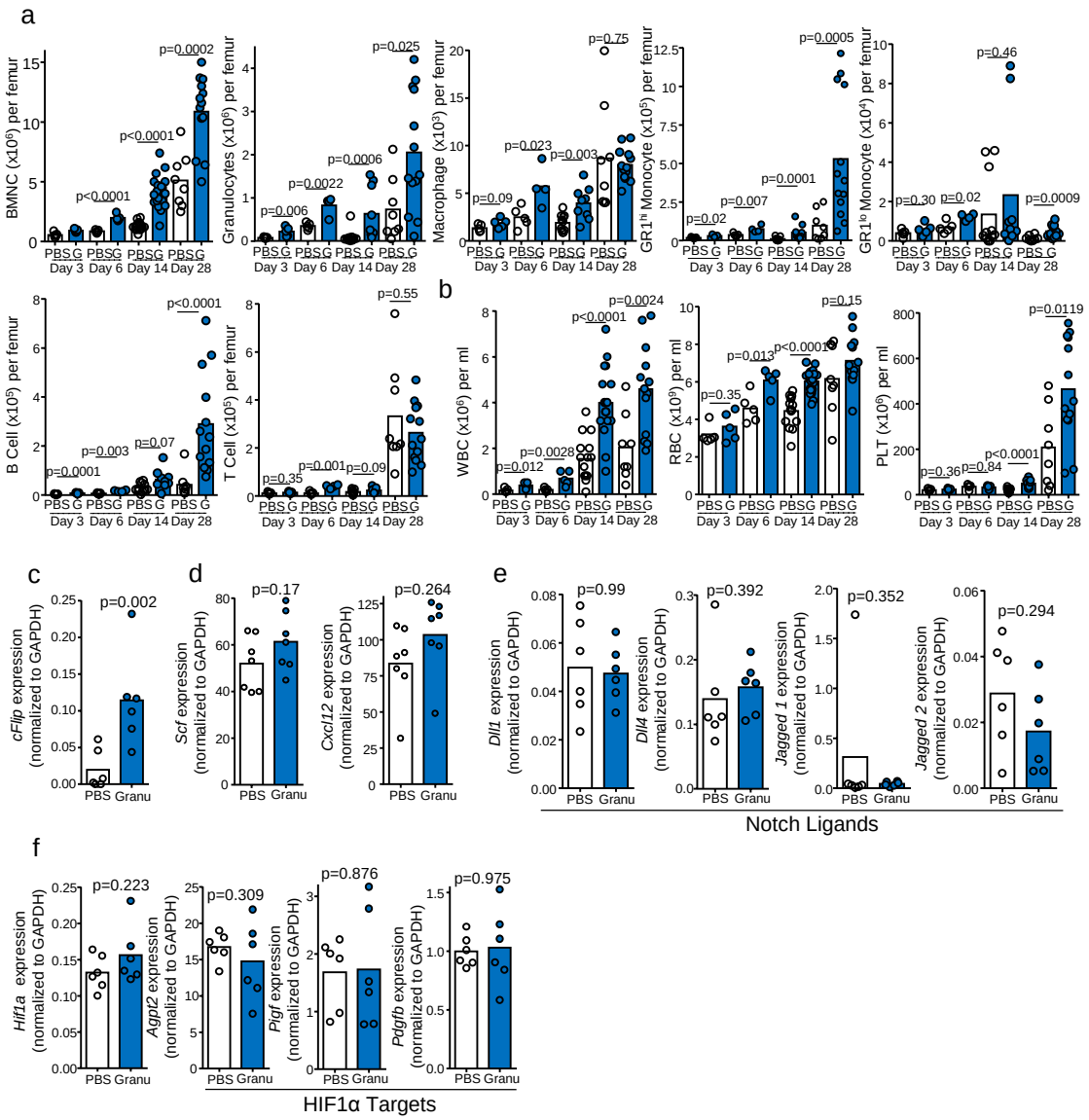

Supplementary Figure 2.4. Kinetics of bone marrow regeneration. (**a**) Number of total BMNC, Gr1+CD115- granulocytes, Gr1-CD115-F4/80+ macrophages, Gr1hiCD115+ monocytes, Gr1loCD115+ monocytes, Gr1-F4/80-B220+ B cells, Gr1-CD4+ and CD8+ T cells per femur in C57BL/6 mice at the indicated time points after lethal irradiation and transplant of 105 BMNC followed by treatment with PBS (D3: n=5, D6: n=5, D14: n=15, D28: n=8) or adoptive granulocyte transfer (D3: n=5, D6: n=5, D14: n=19, D28: n=13). ( ) WBC, RBC and PLT in the peripheral blood of mice treated as in panel a. (**c f**) PCR` analyses for cFlip (**c**), Scf and Ccl12` (**d**) , Dll1, Dll4, agged1,` and agged2` (**e**), and if1a,` Agpt2, Pigf, and Pdgfb (**f**) epression` in endothelial cells sorted from C57BL/6 mice 14 days after lethal irradiation and transplant of 105 BMNC followed by treatment with PBS (n=6) or adoptive granulocyte transfer (n=6). For all eperiments` each dot represents one mouse. p values were calculated using two-tailed Two-sample T-Test. Graphs show the pooled data of at least two independent eperiments.` Bar graphs represent the mean.

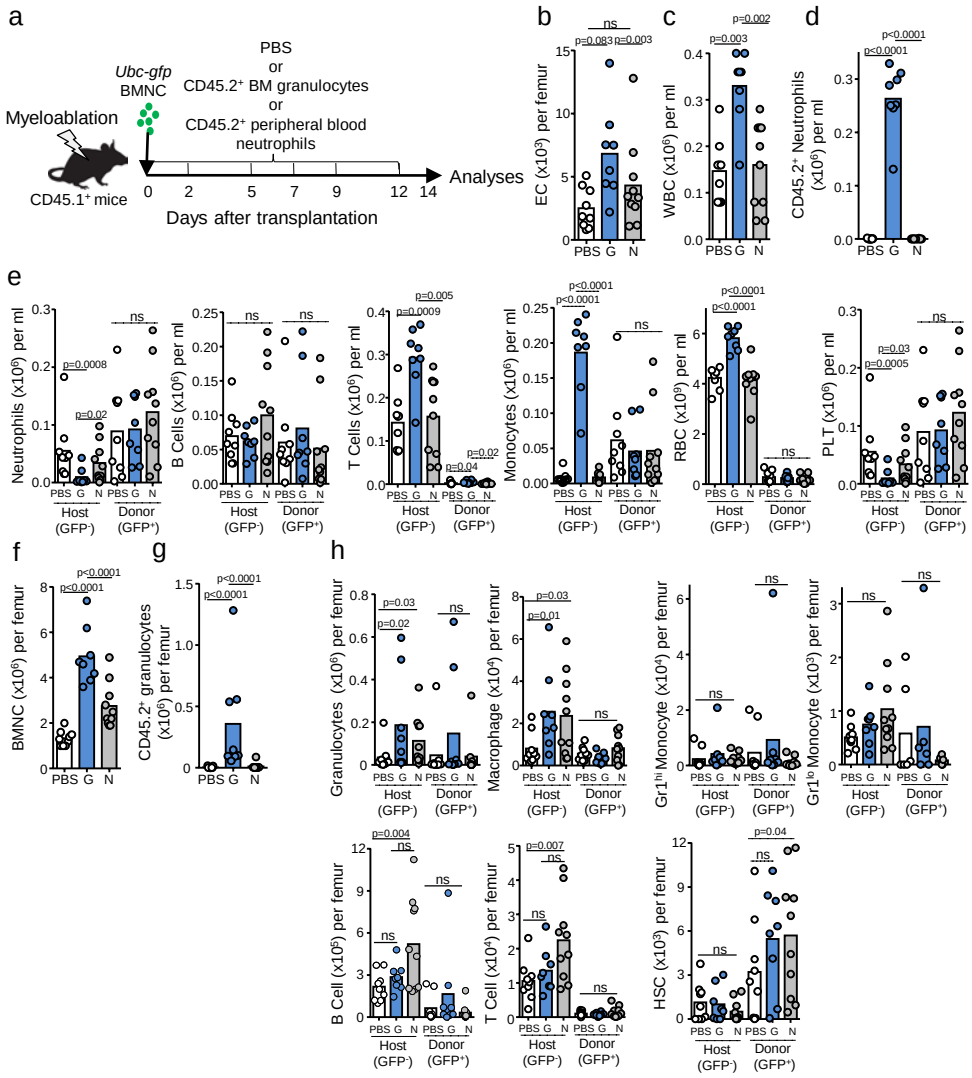

Supplementary Figure 2.5. Lineage trace of hematopoeitic reconstitution. (**a**) Experimental design for lineage tracing donor derived hematopoietic cells. (**b**) Total CD45$^-$Ter119$^-$CD31$^+$CD105$^+$ endothelial cells from C57BL/6 mice 2 weeks after lethal irradiation and transplant of 10^5 CD45.1$^+$ BMNC followed by treatment with PBS or adoptive transfer of BM granulocytes (G) or peripheral blood neutrophils (N). (**c**) WBC in the peripheral blood of mice treated as in panel a. (**d**) CD45.2$^+$ *Ubc-gfp*$^-$ Gr1$^+$CD11b$^+$ neutrophils in the peripheral blood of mice treated as in a. (**e**) Host versus donor-derived Gr1$^+$CD11b$^+$ neutrophils, B220$^+$ B cells, CD4$^+$ or CD8$^+$ T cells, Gr1$^-$CD11b$^+$ monocytes, RBC, and PLT in the peripheral blood of mice treated as in panel a. (**f**) Total BMNC per femur in mice treated as in panel a. (**g**) Total CD45.2$^+$ *Ubc-gfp*$^-$ Gr1$^+$CD115$^-$granulocytes per femur in mice treated as in panel a. (**h**) Host versus donor-derived Gr1$^+$CD115$^-$ granulocytes, Gr1$^-$CD115$^-$F4/80$^+$ macrophages, Gr1^{hi}CD115$^+$ monocytes, Gr1^{lo}CD115$^+$ monocytes, Gr1$^-$F4/80$^-$B220$^+$ B cells, Gr1$^-$CD4$^+$ or CD8$^+$ T cells, and Lin$^-$CD48$^-$CD150$^+$ HSC per femur in mice treated as in panel a. For all experiments each dot represents one mouse (PBS: n=9, G: n=8, N: n=10). Graphs show the pooled data of at least two independent experiments. p values were calculated using one-way ANOVA model. Bar graphs represent the mean.

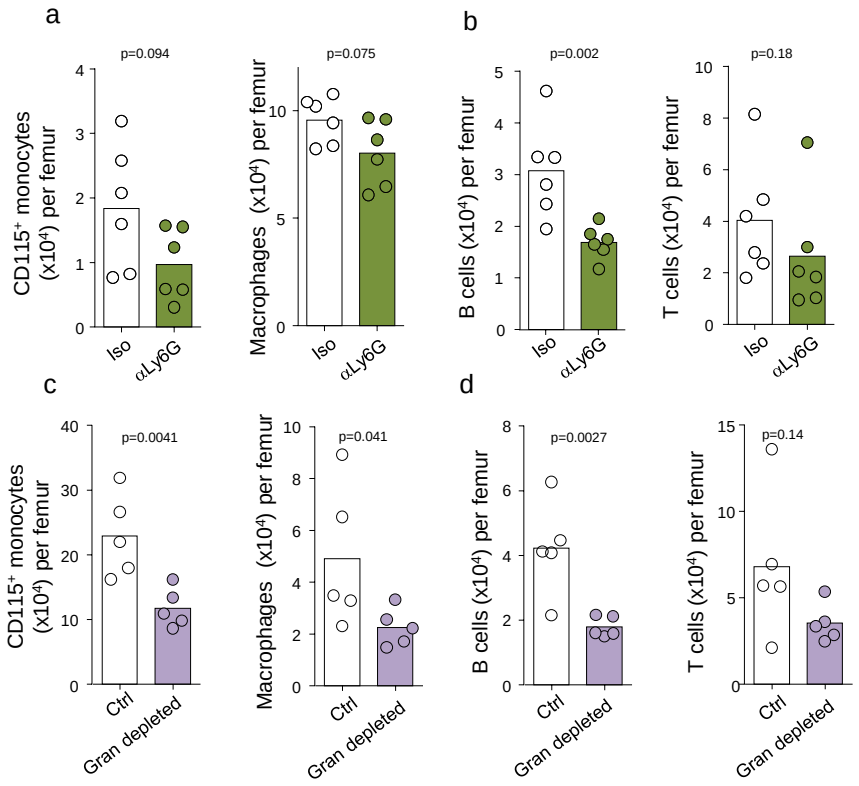

Supplementary Figure 2.6. Alternative methods of granulocyte depletion during regeneration. (**a,b**) Number of monocytes and macrophages (a) or B and T lymphocytes (b) in the bone marrow of lethally irradiated C57BL6/J mice 6 days after transplantation of 10^6 BMNC and treatment with isotype control (Iso: n=6) or αLy6G (n=6) antibodies. (**c,d**) Number of monocytes and macrophages (c) or B and T lymphocytes (d) in the bone marrow of lethally irradiated C57BL6/J mice 6 days after transplantation of 10^6 BMNC (Ctrl: n=5) or a graft containing all other hematopoietic cells but in which granulocytes have been removed via FACS (Gran depleted: n=5). Each dot corresponds to one mouse. p values were calculated using a two-tailed two-sample T-Test. Bar graphs represent the mean.

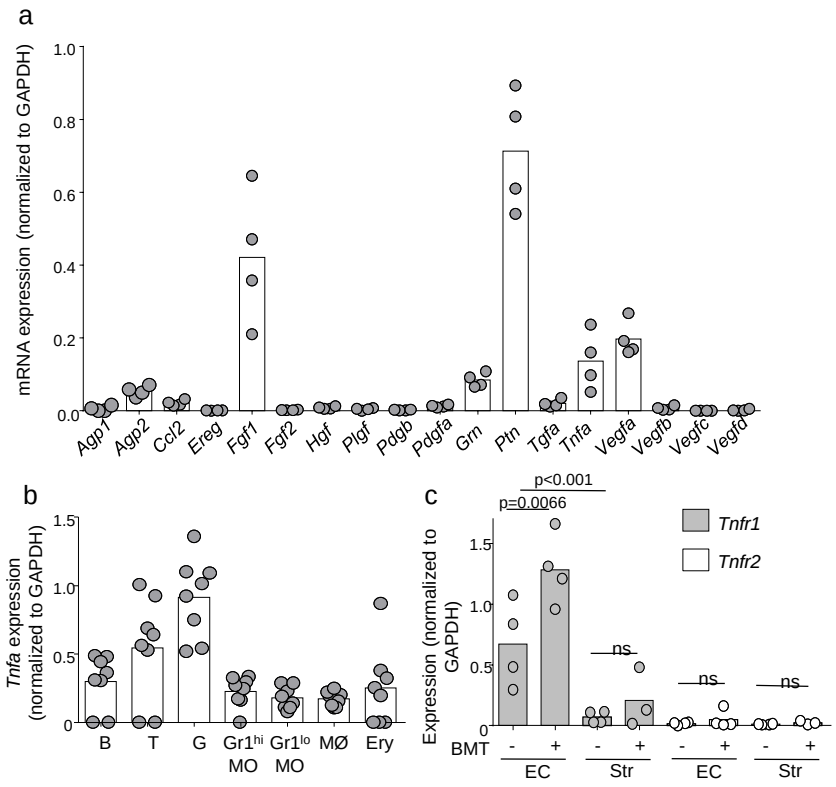

Supplementary Figure 2.7. qPCR analysis for pro-angiogenic factors during regeneration. (**a**) qPCR analyses to detect expression of angiogenic factors in FACS-purified BM granulocytes (n=4). (**b**) *Tnfa* expression in FACS-purified bone marrow cells: B-cells (B, $B220^+$, n=8), T-cells (T, $CD4^+$ or $CD8^+$, n=8), granulocytes (G, $CD115^-Gr1^+$, n=8), $Gr1^{hi}$ monocytes ($Gr1^{hi}$ MO, $Gr\text{-}1^{hi}CD115^+$, n=8), $Gr\text{-}1^{lo}$ monocytes ($Gr1^{lo}$ MO, $Gr1^{lo}$ $B220^-CD4^-CD8^-CD115^+$, n=8), macrophages (MØ, $Gr1^-CD115^-B220^-CD4^-CD8^-F4/80^+$ n=8) or erythroid cells (Ery, $Ter119^+$, n=8). Graphs show the pooled data of at least two independent experiments. (**c**) qPCR analyses for *Tnfr1* and *Tnfr2* expression in BM endothelial cells (EC; steady state: n=4, BMT: n=4) or $CD45^-Ter119^-CD31^-$ stromal cells (Str; steady state: n=4, BMT: n=3) in WT mice in the steady state (-) or 8 days (+) after bone marrow transplantation (BMT) with 10^6 BMNC. For all experiments each dot corresponds to one mouse. p-values were calculated using 1-way ANOVA model. Bar graphs represent the mean.

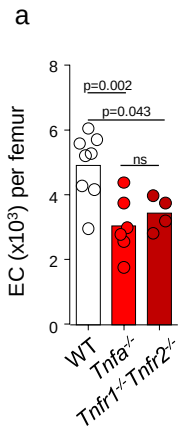

Supplementary Figure 2.8. Endothelial cell numbers in Tnfa and Tnfr1:Tnfr2 null mice. (a) Number of endothelial cells in the bone marrow of wild-type (n=8), Tnfa-/- (n=6), or Tnfr1-/-:Tnfr2-/- (n=4) mice in the steady-state. Each dot corresponds to one mouse. p values were calculated using one way ANOVA. Bar graphs represent the mean.

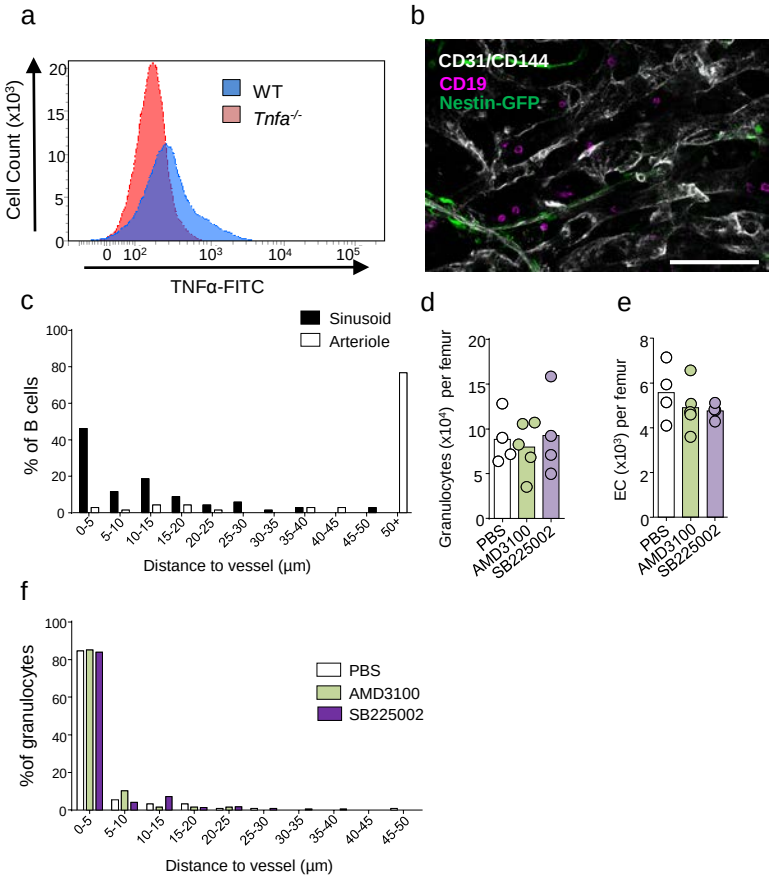

Supplementary Figure 2.9. Donor granulocytes localize to regenerating vasculature. (**a**) Representative flow cytometry FACS plots showing expression of membrane-bound TNFα in $Gr1^{+}CD115^{-}$ BM granulocytes purified from WT or *Tnfa*$^{-/-}$ mice. The experiment was repeated twice with a total of 4 mice per group. (**b**) Immunofluorescence analyses showing the association between transferred B cells (magenta, CD19), regenerating sinusoids (white, CD31/CD144) and arterioles (white and green, $CD31/CD144^{+}$Nestin-GFP^{bright}) in the sternum of *Nestin-gfp* mice 6 days after lethal irradiation and transplant of 10^6 BMNC. Scale bar=100μm. Images are representative of 3 mice in two different experiments. (**c**) Percentage of B cells (n= 69 B cells from three mice) found at the indicated distances from sinusoids (black) or arterioles (white) in *Nestin-gfp* mice 6 days after lethal irradiation and transplant of 10^6 BMNC. Bar graphs represent the pooled data of three mice in two independent experiments. (**d,e**) Number of granulocytes (d) and endothelial cells (e) in the femur of C57BL/6 mice 6 days after transplant of 10^6 BMNC and treatment with PBS (n=4), AMD3100 (CXCR4 antagonist, n=5) or SB225002 (CXCR2 antagonist, n=4). Each dot corresponds to one mouse. Bar graphs represent the mean for each group. (**f**) Percentage of granulocytes found at the indicated distances from $CD31/CD144^{+}$ vessels in the sternum of PBS- (n=91 granulocytes from three mice), AMD3100- (n=67 from three mice) or SB225002–treated (n=222 from three mice) mice. Bar graphs represent the pooled data of three mice in two independent experiments.

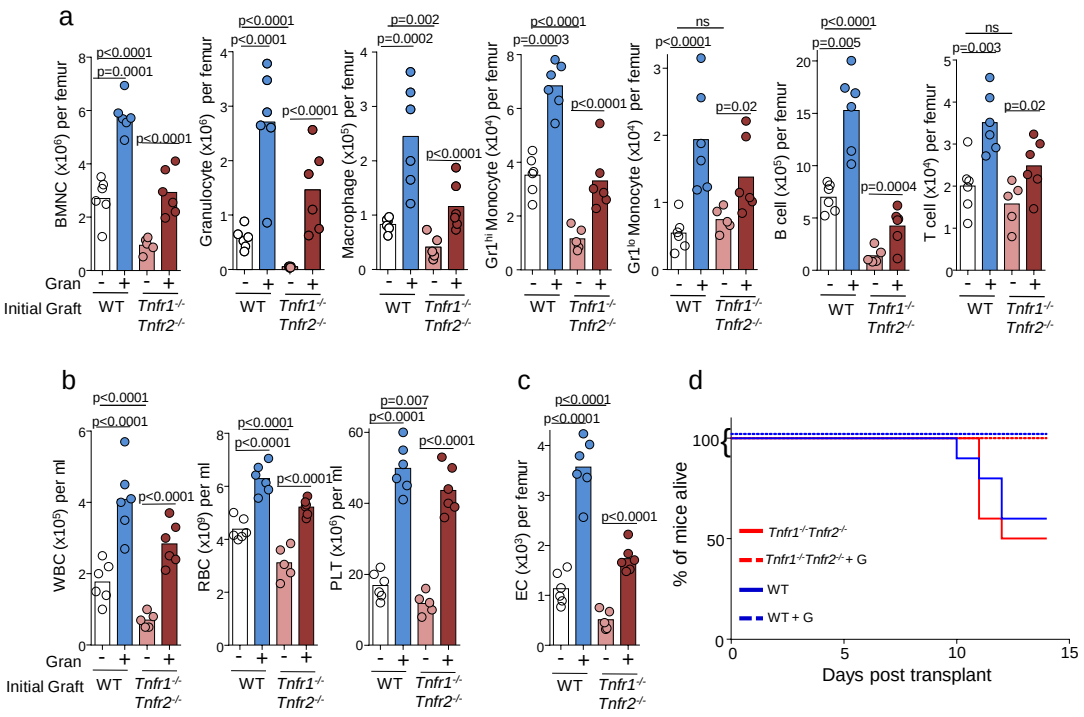

Supplementary Figure 2.10. TNFR1:TNFR2 in hematopoietic cells is dispensible during regeneration. (**a**) Total BMNC, $Gr1^{+}CD115^{-}$ granulocytes, $Gr1^{-}CD115^{-}F4/80^{+}$ macrophages, $Gr1^{hi}CD115^{+}$ monocytes, $Gr1^{lo}CD115^{+}$ monocytes, $Gr1^{-}F4/80^{-}B220^{+}$ B cells, $Gr1^{-}CD4^{+}$ or $CD8^{+}$ T cells per femur in C57BL\6 mice 2 weeks after lethal irradiation and transplant of 10^{5} WT or *Tnfr1*$^{-/-}$*Tnfr2*$^{-/-}$ BMNC followed by adoptive transfer of WT granulocytes. (**b**) WBC, RBC, and PLT in the peripheral blood of mice treated as in panel a.(**c**) Total $CD45^{-}Ter119^{-}CD31^{+}CD105^{+}$ endothelial cells from mice treated as in panel a. WT + PBS n=6, WT + Granulocytes n=6, *Tnfr1*$^{-/-}$*Tnfr2*$^{-/-}$ + PBS n=5, and *Tnfr1*$^{-/-}$*Tnfr2*$^{-/-}$ + Granulocytes n=6. (**d**) Survival curve of mice treated as in panel a. WT + PBS n=10, WT + Granulocytes n=6, *Tnfr1*$^{-/-}$*Tnfr2*$^{-/-}$ + PBS n=10, and *Tnfr1*$^{-/-}$*Tnfr2*$^{-/-}$ + Granulocytes n=6. For all experiments one dot represents one mouse. p values were calculated using one-way ANOVA model. Graphs show the pooled data of at least two independent experiments. Bar graphs represent the mean.

Gene	Forward	Reverse	Reference
Angpt1	CATTCTTCGCTGCCATTCTG	GCACATTGCCCATGTTGAATC	100
Angpt2	TTAGCACAAAGGATTCGGACAAT	TTTTGTGGGTAGTACTGTCCATTCA	100
Ccl2	CCCACTCACCTGCTGCTACTCA	GCTTCTTTGGGACACCTGCTG	101
cFlip	GCTCCAGAATGGGCGAAGTAA	ACGGATGTGCGGAGGTAAAAA	98
Cxcl12	CGCCAAGGTCGTCGCCG	TTGGCTCTGGCGATGTGGC	14
Dll1	ACCTCGGGATGACGCCTTTG	ACTCCCCTGGTTTGTCACAG	95
Dll4	CAGTTGCCCTTCAATTTCACCT	AGCCTTGGATGATGATTTGGC	96
Ereg	TGGGTCTTGACGCTGCTTTGTCTA	AAGCAGTAGCCGTCCATGTCAGAA	102
Fgf1	GTTGACCCTACCATGTTCCCTTG	GCCAGCAGCATCTATGGGAC	103
Fgf2	ACGGCGTCCGGGAGAA	TCTTCTGGTTCGGCATCAC	104
Hif1a	CTATGGAGGCCAGAAGAGGGTAT	CCCACATCAGGTGGCTCATAA	99
Hgf	GAACTGCAAGCATGATGTGG	GATGCTGGAAATAGGGCAGAA	105
Jagged 1	GGTAACACCTTCAATCTCAAGGC	CCACCAGCAAAGTGTAGGACC	106
Jagged 2	TGGTACCTGCGTGGATCAG	AATAGCCGCCAATCAGGTT	106
Plgf	ATGCAGATCTTGAAGATTCCC	CTCTTCCCCTTGGTTTTCCT	92
Pdgb	CATCCGCTCCTTTGATGATCTT	GTGCTCGGGTCATGTTCAAGT	93
Pdgfa	GAGGAAGCCGAGATACCCC	TGCTGTGGATCTGACTTCGAG	93
Grn	GGTTGATGGTTCGTGGGGATGTTG	AAGGCAAAGACACTGCCCTGTTGG	94
Ptn	TGGAGAATGGCAGTGGAGTGTGT	TGGTACTTGCACTCAGCTCCAAACT	95
Scf	CCCTGAAGACTCGGGCCTA	CAATTACAAGCGAAATGAGAGCC	14
Tgfa	ATCCTGTTAGCTGTGTGCCA	GGAATCTGGGCACTTGTTGA	96
Tnfa	CCCTCACACTCAGATCATCTTCT	GCTACGACGTGGGCTACAG	97
Tnfr1	CCG GGAGAAGAGGGATAGCTT	TCGGACAGTCACTCACCAAGT	107
Tnfr2	GCCCAGGTTGTCTTGACACC	CACAGCACATCTGAGCCTTCC	108
Vegfa	CAGAAGGAGAGCAGAAGTCC	CTCCAGGGCTTCATCGTTA	92
Vegfb	CCCAGTTTGATGGCCCCA	TGCCCATGAGTTCCATGC	92
Vegfc	GTAAAAACAAACTTTTCCCTAATTC	TTTAAGGAAGCACTTCTGTGTGT	92
Vegfd	GCAAGACGAGACTCCACTGC	GGTGCTGAATGAGATCTCCC	92

Supplementary Table 2.1. List of oligonucleotides used in qPCR experiments.

CHAPTER THREE:

NEONATAL MICROBES RESTRICT PROLIFERATION AND INSTRUCT LINEAGE COMMITMENT OF HEMATOPOIETIC STEM CELLS

INTRODUCTION AND RESULTS

The work shown in the previous chapter demonstrated a critical role for BM granulocytes in regulating endothelial cells during regeneration. We then decided to investigate whether changing BM granulocyte numbers during homeostasis could also affect the vasculature. A study in the literature showed that gut microbes induced neutrophil production and 6-fold neutrophil accumulation in the bone marrow during neonatal development (**109**). In this study, depletion of the neonatal gut microbiota by antibiotic treatment leads to a significant impairment in production of neutrophils resulting in dramatically lower numbers of neutrophils in the BM and in circulation (**109**). This correlated with a decrease in G-CSF plasma levels and increased susceptibility to *Escherichia coli K1* and *Klebsiella pneumoniae* sepsis (**109**). We hypothesized that neonatal microbe-induced neutrophil expansion would also expand BM endothelial cells. To test this, and in collaboration with Dr. Gabriel Nuñez's laboratory, we compared neutrophil and endothelial cell numbers in germ-free or SPF (P10) neonates housed in the UM vivarium. In contrast to the previous study (**109**) we did not find reduced neutrophil numbers in the germ-free neonates when compared to SPF controls (**Fig. 3.1a**). In agreement, endothelial cell numbers were also unaffected (**Fig. 3.1b**). We interpret the differences between our data and the one described in the literature as due to different gut microbe composition between different institutions, a well-known problem in the field (**110-111**).

While performing these studies we thoroughly characterized the spectrum of mature and progenitor hematopoietic cells. We detected only very mild differences between pups born and raised in GF or SPF conditions (**Supp. Fig 3.1a-d**). However, we did discover a very striking HSC phenotype (**Fig 3.1**). Neonatal mice raised in SPF conditions had equal numbers of BM HSC to the GF cohort (**Fig 3.1c**) but had a significantly higher pool of $Ki67^-$ quiescent HSC compared to the GF group (**Fig 3.1d,e**). Shockingly, this difference in cell cycle status seems to be restricted to the HSC pool as the immediate downstream progenitor, the MPP, had the same total number (**Fig 3.1c**) and same percent of cycling MPPs (**Fig 3.1d**) in either group. To functionally test differences from HSC retrieved from neonates raised in SPF or GF conditions we initiated a competitive transplant where 20% of the BMNC from SPF or GF neonates was co-transplanted with $2.5x10^5$ CD45.1 competitor into CD45.2 lethally irradiated recipients. Blood was taken every 2 weeks for 16 weeks to track tri-lineage reconstitution. Interestingly, HSC isolated from SPF neonates show a skewing towards myeloid and T lymphocyte lineages compared to the HSC isolated from GF neonates (**Fig 3.1f**). Additionally, recipients that received HSC from SPF neonates have high reconstitution in the peripheral blood (measured by total $CD45.2^+$ cells) indicating higher HSC activity (**Fig 3.1f**).

Our research was not the first to note a phenotype in the HSC pool when the gut microbiota is absent. In fact, in a previous report where researchers compared the BM of adult GF and SPF animals, they also noted no change to the size of the HSC pool in the BM (**112**). Additionally, the absence of a gut microbiota also induced large changes to the myeloid compartment including significant reductions in the number of BM and splenic macrophages and neutrophils, as well as, BM granulocyte-monocyte progenitors (GMPs). When these GMPs were placed in

CFU assays, GMPs isolated from GF mice had reduced production of CFU-G and CFU-M colonies, as well as smaller colonies over all, compared to GMPs taken from SPF donors, suggesting that loss of a gut microbiota impairs the differentiation and proliferation of this progenitor population (**112**). While this research further supported the importance of the gut microbiota in maintaining proper production of mature myeloid cells, the function of the HSC in GF mice was never tested. In fact, no other parameters besides total number of HSC were ever investigated in this study. This leaves open the question of whether the GMP is the BM target of this communication emanating from the large intestine or if the reduction in GMPs is the result of impaired lineage differentiation from the HSC.

Recently, a group reported the impact on the hematopoietic stem and progenitor cells in the BM after an antibiotic cocktail regiment including ampicillin, vancomycin, neomycin, metronidazole, and ciprofloxacin (**113**). Long-term exposure to antibiotics leads to bone marrow suppression which can cause anemia, thrombocytopenia, and neutropenia (**113**). If this is left unnoticed, this prolonged impairment to the hematopoietic system can lead to severe infection. While this phenotype is known to occur to patients in the clinic, there is still little known about the exact mechanisms that drive antibiotic-induced hematopoietic suppression. As expected, after two weeks of antibiotic drinking water, mice had suppression throughout the mature blood cell populations in the peripheral blood. More interestingly, however, was the suppression found within the BM as HSC were significantly reduced in mice that received antibiotics (**113**). Additionally, mice receiving antibiotic treatment also have a higher percentage of $BrdU^+$ HSC than the control group. It should also be noted that mice receiving antibiotics have additional BM progenitor phenotypes with MPPs and CLPs also showing significant reductions in number,

however, only the HSC has any significant change in proliferation (**113**). Taken together with the previous research described, this data suggests that the BM phenotype emanates with changes to the HSC pool leading to a shift in the production of progenitors, however, as with the previous work the researchers in this group did not test HSC function. Additionally, germ-free mice were not treated with antibiotics to test for microbiota-independent effects to the BM microenvironment, the HSC niche, and hematopoietic cells themselves.

The results in Fig. 3.1 demonstrated that HSC purified from SPF neonates have reduced proliferation, increased output after transplantation and are biased towards a myeloid fate. We then tested whether this was due to the gut microbiota. For this we initiated foster experiments to determine if the introduction of a gut microbiota to GF neonates following birth could induce the same BM phenotypes as mice born and reared in SPF conditions. SPF and GF females underwent timed breeding to generate litters born at the same time. Half of the pups born in GF conditions were immediately transferred to a SPF foster female. Ten days later, the BM of the SPF, GF, and GF pups fostered in SPF conditions were analyzed (**Fig 3.2a**). As shown in Fig. 1, neonates raised in GF housing have increased proliferation within their HSC pool compared to SPF neonates with no change in the total number of HSC present in the BM (**Fig 3.2b-c**). Interestingly, GF neonates that were fostered in SPF conditions have an HSC profile much closer to SPF neonates than GF neonates (**Fig 3.2c**). HSC taken from fostered GF neonates have a quiescence signature mirroring that of HSC isolated from neonates born and raised in SPF housing (**Fig 3.2c**). While fecal samples were taken for analysis, we are currently waiting for the sequencing data to validate that the composition of the gut microbiota in GF neonates fostered

in SPF conditions mirrors the composition found in SPF neonates. Ultimately, this analysis could aid us in narrowing down the possible microbial candidates driving this communication.

Next, we aimed to determine if this HSC phenotype was solely the result of developmental timing or if the introduction of a neonatal gut microbiota could influence HSC biology in an adult. The cecal contents of adult and neonatal (P5) mice were isolated and then adoptively transferred into adult GF recipients via oral gavage (**Fig 3.2d**). Three weeks after inoculation, bone marrow was harvested to test the HSC function and number. As predicted, the diversity of microbes in the large intestine varied greatly between the group receiving adult microbiota and the group receiving neonatal microbiota even three weeks after inoculation (**Fig 3.2e**). While the total number of HSC – along with other progenitor and mature blood populations – in the BM undergoes no change regardless of bacteria present, GF recipients that received the neonatal mixture contain a larger portion of quiescent HSC compared to GF recipients that received the inoculation of adult gut microbiota (**Fig 3.2f-g, Supp. Fig 3.2a-c**). To test for lineage skewing, we initiated a competitive transplant where $CD45.1^+$ recipient mice received 20% of BMNC from mice inoculated with adult or neonatal gut microbiota along with $2.5x10^5$ $CD45.1^+$ competitor marrow (**Fig 3.2h**). Beginning six weeks post-transplant, recipients transplanted with BM from GF mice inoculated with neonatal microbiota produce a higher portion of myeloid cells in the peripheral blood against the competitor compared to the recipients that were transplanted with BM from GF mice that received adult microbiota (**Fig 3.2h**). As predicted we found increased peripheral blood reconstitution and bias towards myeloid and T cell lineages in recipient mice transplanted with BM cells purified from GF mice adoptive transferred with neonatal microbes (**Fig. 3.2h**). Taken together these experiments conclusively demonstrate that neonatal gut

microbes restrict proliferation and instruct lineage choices of HSC. Additionally, this data does suggest that it is the presence of a specific composition of bacteria in the large intestine that communicate with the BM to inhibit proliferation of the HSC pool and the prime the BM for specific hematopoietic cell production. Interestingly, when we analyzed the BM further we found that adult GF animals that receive a neonatal microbiota exhibit an expansion of their BM neutrophils (**Supp. Fig 3.2c**). However, this is not associated with an increase in BM endothelial cells (**Supp. Fig 3.2d**).

While the GF model system allows us to test the role of the gut microbiota in a lower variable setting compared to treatment with antibiotic cocktails, the ease of using the system is low. The ability to accumulate enough mice for experimentation takes months and ultimately, we would need specific strains bred into the GF facility to test mechanism. In order to get around these issues, we began looking for additional models that mirror the neonatal gut microbiota phenotype. Previous research performed by the Nuñez lab demonstrated that adult SPF mice treated for three weeks with vancomycin induced a neonatal-like gut microbiota (**114**). Mice were treated with 250 µg/mL of vancomycin dissolved in their drinking water and three weeks after initiation of treatment, the mice were harvested for BM analysis. As with the adult GF mice treated with a neonate microbiota, adult SPF mice treated with vancomycin have increased HSC quiescence compared to the PBS control group (**Fig 3.3b**). However, SPF mice treated with vancomycin have mild expansion in several hematopoietic progenitor populations, including HSC (**Fig 3.3a, Supp. Fig 3.3a-c**), which was not an observed phenotype in either the neonatal studies or the adoptive transfer of gut microbiota studies. Interestingly, this data could suggest that vancomycin treatment impacts the gut microbiota composition in a way that induces only part of the

phenotype we see in the previous experiments. This could be due to incomplete removal of "adult" microbes that prevent expanded colonization of a more neonatal-like composition, as well as, impaired kinetics of the phenotype due to an ablation step followed by a recolonization step. Therefore, comparative fecal analysis of vancomycin-treated SPF adult animals, adult GF mice inoculated with neonatal gut microbiota, and true neonates will be necessary to determine any compositional differences in the intestinal bacteria of these groups. Additionally, HSC isolated from the vancomycin-treated and control groups need to be functionally tested in the competitive transplant setting to elucidate differences in engraftment and lineage skewing of mature cells in the peripheral blood. As mentioned previously, it is also important to compare bacterial diversity across the all different groups to 1) validate that our models are truly representative of a neonatal microbiota and 2) to aid in narrowing down potential bacterial candidates that could be important for this communication.

DISCUSSION

The colonization of the neonatal intestine following birth is connected to many alterations to the bone marrow and the secondary lymphoid organs associated with the intestine. These changes appear to be an important step in the maturation of the very naïve immune system for the neonate. Neutrophil production has been shown to dramatically increase following colonization of the gut and is an important step in protecting neonates from potentially life-threatening infections (**109,115**). Our results do not match this, and this could be due to the timing of our analysis, as well as, potential differences in gut microbiota of animals housed in different facilities (**110-111**). More specifically, the biggest differences in neutrophil numbers noted between GF and SPF neonates occur around P3, where SPF neonates have a ~10-fold increase in BM

neutrophils. By P7, that fold difference drops to ~2-fold (**109**). As all of our analyses fell on P10, it is possible that we missed the window for the initial expansion of BM neutrophils and the possible impact this could have on the developing BM vasculature.

Additionally, research has also shown that hematopoietic stem and progenitor cells (HSPCs) are capable of sensing bacterial byproducts through expression of pathogen-associated molecular pattern (PAMP) receptors like the Toll-like receptors (TLR). In particular, activation of TLR4, through its ligand LPS, induces both HSC cycling and a skewing towards myeloid differentiation (**116-121**). In the context of acute infection this is a pathway to induce rapid production of neutrophils and monocytes to aid in the clearing of pathogens with the hematopoietic system returning to normal multi-lineage production following removal of the stressor. However, under the conditions of chronic infection and prolonged stimulation of TLRs, HSC function begins to deteriorate with severe impairment in long-term production of lymphocytes and decreased self-renewal of HSC in a competitive transplant setting suggesting an overall loss of HSC function in the presence of prolonged TLR activation (**117-118**). While this data has implicated an involvement of bacteria on HSC function it is all within the context of infection. As mentioned earlier, more recent studies have also begun elucidating the impact of the gut microbiota on steady-state hematopoiesis (**109,112-113**). While previous GF studies have been done during homeostasis (**112**), the HSC phenotypes do not entirely match ours. However, it is important to note that most of these previous studies do not hone in on the HSC population and fail to commit to functional studies to test the biology of HSC in mice with or without a gut microbiota (**112-113**). Even excluding the HSC phenotype, we do not observe many significant differences to the BM of adult mice raised in GF or SPF conditions (data not shown). It is important to note, our

research using the GF adults for adoptive transfer assays were done strictly using female GF recipients while males are typically used in other studies (**112-113**). This brings into the question the possibility of sex-based differences in how the hematopoietic system responds to the lack of a gut microbiota. Lastly, our research is novel in that we specifically investigated the importance of the composition of the gut microbiota – and not just the absence or presence – on steady-state hematopoiesis. More specifically, we identified the neonatal bacterial diversity of the gut as capable of inducing quiescence and myeloid cell production of the HSC pool. However, as of now we do not have much insight into the possible mechanistic pathways at work to drive this communication.

Due to the increase in HSC quiescence, we can develop some hypotheses for how the gut microbiota might be targeting the BM. In particular, a change in the HSC pool immediately brings into question changes to the BM microenvironment and the HSC niche. Several non-hematopoietic and hematopoietic populations have been shown to provide signals that induce changes in the associated HSC. More specifically, the stromal $Ng2^{+}$ perivascular population (**8**) and the megakaryocyte (**16-19**) have been connected to HSC quiescence. Preliminary data suggests an expansion of megakaryocytes in SPF neonates and in adult GF mice inoculated with neonatal microbiota (data not shown), however, as of now the pool size of these experiments is quite small and we have no mechanistic data to further support this observation. However, these two cell populations are potential mediators of this communication pathway.

While this is interesting from the perspective of stem cell biology, our research might also have potential in the clinical setting. HSC quiescence has been shown to influence their engraftment success following bone marrow transplant with a larger quiescent pool of HSC being associated

with increased engraftment (**122-123**). Additionally, rapid production of myeloid cells following transplant is a necessary step to prevent life-threatening complications induced by rampant infection. Our data suggests that a gut microbiota that compositionally resembles that of a neonate induces a shift in hematopoietic lineage production towards the granulocytic and monocytic lineages. This large shift in neutrophil production was not just present in the bone marrow cavity but was also observed in the peripheral blood. This could be suggesting increased production of matured, functional granulocytes, but this needs to be further tested in an infection animal model with recipients inoculated with adult or neonatal gut microbiota. Taken together our data could suggest an important clinical role for the manipulation of the gut microbiota in aiding the success of bone marrow transplant to increase HSC engraftment and myeloid-skewing to bias production of neutrophils to prevent infection.

MATERIALS AND METHODS

Animals

Specific pathogen free (SPF) C57BL/6J (CD45.2^{+}) and B6.SJL-*Ptprc*^{a}*Pepc*^{b}/BoyJ (B6.SJL, CD45.1^{+}) mice were purchased from the Jackson laboratory and bred in house. SPF mice were housed at the SPF facility managed by the Unit for Laboratory Animal Medicine (ULAM) at the University of Michigan. C57BL/6J mice were also maintained on a germ-free (GF) background and were bred and maintained at the Germ-Free Animal Core Facility at the University of Michigan. GF mice were maintained in flexible film isolators and were checked weekly for GF status by aerobic and anaerobic culture. All experiments were performed on P10 neonates and 8-14 week-old mice. Experiments were approved by the Institutional Animal Care and Use Committee at the University of Michigan.

Reconstitution of GF ice with cecal contents of defined bacteria

Isolation, reconstitution, and inoculation of recipient mice were completed following the methods presented in the Nunez manuscript cited in the references, **114**.

Treatment with Vancomycin

Vancomycin (250 mg/L) was administered in the mouse drinking water for 21 days. Water was replenished and fresh Vancomycin was added every 7 days.

DNA extraction and 16S rRNA gene sequencing from fecal pellets

DNA sequencing of fecal samples were completed following the methods presented in the Nunez manuscript cited in the references, **114**.

Bone marrow isolation

Mice were euthanized with isoflurane overdose. Mouse long bones were flushed with 1 ml of ice-cold PEB (2mM EDTA, 0.5% Bovine serum albumin in PBS) to harvest bone marrow. Red blood cells were lysed once by adding 1 ml of RBC Lysis Buffer (NH4Cl 150mM, NaCO3 10mM, EDTA 0.1mM). Cell suspension was immediately separated by centrifugation, supernatant was decanted, and harvest bone marrow cells were resuspended in ice-cold PEB and used in subsequent assays.

Peripheral blood analyses

Peripheral blood was collected from the facial vein in tubes containing EDTA. White blood cell (WBC), red blood cell (RBC), and platelet counts were obtained using an Advia Counter

(Siemens) or a Hemavet 950 (Drew Scientific). Prior to flow cytometry staining and analyses, red blood cells in peripheral blood were lysed once by adding 1 ml of RBC Lysis Buffer and incubating on ice for 5 minutes. Cells then underwent centrifugation to decant the supernatant. The cell pellet was resuspended in ice-cold PEB and used in subsequent assays.

Collagenase/Dispase digestion

To purify the stromal cell fraction of the bone marrow (including endothelial cells) we used a modified version of the serial digestion protocol developed by the Simmons laboratory (**90**). Digestion buffer was made by dissolving 2 mg/ml Collagenase Type IV (Gibco, 17104-019) and 3 mg/ml Dispase (Gibco, 17105-041) in PBS at room temperature. Bone marrow was harvested by flushing a tibia with 1 ml of digestion buffer into a 5 ml polypropylene snap-cap tube containing another 1 ml of digestion buffer. Tubes were mixed vigorously by hand and incubated at 37°C for 5-7 minutes. Following the first incubation, the tubes were again mixed vigorously by hand and then placed back at 37°C for another 5-7 minutes. After the second incubation, the supernatant was collected (taking care to leave any macroscopic clumps in the digestion tube) and transferred the digested cells to a tube containing 5 ml of ice-cold PEB. Next, 1 ml of digestion buffer was added to the snap-cap tubes and the process above repeated until all macroscopic pieces of bone marrow had been digested. The red blood cells were lysed once using RBC Lysis Bugger, filtered through a 100 μm filter (Greiner Bio-one, 542-000), and immediately spun down in the centrifuge. The cell pellet was resuspended in 1 ml of ice-cold PEB and used for subsequent analyses.

FACS analyses

Cells were stained for 30 minutes in PEB buffer with the indicated antibodies and analyzed in a BD LSRFortessa (BD Biosciences). Antibodies used were against B220 (clone RA3-6B2, Cat No: 103224), CD3 (clone 145-2C11, Cat No:100304), CD4 (clone GK1.5, Cat No:100422), CD8 (clone 53-6.7, Cat No:100722), CD11b (clone M1/70, Cat No:101216 or 101204), CD16/32 (clone 93, Cat No:101328), CD31 (clone A20, Cat No:110724), CD41 (clone MWReg30, Cat No:133921 or clone D7, Cat No: 108104), CD45 (clone 30-F11, Cat No:103116), CD45.1 (clone A20, Cat No:110723 or 110708), CD45.2 (clone 104, Cat No:109845, 109823 or 109814), CD105 (clone MJ7/18, Cat No:120410), CD115 (clone AFS98, Cat No:135506 or 135513), CD144 (clone BV13, Cat No: 138006), CD150 (clone TC15-12F12.2, Cat No:115904), F4/80 (clone BM8, Cat No:123122), Gr1 (clone RB6-8C5, Cat No: 108406 or 108404), Sca-1 (clone D7, Cat No:108106), and Ter119 (clone TER-119, Cat No:116220), all from Biolegend, CD117 (clone 2B8, Cat No:105828 and 105833 from Biolegend or 562417 from BD Biosciences), and Ki67 (clone SolA15, Cat No:50-5698-82 from ThermoFisher Scientific). For cell cycle analyses, cells were first stained for immunophenotype. This was followed by fixation with 4% paraformaldehyde for 20 minutes at 4°C and then by permeabilization of the plasma membrane with 0.1% Triton X-100 for 20 minutes at 4°C. The cells were then stained for 30 minutes in PEB buffer containing 0.1% Triton X-100 with Ki67 (Cat No: 50-5698-82). Lastly, cells were incubated in PEB buffer containing DAPI for one hour at room temperature before being analyzed as described above.

Competitive bone marrow transplants

Recipient SPF female mice were conditioned with two doses of 600 rads, 3 hours apart, and immediately transplanted with the indicated amount of donor BMNC via retroorbital injection.

Statistics

In most graphs, the actual values for each mouse are plotted and the means indicated. In others, the means and standard errors are plotted. Sample size was not predetermined and all mice were included in the analyses. Mice were randomly allocated to the different groups based on cage and litter size. For all experiments, we aimed to have the same number of mice in the control and experimental groups. For all experiments, at the time of analyses, the investigator was blinded to the group allocation. Statistical differences were calculated using two-sample T-tests (for experiments with two groups) and ANOVA (for experiments with 3 or more groups) on log transformed data.

References

Can be found at the end of dissertation.

Publication

This manuscript is currently ongoing in the Lucas lab as several experiments remain to be completed.

CHAPTER FOUR:

CONCLUSION

The BM is a complex structure containing many hematopoietic and non-hematopoietic cell populations that crosstalk to create a microenvironment that supports and regulates the production of mature blood cells. The best studied example of this complex crosstalk is the HSC niche. These niches are absolutely necessary for HSC maintenance through the production of a variety of signaling molecules. While many groups have and continue to investigate the mechanisms through which the niche regulates HSC much less is known about how the microenvironment functions downstream of HSC and how the different components of the microenvironment are regulated. The work done during my thesis has identified two novel forms of hematopoiesis regulation that impact the niche and hematopoietic cell production.

Prior to my thesis, research had already discovered that BM endothelial cells are a large component of the HSC niche with production of critical HSC regulatory factors like SCF and CXCL12 (**10-11**). Additionally, studies performed in the context of regeneration and BMT placed vascular regeneration as a necessary precedent for the successful engraftment of the transplanted hematopoietic system (**42,48**). However, until now, very few mechanisms had been identified that induced vascular regeneration in the transplant setting. My thesis work uncovered a novel role for BM granulocytes in the regeneration and recovery of the vascular network and hematopoietic system in the BM. The adoptive transfer of BM-derived granulocytes increased

FIGURES

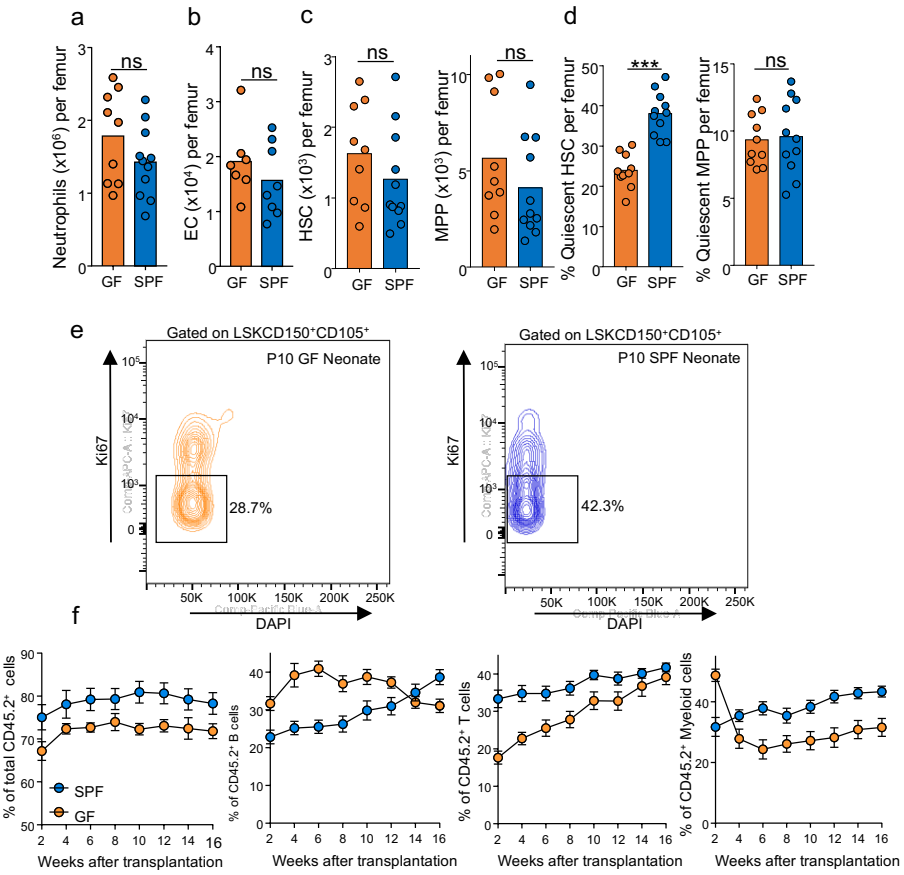

Figure 3.1 Gut microbes induce HSC quiescence in neonates. (**a**) Number of Gr1^{+}CD115^{-} neutrophils in the femur of P10 neonates raised in germ-free (GF) or specific pathogen free (SPF) housing (n=9-11). (**b**) Number of CD45^{-} TER119^{-}CD31^{+}CD105^{+} endothelial cells in the femur of the mice in a (n=9-11). (**c**) Number of LSKCD150^{+}CD105^{+} HSC (left, n=9-11) and of LSKCD150^{-} CD105^{-} MPP (right, n=9-11) in the femur of mice in a. (**d**) Percent of quiescent (Ki67^{-}) LSKCD150^{+}CD105^{+} HSC (left, n=9-11) and LSKCD150^{-}CD105^{-} MPP (right, n=9-11) in the femur of the mice in a. (**e**) Representative FACS plots showing the percent of Ki67^{-} HSC from P10 GF (orange) or SPF (blue) neonatal mice. (**f**) CD45.2^{+} cell engraftment of total, B, T, and myeloid cells in secondary recipients after transplantation of 2.5x10^{5} CD45.1^{+}:CD45.2^{+} competitor BMNC and 20% of the CD45.2^{+} cell in one femur of GF or SPF P10 neonates (n=7-10). For all experiments each dot represents one mouse. p values were calculated using two-tailed Two-sample T-Test. Graphs show the pooled data of at least two independent experiments. Bar graphs represent the mean.

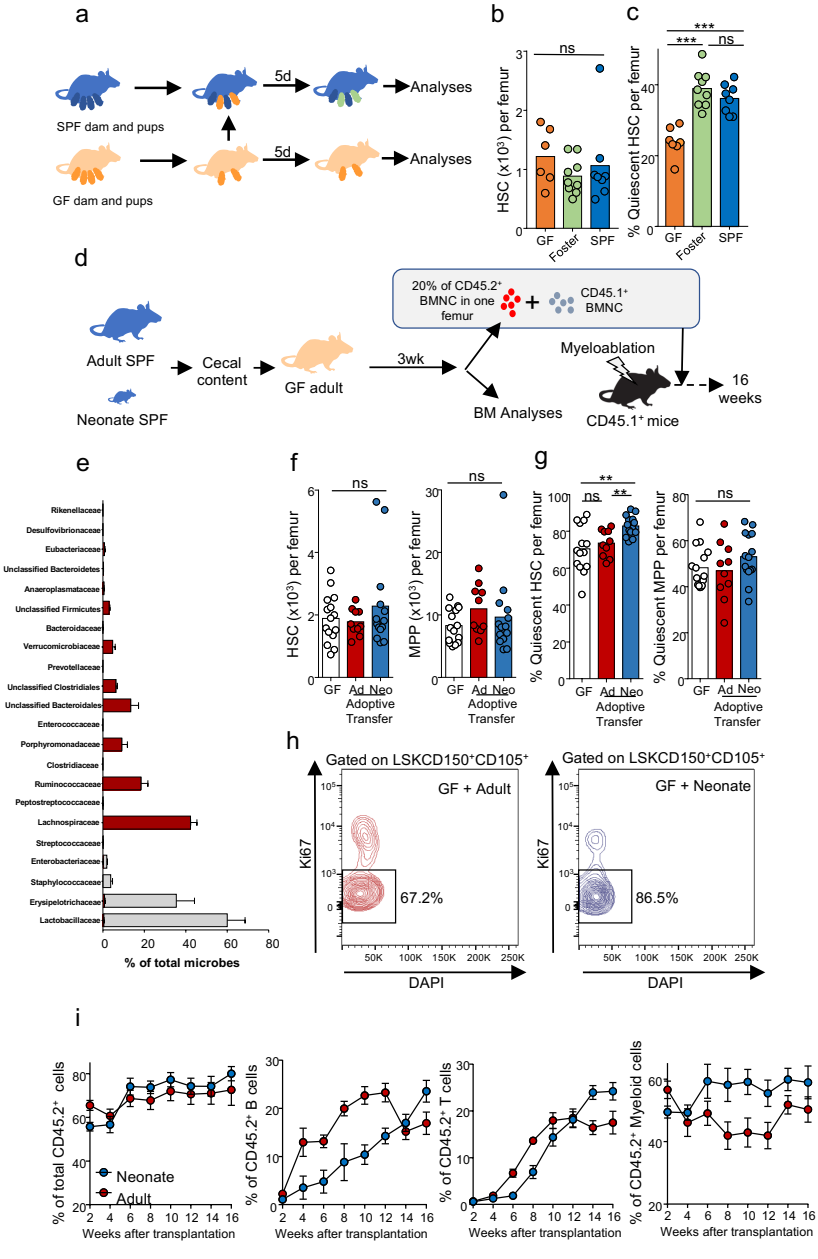
a
SPF dam and pups
GF dam and pups
5d
5d
Analyses
Analyses
b
ns
HSC (x10³) per femur
GF
Foster
SPF
c
***
***
ns
% Quiescent HSC per femur
GF
Foster
SPF
d
Adult SPF
Neonate SPF
Cecal content
GF adult
3wk
20% of CD45.2⁺ BMNC in one femur
CD45.1⁺ BMNC
Myeloablation
16 weeks
BM Analyses
CD45.1⁺ mice
e
Rikenellaceae
Desulfovibrionaceae
Eubacteriaceae
Unclassified Bacteroidetes
Anaeroplasmataceae
Unclassified Firmicutes
Bacteroidaceae
Verrucomicrobiaceae
Prevotellaceae
Unclassified Clostridiales
Unclassified Bacteroidales
Enterococcaceae
Porphyromonadaceae
Clostridiaceae
Ruminococcaceae
Peptostreptococcaceae
Lachnospiraceae
Streptococcaceae
Enterobacteriaceae
Staphylococcaceae
Erysipelotrichaceae
Lactobacillaceae
0 20 40 60 80
% of total microbes
f
ns
HSC (x10³) per femur
ns
MPP (x10³) per femur
GF Ad Neo
Adoptive Transfer
g
**
ns
**
% Quiescent HSC per femur
ns
% Quiescent MPP per femur
GF Ad Neo
Adoptive Transfer
h
Gated on LSKCD150⁺CD105⁺
GF + Adult
Ki67
67.2%
DAPI
Gated on LSKCD150⁺CD105⁺
GF + Neonate
Ki67
86.5%
DAPI
i
% of total CD45.2⁺ cells
Neonate
Adult
Weeks after transplantation
% of CD45.2⁺ B cells
Weeks after transplantation
% of CD45.2⁺ T cells
Weeks after transplantation
% of CD45.2⁺ Myeloid cells
Weeks after transplantation

Figure 3.2. Neonatal gut microbes restrict HSC proliferation. (**a**) Experimental design for fostering GF pups with a SPF dam. (**b**) Number of LSKCD150^{+}CD105^{+} HSC in the femur of P10 neonates raised in GF, SPF, or GF fostered with a SPF dam housing (n=6-9). (**c**) Percent of quiescent (Ki67^{-}) LSKCD150^{+}CD105^{+} HSC in the femur of mice described in b (n=7-9). (**d**) Experimental design for adoptive transfer of gut microbes. (**e**) Microbial diversity in the large intestine of GF mice inoculated with adult (red) or neonatal (grey) gut microbiota. (**f**) Number of LSKCD150^{+}CD105^{+} HSC (left, n=10-15) and LSKCD150^{-}CD105^{-} MPP (right, n=10-15) in the femur of GF mice (white) or GF mice inoculated with adult (red) or neonatal (blue) microbiota. (**g**) Percent of quiescent (Ki67^{-}) LSKCD150^{+}CD105^{+} HSC (left, n=10-14) and LSKCD150^{-}CD105^{-}MPP (right, n=10-14) in the femur of the mice in f. (**h**)
Representative FACS plots showing the percent of Ki67^{-} HSC from GF mice inoculated with adult (left, red) or neonate (right, blue) microbiota.(**i**) CD45.2^{+} cell engraftment of total, B, T, and myeloid cells in secondary recipients after transplantation of 2.5x10^{5} CD45.1^{+}:CD45.2^{+} competitor BMNC and 20% of the CD45.2^{+} cell in one femur of GF mice inoculated with adult (red) or neonatal (blue) microbiota (n=7-10). For all experiments each dot represents one mouse. p values were calculated using two-tailed Two-sample T-Test. Graphs show the pooled data of at least two independent experiments. Bar graphs represent the mean.

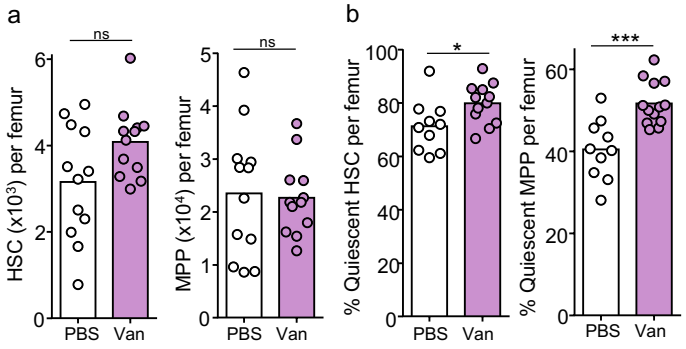

Figure 3.3. Vancomycin-induced gut microbiota induces HSC quiescence. (**a**) Number of LSKCD150^{+}CD105^{+} HSC (left) and LSKCD150^{-}CD105^{-} MPP (right) in the femur of mice treated with Vancomycin (purple) or PBS (white), n=12. (b) Percent of quiescent (Ki67^{-}) LSKCD150^{+}CD105^{+} HSC (left, n=12) and LSKCD150^{-}CD105^{-} MPP (right, n=12) in the femur of the mice in a. For all experiments each dot represents one mouse. p values were calculated using two-tailed Two-sample T-Test. Graphs show the pooled data of at least two independent experiments. Bar graphs represent the mean.

SUPPLEMENTAL FIGURES

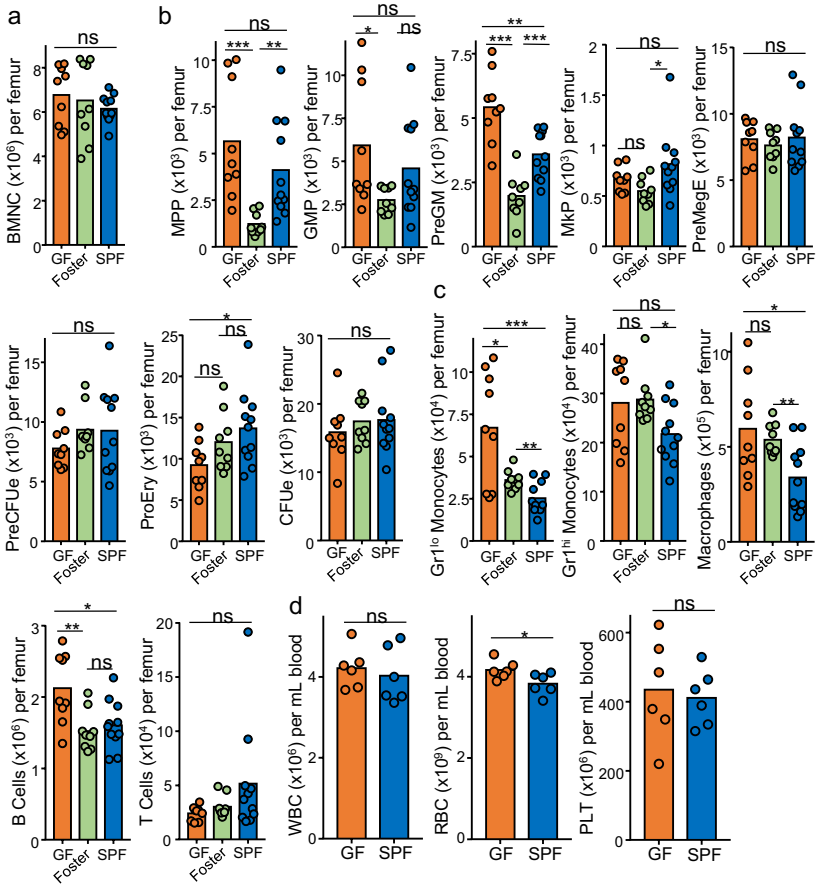

Supplemental Figure 3.1. (**a**) Number of total BMNC in the femur of P10 neonates raised in germ-free (GF, n=9), germ-free fostered in specific-pathogen free (Foster, n=9), and specific pathogen free (SPF, n=11) housing. (**b**) Number of LSKCD150$^-$CD105$^-$ MPP, LKCD41$^-$CD150$^-$CD16/32$^+$ GMP, LKCD41$^-$CD150$^-$CD105$^-$CD16/32$^-$ PreGM, LKCD150$^+$CD41$^+$ MkP, LKCD41$^-$CD16/32$^-$CD150$^+$CD105$^-$ PreMegE, LKCD41$^-$CD16/32$^-$CD150$^+$CD105$^+$ PreCFUe, LKCD41$^-$CD16/32$^-$CD150$^-$CD105$^+$TER119$^-$ ProEry, and LKCD41$^-$CD16/32$^-$CD150$^-$CD105$^+$TER119$^+$ CFUe in the femur of the mice described in a, n=9-11. (**c**) Number of Gr1^{lo}CD115$^+$ Monocytes, Gr1^{hi}CD1115$^+$ Monocytes, Gr1$^-$CD115$^-$F4/80$^+$ Macrophages, Gr1$^-$CD115$^-$F4/80$^-$B220$^+$ B cells, and Gr1$^-$CD115$^-$CD4$^+$ and Gr1$^-$CD115$^-$CD8$^+$ T cells in the femur of mice described as in a, n=9-11. (**d**) WBC, RBC and PLT in the peripheral blood of mice treated as in a, n=6. For all experiments each dot represents one mouse. p values were calculated using two-tailed Two-sample T-Test. Graphs show the pooled data of at least two independent experiments. Bar graphs represent the mean.

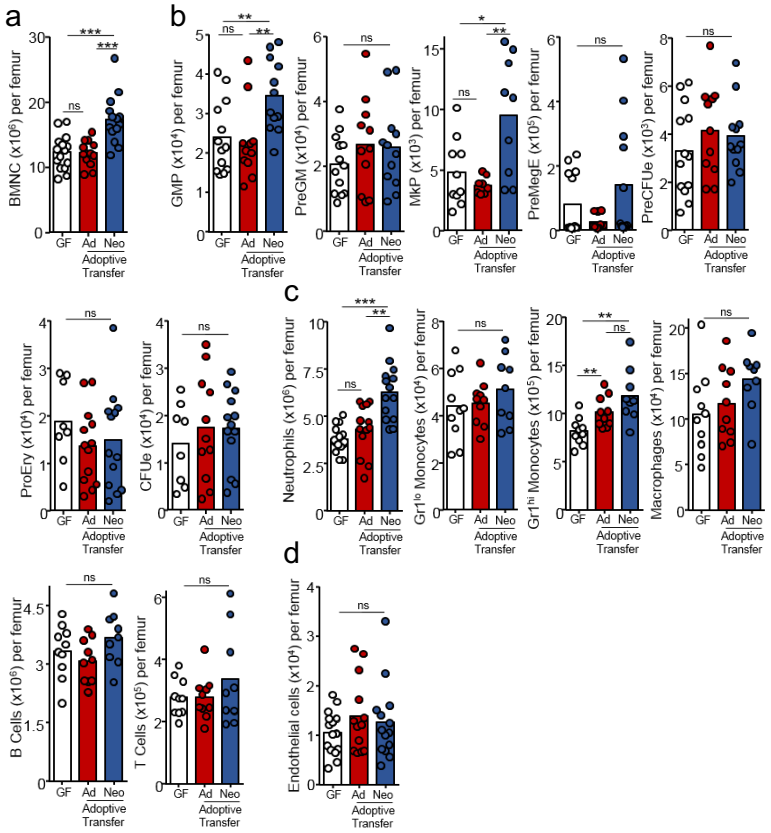

Supplemental Figure 3.2. (**a**) Number of total BMNC in the femur of GF mice (white, n=15) or GF mice inoculated with adult (red, n=13) or neonatal (blue, n=14) microbiota. (**b**) Number of LKCD41$^-$CD150$^-$CD16/32$^+$ GMP, LKCD41$^-$CD150$^-$CD105$^-$CD16/32$^-$ PreGM, LKCD150$^+$CD41$^+$ MkP, LKCD41$^-$CD16/32$^-$CD150$^+$CD105$^-$ PreMegE, LKCD41$^-$CD16/32$^-$CD150$^+$CD105$^+$ PreCFUe, LKCD41$^-$CD16/32$^-$CD150$^-$CD105$^+$TER119$^-$ ProEry, and LKCD41$^-$CD16/32$^-$CD150$^-$CD105$^+$TER119$^+$ CFUe in the femur of the mice described in a, n=13-15. (**c**) Number of Gr1$^+$CD115$^-$ Neutrophils, Gr1^{lo}CD115$^+$ Monocytes, Gr1^{hi}CD1115$^+$ Monocytes, Gr1$^-$CD115$^-$F4/80$^+$ Macrophages, Gr1$^-$CD115$^-$F4/80$^-$B220$^+$ B cells, and Gr1$^-$CD115$^-$CD4$^+$ and Gr1$^-$CD115$^-$CD8$^+$ T cells in the femur of mice described as in a, n=9-11. (**d**) Number of CD45$^-$TER119$^-$CD31$^+$CD105$^+$ endothelial cells of mice treated as in a, n=13-15. For all experiments each dot represents one mouse. p values were calculated using two-tailed Two-sample T-Test. Graphs show the pooled data of at least two independent experiments. Bar graphs represent the mean.

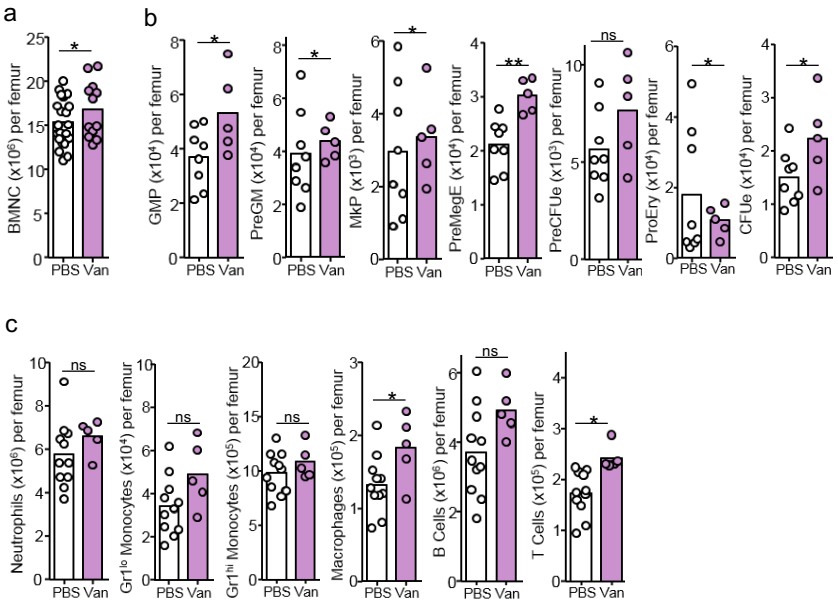

Supplemental Figure 3.3. (**a**) Number of total BMNC in the femur of mice treated with vancomycin (purple, n=18) or PBS (white, n=18). (**b**) Number of LKCD41$^-$CD150$^-$CD16/32$^+$ GMP, LKCD41$^-$CD150$^-$CD105$^-$CD16/32$^-$ PreGM, LKCD150$^+$CD41$^+$ MkP, LKCD41$^-$CD16/32$^-$CD150$^+$CD105$^-$ PreMegE, LKCD41$^-$CD16/32$^-$CD150$^+$CD105$^+$ PreCFUe, LKCD41$^-$CD16/32$^-$CD150$^-$CD105$^+$TER119$^-$ ProEry, and LKCD41$^-$CD16/32$^-$CD150$^-$CD105$^+$TER119$^+$ CFUe in the femur of the mice described in a, n=5-10. (**c**) Number of Gr1$^+$CD115$^-$ Neutrophils, Gr1^{lo}CD115$^+$ Monocytes, Gr1^{hi}CD1115$^+$ Monocytes, Gr1$^-$CD115$^-$F4/80$^+$ Macrophages, Gr1$^-$CD115$^-$F4/80$^-$B220$^+$ B cells, and Gr1$^-$CD115$^-$CD4$^+$ and Gr1$^-$CD115$^-$CD8$^+$ T cells in the femur of mice described as in a, n=5-10. For all experiments each dot represents one mouse. p values were calculated using two-tailed Two-sample T-Test. Graphs show the pooled data of at least two independent experiments. Bar graphs represent the mean.

the overall number of endothelial cells present in the BM, as well as, the overall function of that vasculature (I.e. less permeability of the blood vessels) and significantly improved production of mature blood cells in circulation. Additionally, I also discovered that this crosstalk is in part mediated through the production of TNFα as the adoptive transfer of *Tnfa*$^{-/-}$ granulocytes into transplant recipients completely lost the ability to increase vascular and hematopoietic regeneration. While recombinant injection of TNFα does lead to some improvement in the regeneration of the BM, the regenerative effect is much milder in comparison to the adoptive transfer experiments. It is also interesting to note that imaging analysis of the adoptively transferred granulocytes suggests a specific localization of these cells compared to the same analysis done with adoptively transferred B lymphocytes, which appear to localize randomly in the regenerating BM, suggesting that membrane-bound TNFα may have a stronger regenerative effect than soluble forms. This observation could be important when discussing the clinical implications of this research. While this research was able to add to the growing mechanism that is BM regeneration, it has also opened up several other questions. While the adoptive transfer of granulocytes does increase vascular regeneration, we have very limited information regarding how the vasculature itself regenerates following BM damage. Initial mechanistic studies from this research suggest that granulocytes induce survival of the damaged endothelial cells as we noted increased expression of the pro-survival gene c-FLIP. However, the actual process that occurs to regenerate the damaged vasculature is unknown and is a current area of interest in our lab. Very preliminary studies using the *Confetti* mouse model under control of the vascular specific promoter VE-Cadherin suggests a possible patchwork mechanism where in damaged sinusoids re-associate with one another to reform the blood vessels (data not presented). This is contrary to the more well-defined mechanisms of sprouting and intussusceptive angiogenesis

and could provide insight into a novel form of blood vessel formation following severe vascular damage.

The observation that granulocytes drive vascular regeneration fit within a larger narrative showing bidirectional communication between granulocytes and the vasculature. Granulocytes are the most abundant hematopoietic cell in the BM and are a critical component of the innate immune system and the inflammatory response. In order for granulocytes to egress from and home to the BM, they must migrate across an endothelial cell barrier. This process is dependent on the chemokine receptors CXCR2 and CXCR4, both expressed by granulocytes (**74**). CXCL1, CXCL2, and CXCL12 are all expressed by the BM vasculature and serve as ligands for these two receptors (**74**). Lack of CXCR2 expression leads to an accumulation of granulocytes in the BM space (**124**) while lack of CXCR4 in the BM leads to constitutive mobilization of granulocytes into the peripheral blood (**125**). The CXCR2/CXCR4 chemokine axis helps maintain the balance of granulocytes in the BM and in circulation. Similarly, granulocyte recruitment to tissues is regulated by the expression of adhesion molecules like selectins in the endothelial cell (**126-127**). Granulocytes produce several known pro-angiogenic proteins like VEGF-A (**128-129**), CXCL8/IL-1 (**130**), CXCL1 (**130**), and HGF (**131-132**). Mice that have undergone antibody-depletion of granulocytes lack the ability to induce angiogenesis into a Metrigel plug *in vivo* (**133**) from lack of release of VEGF-A (**134-135**), suggesting that recruitment of granulocytes to sites of wound healing or infection is required for the reformation of damaged blood vessels. Interestingly, this process is not restricted to the adult animal as research in zebrafish embryos has suggested a role for granulocyte-derived TNFα in the emergence of HSC from hemogenic endothelium (**136**). Loss of TNFα, its receptor TNFR2, or primitive granulocytes during

embryogenesis significantly impairs the budding of definitive HSC leading to a ~2-fold reduction in the HSC population (**136**). Thus, granulocytes and endothelial cells regulate each other in many biological processes including bone marrow regeneration.

As mentioned, the data presented in chapter two of this thesis has clinical implication in the context of bone marrow transplantation. However, as presented, the process of granulocyte adoptive transfer would likely not be feasible, as the removal of bone marrow granulocytes from a healthy donor at multiple timepoints over the course of several weeks would be a technical challenge. While the research presented in chapter 2 discounts the use of peripheral blood neutrophils as an alternative source of TNFα (**Supplementary Fig. 2.4b-h**), this does not discount the possibility of 1) isolating G-CSF mobilized granulocytes from a healthy donor or 2) storing aliquots of bone marrow derived granulocytes from a healthy donor to be used for successive adoptive transfers. However, both of these potential alternative approaches have yet to be tested and are a continued focus of the research being conducted.

We have also discovered that the composition of the gut microbiota is capable of influencing lineage differentiation decisions in the BM through alterations to the HSC pool. More specifically, we observed that the presence of a gut microbiota compositionally similar to a neonate leads to an increase in the fraction of HSCs that are quiescent and a skewing towards myeloid cell production that is maintained in competitive transplants. This was novel because we are the first lab to identify that signals emanating from the large intestine can influence HSC decisions in the BM during homeostasis as prior to this research most analysis concerning HSCs and the gut microbiota focused on infection and gut dysbiosis. However, there are many questions

surrounding the mechanism of communication that are still unknown. The most obvious open questions involve the bacterial species that are actively involved in this crosstalk. While we plan to do cross-comparative analysis of the fecal samples taken from all our experimental mice to hopefully narrow down potential bacterial candidates, it is likely to be more complex than a single species of bacteria. Additionally, the current signal(s) that are being sent to the BM to alter HSC function are unknown. Previous work investigating the increase in neutrophil production following the introduction of the gut microbiota after birth have identified G-CSF as a protein that increases in production after colonization (**109**) suggesting that known hematopoietic regulatory factors are likely involved in the phenotype we observe in the HSC pool. In addition, HSC quiescence has previously been linked to specific niche populations within the BM and an increase in the fraction of quiescent HSCs, with no change to the total number of HSC present, could suggest either 1) HSCs are re-localizing to niches that confer quiescence or 2) the niches are undergoing identity changes to switch from an "active" niche to a quiescent niche. While we do not observe any significant changes to the number of endothelial or $LepR^{+}$ cells in the BM of mice with a neonatal gut microbiota, we have preliminary data that the neonatal composition leads to an increase in BM megakaryocytes – a known quiescent HSC niche (data not shown).

In this thesis, we have identified two novel regulators of the hematopoietic microenvironment during regeneration (granulocytes) and homeostasis/development (gut microbes). These studies highlight the complex crosstalk that ensures that the hematopoietic system can adjust blood cell production to physiological demand.

REFERENCES

1. Asada N, Takeishi S, Frenette PS. Complexity of bone marrow hematopoietic stem cell niche. Int J Hematol. 106;45-54 (2017).

2. Bribrair A, Frenette PS. Niche heterogeneity in the bone marrow. Ann NY Acad Sci. 1370;82-96 (2016).

3. Crane GM, Jeffery E, Morrison SJ. Adult haematopoietic stem cell niches. Nat Rev Immunol. 17;573-590 (2017).

4. Ramalingam P, Poulos MG, Butler JM. Regulation of the hematopoietic stem cell lifecycle by the endothelial niche. Curr Opin Hematol. 24;289-299 (2017).

5. Sanchez-Aguilera A, Mendez-Ferrer S. The hematopoietic stem-cell niche in health and leukemia. Cell Mol Life Sci. 74;579-590 (2017).

6. Yu VW, Scadden DT. Heterogeneity of the bone marrow niche. Curr Opin Hematol. 23;331-338 (2016).

7. Chan CK, Chen CC, Luppen CA, Kim JB, DeBoer AT, Wei K, Helms JA, Kuo CJ, Kraft DL, Weissman IL. Endochondral ossification is required for haematopoietic stem-cell niche formation. Nature. 457;490-494 (2009).

8. Kunisaki Y, Bruns I, Scheiermann C, Ahmed J, Pinho S, Zhang D, Mizoguchi T, Wei Q, Lucas D, Ito K, Mar JC, Bergman A, Frenette PS. Arteriolar niches maintain haematopoietic stem cell quiescence. Nature. 502;637-643 (2013).

9. Mendez-Ferrer S, Michurina TV, Ferraro F, Mazloom AR, Macarthur BD, Lira SA, Scadden DT, Ma'ayan A, Enikolopov GN, Frenette PS. Mesenchymal and haematopoietic stem cells form a unique bone marrow niche. Nature. 466;829-834 (2010).

10. Ding L, Saunders TL, Enikopolov G, Morrison SJ. Endothelial and perivascular cells maintain haematopoietic stem cells. Nature. 481;457-462 (2012).

11. Ding L, Morrison SJ. Haematopoietic stem cells and early lymphoid progenitors occupy distinct bone marrow niches. Nature. 495;231-235 (2013).

12. Pinho S, Lacombe J, Hanoun M, Mizoguchi T, Bruns I, Kunisaki Y, Frenette PS. PDGFRα and CD51 mark human nestin+ sphere-forming mesenchymal stem cells capable of hematopoietic progenitor expansion. J Exp Med. 210;1351-1367 (2013).

13. Asada N, Kunisaki Y, Pierce H, Wang Z, Fernandez NF, Birbrair A, Ma'ayan A, Frenette PS. Differential cytokine contributions of perivascular haematopoietic stem cell niches. Nat Cell Biol. 19;241-223 (2017).

14. Mendez-Ferrer S, Lucas D, Battista M, Frenette PS. Heamatopoietic stem cell release is regulated by circadian oscillations. Nature. 452;442-447 (2008).

15. Katayama Y, Battista M, Kao WM, Hidalgo A, Peired AJ, Thomas SA, Frenette PS. Signals from the sympathetic nervous system regulate hematopoietic stem cell egress from the bone marrow. Cell. 124;407-421 (2006).

16. Bruns I, Lucas D, Pinho S, Ahmed J, Lambert MP, Kunisaki Y, Scheiermann C, Schiff L, Poncz M, Bergman A, Frenette PS. Megakaryocytes regulate hematopoietic stem cell quiescence thtough CXCL4 secretion. Nat Med. 20;1315-1320 (2014).

17. Zhao M, Perry JM, Marshall H, Venkatraman A, Qian P, He XC, Ahamed J, Li L. Megakaryocytes maintain homeostatic quiescence and promote post-injury regeneration of the hematopoietic stem cells. Nat Med. 20;1321-1326 (2014).

18. Nakamura-Ishizu A, Takubo K, Fujioka M, Suda T. Megakaryocytes are essential for HSC quiescence through production of thrombopoietin. Biochem Biophys Res Commun. 454;353-357 (2014).

19. Nakamura-Ishizu A, Takubo K, Kobayashi H, Suzuki-Onoue K, Suda T. CLEC-2 in megakaryocytes is critical for maintenance of the hematopoietic stem cells in the bone marrow. J Exp Med. 212;2133-2146 (2015).

20. Winkler IG, Sims NA, Pettit AR, Barbier V, Nowlan B, Helwani F, Poulton IJ, van Rooijen N, Alexander KA, Raggatt LJ, Levesque JP. Bone marrow macrophages maintain hematopoietic stem cell (HSC) niches and their depletion mobilizes HSCs. Blood. 116;4815-4828 (2010).

21. Chow A, Lucas D. Hidalgo A, Mendez-Ferrer S, Hashimoto D, Scheiermann C, Battista M, Leboeuf M, Prophete C, van Rooijen N, Tanaka M, Merad M, Frenette PS. Bone marrow CD169+ macrophages promote the retention of hematopoietic stem and progenitor cells in the mesenchymal stem cell niche. J Exp Med. 208;261-271 (2011).

22. Casanova-Acebes M, Pitaval C, Weiss LA, Nombela-Arrieta C, Chevre R, A-Gonzalez N, Kunisaki Y, Zhang D, van Rooijen N, Silberstein LE, Weber C, Nagasawa T, Frenette PS, Castrillo A, Hidalgo A. Rhythmic modulation of the hematopoietic niche through neutrophil clearance. Cell. 153;1025-1035 (2013).

23. Nilsson SK, Johnston HM, Coverdale JA. Spatial localization of transplanted hematopoietic stem cells: inferences for the localization of stem cell niches. Blood. 97;2293–9 (2001).

24. Kiel MJ, Yilmaz OH, Iwashita T, Yilmaz OH, Terhorst C, Morrison SJ. SLAM family receptors distinguish hematopoietic stem and progenitor cells and reveal endothelial niches for stem cells. Cell. 121;1109–21 (2005).

25. Itkin T, Gur-Cohen S, Spencer JA, Schajnovitz A, Ramasamy SK, Kusumbe AP, Ledergor G, Jung Y, Milo I, Poulos MG, Kalinkovich A, Ludin A, Kollet O, Shakhar G, Butler JM, Rafii S, Adams RH, Scadden DT, Lin CP, Lapidot T. Distinct bone marrow blood vessels differentially regulate hematopoiesis. Nature. 532;323-328 (2016).

26. Zou YR, Kottmann AH, Kuroda M, Taniuchi I, Littman DR. Function of the chemokine receptor CXCR4 in haematopoiesis and in cerebellar development. Nature. 393;595–599 (1998).

27. Nagasawa T, Hirota S, Tachibana K, Takakura N, Nishikawa S, Kitamura Y, Yoshida N, Kikutani H, Kishimoto T. Defects in B-cell lymphopoiesis and bone-marrow myelopoiesis in mice lacking CXC chemokine PBSF/SDF-1. Nature. 382;635-638 (1996).

28. Ara T, Tokoyoda K, Sugiyama T, Egawa T, Kawabata K, Nagasawa T. Long-term hematopoietic stem cells require stromal cell-derived factor-1 for colonizing bone marrow ontogeny. Immunity. 19;254-267 (2003).

29. Tzeng YS, Li H, Kang YL, Chen WC, Lai DM. Loss of Cxcl12/Sdf-1 in adult mice decreases the quiescent state of hematopoietic stem/progenitor cells and alters the pattern of hematopoietic regeneration after myelosuppression. Blood. 117;429-439 (2011).

30. Sugiyama T, Kohara H, Noda M, Nagasawa T. Maintenance of the hematopoietic stem cell pool by CXCL12–CXCR4 chemokine signaling in bone marrow stromal cell niches. Immunity. 25;977–988 (2006).

31. Barker JE. Sl/Sld hematopoietic progenitors are deficient in situ. Exp Hematol. 22;174-177 (1994).

32. Himburg HA, Harris JR, Ito T, Daher P, Russell JL, Quarmyne M, Doan PL, Helms K, Nakamura M, Fixsen E, Herradon G, Reya T, Chao NJ, Harroch S, Chute JP. Pleiotrophin regulates the retention and self-renewal of hematopoietic stem cells in the bone marrow vascular niche. Cell Rep. 2;964-975 (2012).

33. Himburg HA, Muramoto GG, Daher P, Meadows SK, Russell JL, Doan P, Chi JT, Salter AB, Lento WE, Reya T, Chao NJ, Chute JP. Pleiotrophin regulates the expansion and regeneration of the hematopoietic stem cells. Nat Med. 16; 475-482 (2010).

34. Butler JM, Nolan DJ, Vertes EL, Varnum-Finney B, Kobayashi H, Hooper AT, Seandel M, Shido K, White IA, Kobayashi M, Witte L, May C, Shawber C, Kimura Y, Kitajewski J, Rosenwaks Z, Bernstein ID, Rafii S. Endothelial cells are essential for the self-renewal and repopulation of Notch-dependent hematopoietic stem cells. Cell Stem Cell. 6;251-264 (2010).

35. Poulos MG, Guo P, Kofler NM, Pinho S, Gutkin MC, Tikhonova A, Aifantis I, Frenette PS, Kitajewski J, Rafii S, Butler JM. Endothelial Jagged-1 is necessary for homeostatic and regenerative hematopoiesis. Cell Rep. 4;1022-1034 (2013).

36. Rafii S, Shapiro F, Pettengell R, Ferris B, Nachman RL, Moore MA, Asch AS. Human bone marrow microvascular endothelial cells support long-term proliferation and differentiation of myeloid and megakaryocytic progenitors. Blood. 86;3353–3363 (1995).

37. Lu LS, Wang SJ, Auerbach R. In vitro and in vivo differentiation into B cells, T cells, and myeloid cells of primitive yolk sac hematopoietic precursor cells expanded >100-fold by coculture with a clonal yolk sac endothelial cell line. P Natl Acad Sci USA. 93;14782–14787 (1996).

38. Ohneda O, Fennie C, Zheng Z, Donahue C, La H, Villacorta R, Cairns B, Lasky LA. Hematopoietic stem cell maintenance and differentiation are supported by embryonic aorta-gonad-mesonephros region-derived endothelium. Blood. 92;908–919 (1998).

39. Li W, Johnson SA, Shelley WC, Ferkowicz M, Morrison P, Li Y, Yoder MC. Primary endothelial cells isolated from the yolk sac and para-aortic splanchnopleura support the expansion of adult marrow stem cells in vitro. Blood. 102;4345–4353 (2003).

40. Maillard I, Koch U, Dumortier A, Shestova O, Xu L, Sai H, Pross SE, Aster JC, Bhandoola A, Radtke F, Pear WS. Canonical notch signaling is dispensable for the maintenance of adult hematopoietic stem cells. Cell Stem Cell. 2;356-366 (2008).

41. Poulos MG, Ramalingam P, Gutkin MC, Kleppe M, Ginsberg M, Crowley MJ, Elemento O, Levine RL, Rafii S, Kitajewski J, Greenblatt MB, Shim JH, Butler JM. Endothelial-specific inhibition of NF-κB enhances functional hematopoiesis. Nat Commun. 7;13829 (2016).

42. Hooper AT, Butler JM, Nolan DJ, Kranz A, Iida K, Kobayashi M, Kopp HG, Shido K, Petit I, Yanger K, James D, Witte L, Zhu Z, Wu Y, Pytowski B, Rosenwaks Z, Mittal V, Sato TN, Rafii S. Engraftment and reconstitution of hematopoiesis is dependent on VEGFR2-mediated regeneration of sinusoidal endothelial cells. Cell Stem Cell. 4;263-74 (2009).

43. Knospe WH, Blom J, Crosby WH. Regeneration of locally irradiated bone marrow. I. Dose dependent, long-term changes in the rat, with particular emphasis upon vascular and stromal reaction. Blood. 28;398-415 (1966).

44. Shirota T, Tavassoli M. Cyclophosphamide-induced alterations of bone marrow endothelium: implications in homing of marrow cells after transplantation. Exp Hematol. 19;369-373 (1991).

45. Kopp HG, Avecilla ST, Hooper AT, Shmelkov SV, Ramos CA, Zhang F, Rafii S. Tie2 activation contributes to hemangiogenic regeneration after myelosuppression. Blood. 106;505-13 (2005).

46. Zhou BO, Ding L, Morrison SJ. Hematopoietic stem and progenitor cells regulate the regeneration of their niche by secreting Angiopoietin-1. Elife. 4;e05521 (2015).

47. Li XM, Hu Z, Jorgenson ML, Wingard JR, Slayton WB. Bone marrow sinusoidal endothelial cells undergo nonapoptotic cell death and are replaced by proliferating sinusoidal cells in situ to maintain the vascular niche following lethal irradiation. Exp Hematol. 36;1143-1156 (2008).

48. Doan PL, Russell JL, Himburg HA, Helms K, Harris JR, Lucas J, Holshausen KC, Meadows SK, Daher P, Jeffords LB, Chao NJ, Kirsch DG, Chute JP. Tie2(+) bone marrow endothelial cells regulate hematopoietic stem cell regeneration following radiation injury. Stem Cells. 31;327-37 (2013).

49. Kopp HG, Avecilla ST, Hooper AT, Shmelkov SV, Ramos CA, Zhang F, Rafii S. Tie2 activation contributes to hemangiogenic regeneration after myelosuppression. Blood. 106;505-513 (2005).

50. T.M. Dexter, M.A. Moore, A.P. Sheridan. Maintenance of hemopoietic stem cells and production of differentiated progeny in allogeneic and semiallogeneic bone marrow chimeras in vitro. J. Exp. Med. 145;1612–1616 (1977).

51. Möhle R, Green D, Moore MA, Nachman RL, Rafii S. Constitutive production and thrombin-induced release of vascular endothelial growth factor by human megakaryocytes and platelets. Proc Natl Acad Sci USA. 94;663-668 (1997).

52. Pintucci G, Froum S, Pinnell J, Mignatti P, Rafii S, Green D. Trophic effects of platelets on cultured endothelial cells are mediated by platelet-associated fibroblast growth factor-2 (FGF-2) and vascular endothelial growth factor (VEGF). Thromb Haemost. 88;834-842 (2002).

53. Fernandez-Patron C, Martinez-Cuesta MA, Salas E, Sawicki G, Wozniak M, Radomski MW, Davidge ST. Differential regulation of platelet aggregation by matrix metalloproteinases-9 and -2. Thromb Haemost. 82;1730-1735 (1999).

54. Pipili-Synetos E, Papadimitriou E, Maragoudakis ME. Evidence that platelets promote tube formation by endothelial cells on matrigel. Br J Pharmacol. 125;1252-1257 (1998).

55. Amano H, Hackett NR, Rafii S, Crystal RG. Thrombopoietin gene transfer-mediated enhancement of angiogenic responses to acute ischemia. Circ Res. 97;337-345 (2005).

56. Kopp HG, Hooper AT, Broekman MJ, Avecilla ST, Petit I, Luo M, Milde T, Ramos CA, Zhang F, Kopp T, Bornstein P, Jin DK, Marcus AJ, Rafii S. Thrombospondins deployed by thrombopoietic cells determine angiogenic switch and extent of revascularization. J Clin Invest. 116;3277-3291 (2006).

57. Jin DK, Shido K, Hopp HG, Petit I, Shmelkov SV, Young LM, Hooper AT, Amano H, Avecilla ST, Heissig B, Hattori K, Zhang F, Hicklin DJ, Wu Y, Zhu Z, Dunn A, Salari H,

Werb Z, Hackett NR, Crystal RG, Lyden D, Rafii S. Cytokine-mediated deployment of SDF-1 induces revascularization through recruitment of CXCR4+ hemangiocytes. Nat Med. 12;557-567 (2006).

58. Suri C, Jones PF, Patan S, Bartunkova S, Maisonpierre PC, Davis S, Sato TN, Yancopoulos GD. Requisite role of angiopoietin-1, a ligand for the TIE2 receptor, during embryonic angiogenesis. Cell. 87;1171-1180 (1996).

59. Kobayashi H, Butler JM, O'Donnell R, Kobayashi M, Ding BS, Bonner B, Chiu VK, Nolan DJ, Shido K, Benjamin L, Rafii S. Angiocrine factors from Akt-activated endothelial cells balance self-renewal and differentiation of haematopoietic stem cells. Nat Cell Biol. 12;1046-1056 (2010).

60. Greenbaum A, Hsu YM, Day RB, Schuettpelz LG, Christopher MJ, Borgerding JN, Nagasawa T, Link DC. CXCL12 in early mesenchymal progenitors is required for haematopoietic stem-cell maintenance. Nature. 495;227-230 (2013).

61. Christopher MJ, Rao M, Liu F, Woloszynek JR, Link DC. Expression of the G-CSF receptor in monocytic cells is sufficient to mediate hematopoietic progenitor mobilization by G-CSF in mice. J. Exp. Med. 208;251-260 (2011).

62. Himburg HA, Yan X, Doan PL, Quarmyne M, Micewicz E, McBride W, Chao NJ, Slamon DJ, Chute JP. Pleiotrophin mediates hematopoietic regeneration via activation of RAS. J Clin Invest. 124;4753-4758 (2014).

63. Schaefer BC, Schaefer ML, Kappler JW, Marrack P, Kedl RM. Observation of antigen-dependent CD8+ T-cell/ dendritic cell interactions in vivo. Cell Immunol. 214;110-122 (2001).

64. Na Nakorn T, Traver D, Weissman, IL, Akashi K. Myeloerythroid-restricted progenitors are sufficient to confer radioprotection and provide the majority of day 8 CFU-S. J Clin Invest. 109;1579-1585 (2002).

65. Tsuchiya Y, Nakabayashi O, Nakano H. FLIP the Switch: Regulation of Apoptosis and Necroptosis by cFLIP. Int J Mol Sci. 16;30321-30341 (2015).

66. Passegue E, Wagner EF, Weissman IL. JunB deficiency leads to a myeloproliferative disorder arising from hematopoietic stem cells. Cell. 119;431-443 (2004).

67. Abram CL, Roberge GL, Hu Y, Lowell CA. Comparative analysis of the efficiency and specificity of myeloid-Cre deleting strains using ROSA-EYFP reporter mice. J Immunol Methods. 408;89-100 (2014).

68. Buch T, Heppner FL, Tertilt C, Heinen TJ, Kremer M, Wunderlich FT, Jung S, Waisman A. A Cre-inducible diphtheria toxin receptor mediates cell lineage ablation after toxin administration. Nat Methods. 2;419-426 (2005).

69. Daley JM, Thomay AA, Connolly MD, Reichner JS, Albina JE. Use of Ly6G-specific monoclonal antibody to deplete neutrophils in mice. J Leukoc Biol. 83;64-70 (2008).

70. Brenner D, Blaser H, Mak TW. Regulation of tumour necrosis factor signalling: live or let die. Nat Rev Immunol. 15;362-374 (2015).

71. Leibovich SJ, Polverini PJ, Shephard HM, Wiseman DM, Shively V, Nuseir N. Macrophage-induced angiogenesis is mediated by tumor necrosis factor-alpha. Nature. 329;630-632 (1987).

72. Baluk P, Yao LC, Feng J, Romano T, Jung SS, Schreiter JL, Yan L, Shealy DJ, McDonald DM. TNF-alpha drives remodeling of blood vessels and lymphatics in sustained airway inflammation in mice. J Clin Invest. 119;2954-2964 (2009).

73. Espin R, Roca FJ, Candel S, Sepulcre MP, Gonzalez-Rosa JM, Alcaraz-Perez F, Meseguer J, Cayuela ML, Mercader N, Mulero V. TNF receptors regulate vascular homeostasis in zebrafish through a caspase-8, caspase-2 and P53 apoptotic program that bypasses caspase-3. Dis Model Mech. 6;383-396 (2013).

74. Eash KJ, Greenbaum AM, Gopalan PK, Link DC. CXCR2 and CXCR4 antagonistically regulate neutrophil trafficking from murine bone marrow. J Clin Invest. 120; 2423-2431 (2010).

75. Rezzoug F, Huang Y, Tanner MK, Wysoczynski M, Schanie CL, Chilton PM, Ratajczak MZ, Fugier-Vivier IJ, Ildstad ST. TNF-alpha is critical to facilitate hemopoietic stem cell engraftment and function. J Immunol. 180;49-57 (2008).

76. Grunewald M, Avraham I, Dor Y, Bachar-Lustig E, Itin A, Jung S, Chimenti S, Landsman L, Abramovitch R, Keshet E. VEGF-induced adult neovascularization: recruitment, retention, and role of accessory cells. Cell. 124;175-189 (2006).

77. Doan PL, Himburg HA, Helms K, Russell JL, Fixsen E, Quarmyne M, Harris JR, Deoliviera D, Sullivan JM, Chao NJ, Kirsch DG, Chute JP. Epidermal growth factor regulates hematopoietic regeneration after radiation injury. Nat Med. 19;295-304 (2013).

78. Pearl-Yafe M, Mizrahi K, Stein J, Yolcu ES, Kaplan O, Shirwan H, Yaniv I, Askenasy N. Tumor necrosis factor receptors support murine hematopoietic progenitor function in the early stages of engraftment. Stem Cells. 28;1270-1280 (2010).

79. Rebel VI, Hartnett S, Hill GR, Lazo-Kallanian SB, Ferrara JL, Sieff CA. Essential role for the p55 tumor necrosis factor receptor in regulating hematopoiesis at a stem cell level. J. Exp. Med. 190;1493-1504 (1999).

80. Slordal L, Warren DJ, Moore MA. Protective effects of tumor necrosis factor on murine hematopoiesis during cycle-specific cytotoxic chemotherapy. Cancer Res. 50;4216-4220 (1990).

81. Pronk CJ, Veiby OP, Bryder D, Jacobsen SE. Tumor necrosis factor restricts hematopoietic stem cell activity in mice: involvement of two distinct receptors. J. Exp. Med. 208;1563-1570 (2011).

82. Ishida T, Suzuki S, Lai CY, Yamazaki S, Kakuta S, Iwakura Y, Nojima M, Takeuchi Y, Higashihara M, Nakauchi H, Otsu M. Pre-Transplantation Blockade of TNF-alpha-Mediated Oxygen Species Accumulation Protects Hematopoietic Stem Cells. Stem cells. 35;989-1002 (2017).

83. Lucas D, Scheiermann C, Chow A, Kunisaki Y, Bruns I, Barrick C, Tessarollo L, Frenette PS. Chemotherapy-induced bone marrow nerve injury impairs hematopoietic regeneration. Nat Med. 19;695-703 (2013).

84. Galotto M, Berisso G, Delfino L, Podesto M, Ottaggio L, Dallorso S, Dufour C, Ferrara GB, Abbondandolo A, Dini G, Bacigalupo A, Cancedda R, Quarto R. Stromal damage as consequence of high-dose chemo/radiotherapy in bone marrow transplant recipients. Exp Hematol. 27;1460-1466 (1999).

85. Kemp K, Morse R, Wexler S, Cox C, Mallam E, Hows J, Donaldson C. Chemotherapy-induced mesenchymal stem cell damage in patients with hematological malignancy. Ann Hematol. 89;701-713 (2010).

86. Pasparakis M, Alexopoulou L, Episkopou V, Kollias G. Immune and inflammatory responses in follicular dendritic cell networks and germinal centers, and in the maturation of the humoral immune response. J Exp Med. 184;1397-1411 (1996).

87. Peschon JJ, Torrance DS, Stocking KL, Glaccum MB, Otten C, Willis CR, Charrier K, Morrissey PJ, Ware CB, Mohler KM. TNF receptor-deficient mice reveal divergent roles for p55 and p75 in several models of inflammation. J Immunol. 160;943-952 (1998).

88. Lucas D, Battista M, Shi PA, Isola L, Frenette PS. Mobilized hematopoietic stem cell yield depends on species-specific circadian timing. Cell stem cell. 3;364-366 (2008).

89. Puram RV, Kowalczyk MS, de Boer CG, Schneider RK, Miller PG, McConkey M, Tothova Z, Tejero H, Heckl D, Jaras M, Chen MC, Li H, Tamayo A, Cowley GS, Rozenblatt-Rosen O, Al-Shahrour F, Regev A, Ebert BL. Core circadian clock genes regulate leukemia stem cells in AML. Cell. 165;303-316 (2016).

90. Suire C, Brouard N, Hirschi K, Simmons PJ. Isolation of the stromal-vascular fraction of mouse bone marrow markedly enhances the yield of clonogenic stromal progenitors. Blood. 119;e86-95 (2012).

91. Schindelin J, Arganda-Carreras I, Frise E, Kaynig V, Longair M, Pietzsch T, Preibisch S, Rueden C, Saalfield S, Schmid B, Tinevez JY, White DJ, Hartenstein V, Eliceiri K, Tomancak P, Cardona A. Fiji: an open-source platform for biological-image analysis. Nat Methods. 9;676-682 (2012).

92. Thijssen VL, Brandwijk RJ, Dings RP, Griffioen AW. Angiogenesis gene expression profiling in xenograft models to study cellular interactions. Exp Cell Res. 299;286-293 (2004).

93. Tripurani SK, Cook RW, Eldin KW, Pangas SA. BMP-specific SMADs function as novel repressors of PDGFA and modulate its expression in ovarian granulosa cells and tumors. Oncogene. 32;3877-3885 (2013).

94. Yu Y, Xu X, Liu L, Mao S, Feng T, Lu Y, Cheng Y, Wang H, Zhao W, Tang W. Progranulin deficiency leads to severe inflammation, lung injury and cell death in a mouse model of endotoxic shock. J Cell Mol Med. 20;506-517 (2016).

95. Rosenfield SM, Bowden ET, Cohen-Missner S, Gibby KA, Ory V, Henke RT, Riegel AT, Wellstein A. Pleiotrophin (PTN) expression and function and in the mouse mammary gland and mammary epithelial cells. PLoS One. 7;e47876 (2012).

96. Maekawa T, Sakuma A, Taniuchi S, Ogo Y, Iguchi T, Takeuchi S, Takahashi S. Transforming growth factor-alpha mRNA expression and its possible roles in mouse endometrial stromal cells. Zoolog Sci. 29;377-383 (2012).

97. Tomita K, Freeman BL, Bronk SF, LeBrasseur NK, White TA, Hirsova P, Ibrahim SH. CXCL10-Mediates Macrophage, but not Other Innate Immune Cells-Associated Inflammation in Murine Nonalcoholic Steatohepatitis. Sci Rep. 6;28786 (2016).

98. Wu YJ, Wu YH, Mo ST, Hsiao HW, He TW, Lai MZ. Cellular FLIP inhibits myeloid cell activation by suppressing selective innate signaling. J Immunol. 195;2612-2623 (2015).

99. Aro E, Khatri R, Gerard-O'Riley R, Mangiavini L, Myllyharju J, Schipani E. Hypoxia-inducible Factor-1 (HIF-1) but not HIF-2 is essential for hypoxic induction of collagen prolyl 4-hydroxylases in primary newborn mouse epiphyseal growth plate chondrocytes. J Biol Chem. 287;37134-37144 (2012).

100. Shih SC, Robinson GS, Perruzzi CA, Calvo A, Desai K, Green JE, Ali IU, Smith LE, Senger DR. Molecular profiling of angiogenesis markers. Am J Pathol. 161;35-41 (2002).

101. Aung HT, Schroder K, Himes SR, Brion K, van Zuylen W, Trieu A, Suzuki H, Hayashizaki Y, Hume DA, Sweet MJ, Ravasi T. LPS regulates proinflammatory gene

expression in macrophages by altering histone deacetylase expression. FASEB J. 20;1315-1327 (2006).

102. Patel RD, Kim DJ, Peters JM, Perdew GH. The aryl hydrocarbon receptor directly regulates expression of the potent mitogen epiregulin. Toxicol Sci. 89;75-82 (2006).

103. Du W, Prochazka J, Prochazkova M, Klein OD. Expression of FGFs during early mouse tongue development. Gene Expr Patterns. 20;81-87 (2016).

104. Izikki M, Guignabert C, Fadel E, Humbert M, Tu L, Zadigue P, Dartevelle P, Simonneau G, Adnot S, Maitre B, Raffestin B, Eddahibi S. Endothelial-derived FGF2 contributes to the progression of pulmonary hypertension in humans and rodents. J Clin Invest. 119;512-523 (2009).

105. Hoot KE, Oka M, Han G, Bottinger E, Zhang Q, Wang XJ. HGF upregulation contributes to angiogenesis in mice with keratinocyte-specific Smad2 deletion. J Clin Invest. 120;3606-3616 (2010).

106. Mourikis P, Gopalakrishnan S, Sambasivan R, Tajbakhsh S. Cell-autonomous Notch activity maintains the temporal specification potential of skeletal muscle stem cells. Development. 139;4536-48 (2012).

107. White LE, Santora RJ, Cui Y, Moore FA, Hassoun HT. TNFR1-dependent pulmonary apoptosis during ischemic acute kidney injury. Am J Physiol Lung Cell Mol Physiol. 303; L449-459 (2012).

108. Shanmugam G, Narasimhan M, Sakthivel R, Kumar RR, Davidson C, Palaniappan S, Claycomb WW, Hoidal JR, Darley-Usmar VM, Rajasekaran NS. A biphasic effect of TNF-alpha in regulation of the Keap1/Nrf2 pathway in cardiomyocytes. Redox Biol. 9;77-89 (2016).

109. Deshmukh HS, Liu Y, Menkiti OR, Mei J, Dai N, O'Leary CE, Oliver PM, Kolls JK, Weiser JN, Worthen GS. The microbiota regulates neutrophil homeostasis and host resistance to Escherichia coli K1 sepsis in neonatal mice. Nat Med. 20;524-530 (2017).

110. Friswell MK, Gika H, Stratford IJ, Theodoridis G, Telfer B, Wilson ID, McBain AJ. Site and strain-specific variation in gut microbiota profiles and metabolism in experimental mice. PLoS One. 5;e8584 (2010).

111. Moore RJ, Stanley D. Experimental design considerations in microbiota/inflammation studies. Clin Transl Immunology. 5;e92 (2016).

112. Khosravi A, Yanez A, Price JG, Chow A, Merad M, Goodridge HS, Mazmanian SK. Gut microbiota promote hematopoiesis to control bacterial infection. Cell Host Microbe. 15;374-381 (2014).

113. Josefsdottir KS, Baldridge MT, Kadmon CS, King KY. Antibiotics impair murine hematopoiesis by depleting the intestinal microbiota. Blood. 129;729-739 (2017).

114. Kim YG, Sakamoto K, Seo SU, Pickard JM, Gillilland MG 3rd, Pudlo NA, Hoostal M, Li X, Wang TD, Feehley T, Stefka AT, Schmidt TM, Martens EC, Fukuda S, Inohara N, Nagler CR, Nunez G. Neonatal acquisition of *Clostridia* species protects against colonization by bacterial pathogens. Science. 356;315-319 (2017).

115. Sarkar S, Bhagat I, Hieber S, Donn SM. Can neutrophil responses in very low birth weight infants predict the organisms responsible for late-onset bacterial or fungal sepsis? J Perinatol. 26;501-505 (2006).

116. Nagai Y, Garrett KP, Ohta S, Bahrun U, Kouro T, Akira S, Takatsu K, Kincade PW. Toll-like receptors on hematopoietic progenitor cells stimulate innate immune system replenishment. Immunity. 24;801-812 (2006).

117. Zhao Y, Ling F, Wang HC, Sun XH. Chronic TLR signaling impairs the long-term repopulating potential of hematopoietic stem cells of wild type but not Id1 deficient mice. PLoS One. 8;e55552 (2013).

118. Esplin BL, Shimazu T, Welner RS, Garrett KP, Nie L, Zhang Q, Humphrey MB, Yang Q, Borghesi LA, Kincade PW. Chronic exposure to a TLR ligand injures hematopoietic stem cells. J Immunol. 186;5367-5375 (2011).

119. Liu A, Wang Y, Ding Y, Baez I, Payne KJ, Borghesi L. Cutting Edge: Hematopoietic stem cell expansion and common lymphoid progenitor depletion require hematopoietic-derived, cell-autonomous TLR4 in a model of chronic endotoxin. J Immunol. 195;2524-2528 (2015).

120. Herman AC, Monlish DA, Romine MP, Bhatt ST, Zippel S, Schuettpelz LG. Systemic TLR2 agonist exposure regulates hematopoietic stem cells via cell-autonomous and cell-non-autonomous mechanisms. Blood Cancer J. 6;e437 (2016).

121. Takizawa H, Regoes RR, Boddupalli CS, Bonhoeffer S, Manz MG. Dynamic variation in cycling of hematopoietic stem cells in steady state and inflammation. J Exp Med. 208;273-284 (2011).

122. Lacorazza HD, Yamada T, Liu Y, Miyata Y, Sivina M, Nunes J, Nimer SD. The transcription factor MEF/ELF4 regulates the quiescence of primitive hematopoietic cells. Cancer Cell. 9;175-187 (2006).

123. Yan L, Womack B, Wotton D, Guo Y, Shyr Y, Dave U, Li C, Hiebert S, Brandt S, Hamid R. Tgif1 regulates quiescence and self-renewal of hematopoietic stem cells. Mol Cell Biol. 33;4824-4833 (2013).

124. Carcalano G, Lee J, Kikly K, Ryan AM, Pitts-Meek S, Hultgren B, Wood WI, Moore MW. Neutrophil and B cell expansion in mice that lack the murine IL-8 receptor homolog. Science. 265;682-684 (1994).

125. Eash KJ, Means JM, White DW, Link DC. CXCR4 is a key regulator of neutrophil release from the bone marrow under basal and stress granulopoiesis conditions. Blood. 113;4711-4719 (2009).

126. Zarbock A, Ley K. Mechanisms and consequences of neutrophil interaction with the endothelium. Am J Pathol. 172;1-7 (2008).

127. McEver RP. Selectins: initiators of leucocyte adhesion and signalling at the vascular wall. Cardiovasc Res. 107;331-339 (2015).

128. Gaudry M, Bregerie O, Andrieu V, El Benna J, Pocidalo MA, Hakim J. Intracellular pool of vascular endothelial growth factor in human neutrophils. Blood. 90;4153 (1997).

129. Scapini P, Calzetti F, Cassatella MA. On the detection of neutrophil-derived vascular endothelial growth factor (VEGF). J Immunol Methods. 232;121 (1999).

130. Cassatella MA. Neutrophil-derived proteins: selling cytokines by the pound. Adv Immunol. 1999.

131. Sakaguchi H, Seki S, Tsubouchi H, Daikuhara Y, Niitani Y, Kobayashi K. Ultrastructural location of human hepatocyte growth factor in human liver. Hepatology. 19;1157 (1994).

132. McCourt M, Wang JH, Sookhai S, Redmond HP. Activated human neutrophils release hepatocyte growth factor/scatter factor. Eur J Surg Oncol. 27;396 (2001).

133. Benelli R, Morini M, Carrozzino F, Ferrari N, Minghelli S, Santi L, Cassatella M, Noonan DM, Albini A. Neutrophils as a key cellular target for angiostatin: implications for regulation of angiogenesis and inflammation. FASEB J. 16;267 (2002).

134. Scapini P, Morini M, Tecchio C, Minghello S, Di Carlo E, Tanghetti E, Albini A, Lowell C, Berton G, Noonan DM, Cassatella MA. CXCL1/macrophage inflammatory protein-2-induced angiogenesis in vivo is mediated by neutrophil-derived vascular endothelial growth factor-A. J Immunol. 172;5034-5040 (2004).

135. Gong Y, Koh DR. Neutrophils promote inflammatory angiogenesis via release of preformed VEGF in an in vivo corneal model. Cell Tissue Res. 339;437-448 (2010).

136. Espin-Palazon R, Stachura DL, Campbell CA, Garcia-Moreno D, Cid ND, Kim AD, Candel S, Meseguer J, Mulero V, Traver D. Proinflammatory signaling regulates hematopoietic stem cell emergence. Cell. 159;1070-1085 (2014).